Caractérisation de variables de structure forestière à partir du nuage de points du lidar aéroporté

Thèse

Étienne Bellemare Racine

Doctorat en sciences forestières
Philosophiæ doctor (Ph. D.)

Québec, Canada

Caractérisation de variables de structure forestière à partir du nuage de points du lidar aéroporté

Thèse

Etienne Bellemare Racine

Sous la direction de :

Jean Bégin, directeur de recherche

Résumé

Les pratiques d'aménagement forestier doivent être adaptées aux particularités des écosystèmes. L'inventaire de la structure forestière permet de fournir les informations de base pour décrire la diversité des écosystèmes. La télédétection est une solution économique pour mesurer de manière détaillée et extensive la structure forestière. Le lidar (*Light Detection and Ranging*) aéroporté est une technologie qui permet d'observer la structure tridimensionnelle de la végétation sur de grandes superficies. Cette thèse s'intéresse à trois éléments de la structure forestière : l'âge, la composition et la densité de couvert. Dans le premier chapitre, nous utilisons la distribution verticale des retours lidar ainsi que d'autres indicateurs de structure forestière (hauteur, taux de pénétration des premiers retours, paramètres de distribution Weibull) et de station (altitude, pente, orientation, radiation solaire, indice d'humidité, aire du bassin versant et longueur de pente arrière) pour prédire l'âge moyen des placettes avec une erreur de prédiction de 8.8 ans (R^2 0.83, racine de l'erreur quadratique moyenne (RMSE) 19%). Dans le deuxième chapitre, nous avons associé la distribution verticale des retours lidar à l'espèce, l'âge et la densité de couvert en utilisant un GLM fonctionnel et un nouveau test de signifiance non paramétrique graphique permettant d'identifier les variations associées à chacune des variables. Nos résultats indiquent que les trois variables peuvent expliquer jusqu'à 47% de la variation de la distribution verticale des retours lidar. Chaque espèce présentait des caractéristiques discriminantes, mais trois groupes se démarquaient : les peuplements de peuplier faux-tremble affichaient la distribution verticale la plus uniforme ; les peuplements de sapin baumier et de bouleau à papier présentaient une distribution centrée autour de 50% de la hauteur. Les peuplements dominés par les épinettes blanche et noire présentaient une distribution plutôt concentrée à 30% de la hauteur du peuplement. Une augmentation de la fermeture du couvert était associée à une concentration de la distribution autour de 50% de la hauteur du peuplement. L'augmentation de l'âge déplaçait la distribution dans la partie supérieure du peuplement jusqu'à 50–70 ans, puis se stabilisait et redescendait à 90–120 ans. Finalement, nous avons étudié l'influence du seuil de hauteur et de la résolution spatiale de la grille sur la répétabilité des mesures de densité de couvert par lidar aéroporté en utilisant trois survols, dont deux conduits la même année (respectivement 2016 et 2018). En utilisant une mesure d'asymétrie (skewness) et la variance des différences décalées de la densité de couvert, nous avons identifié des mesures qui étaient plus répétables entre les survols. Les résultats

montrent que les paramètres suivants étaient optimaux : seuil de hauteur à 3 m, résolution de grille de 25 m (RMSE de 7% et 5% ; biais de 4% et 0% pour les relevés à basse densité de 2016 et 2018). Ces résultats montrent que le lidar est un outil important pour l'enrichissement des données d'inventaire par des données de structure et pourrait contribuer à cibler les pratiques d'aménagement adaptées aux particularités des écosystèmes.

Table des matières

Liste des tableaux

Liste des figures

Liste des acronymes

k-MSN	k-Voisins les plus similaires (*k-Most Similar Neighbors*)
k-NN	k-Plus proches voisins (*k-Nearest Neighbor*)
ALTM	*Airborne Laser Terrain Mapper*
DSM	Modèle numérique de surface (*Digital surface model*)
DTM	Modèle numérique d'altitude (*Digital terrain model*)
FDA	Analyse de données fonctionnelles (*Functional data analysis*)
GEDI	*Global Ecosystem Dynamics Investigation*
GLM	Modèle linéaire généralisé (*Generalized linear model*)
GPS	*Global positionning system*
HD	Haute densité (*High density*)
LD	Faible densité (*Low density*)
Lidar (LiDAR)	*Light detection and ranging*
MSE	Erreur quadratique moyenne (*Mean square error*)
NIR	Proche infrarouge (*Near infrared*)
R^2	Coefficient de détermination
RMSE	Racine de l'erreur quadratique moyenne (*Root mean square error*)
TIN	Réseau irrégulier triangulé (*Triangulated Irregular Network*)
UAF	Unité d'aménagement forestier

Remerciements

Je veux d'abord remercier mon directeur, Jean Bégin pour sa confiance, sa disponibilité et sa complicité dont je n'aurais pu me passer. Merci aussi à Benoît St-Onge pour sa rigueur et sa très grande compétence ; ce fut un plaisir de collaborer avec lui.

Merci à mon comité de thèse, Chhun-Huor Ung et Jean-Claude Ruel de m'avoir encouragé et expliqué le contexte de la sylviculture et de l'inventaire forestier. Merci à Nicholas Coops de m'avoir accueilli dans son laboratoire, de m'avoir appris tant de choses sur la recherche et sur la vie d'humain aussi.

Merci à mes collègues ; ceux du laboratoire de dendrométrie et ceux du Ministère des Forêts, de la Faune et des Parcs. Particulièrement Anick Patry qui m'a orienté vers le lidar, la structure, la créativité et la rigueur, Antoine Leboeuf et Marc-Olivier Lemonde pour avoir partagé tant d'idées avec moi. Merci à mes amis de m'avoir écouté, encouragé, conseillé et surtout diverti de mon travail. Merci à ma famille, particulièrement ma mère pour son soutien et ses encouragements qui ont été essentiels pour terminer cette thèse.

Finalement, écrire une thèse, surtout avec une jeune famille, demande une partenaire exceptionnelle et des enfants qui le sont tout autant. Merci Marianne, Camille et Florence de m'avoir accompagné, encouragé et soutenu. Je vous aime.

Avant-propos

Cette thèse consiste en trois chapitres, tous rédigés sous la forme d'articles scientifiques, en anglais, et publiés ou soumis pour évaluation à des revues scientifiques. Je suis l'auteur principal des chapitres de cette thèse et les coauteurs des articles inclus dans cette thèse ont tous fourni leur accord à l'insertion des articles. Tous les chapitres sont identiques aux versions soumises ou publiées, à l'exception de la mise en page.

Le premier chapitre est publié dans la revue *Forest Science* : Racine E. B., Coops N. C., St-Onge B., Bégin J. (2014) Estimating Forest Stand Age from LiDAR-Derived Predictors and Nearest Neighbor Imputation. Forest Science 60 :128–136. http://dx.doi.org/10.5849/forsci.12-088. Le deuxième chapitre est publié dans *Trees – Structure and function* : Racine E. B., Coops N. C., Bégin J., Myllymäki M. (2021) Tree species, crown cover, and age as determinants of the vertical distribution of airborne LiDAR returns. Trees. https://doi.org/10.1007/s00468-021-02155-2 , et le troisième chapitre (par Etienne Racine, Antoine Leboeuf et Jean Bégin) a été soumis à la revue *Remote Sensing*.

Introduction générale

La capacité des écosystèmes à se maintenir dans le temps et à évoluer lorsque leurs conditions changent repose en grande partie sur leur diversité (Schütz 1997). Dans les dernières années, les aménagistes [1] de la forêt ont adapté leurs pratiques aux particularités des écosystèmes forestiers (Puettmann et al. 2009). Au Québec et ailleurs, on réclame que l'aménagement de la forêt se détache des pratiques agricoles et aille au-delà de l'approvisionnement en bois pour produire des écosystèmes diversifiés, résilients face aux changements climatiques, et représentatifs de la variabilité naturelle historique (Gauthier et al. 2008 ; Puettmann et al. 2009).

On réfère généralement à la variabilité des écosystèmes par la structure forestière : l'organisation des arbres dans l'écosystème. La structure détermine les conditions immédiates des processus écologiques ayant cours, lesquelles modifient à leur tour les conditions futures dans un processus de rétroaction (Pretzsch 2009). En sylviculture, la structure réfère traditionnellement à la distribution des âges, des diamètres ou des hauteurs dans un écosystème ou une placette-échantillon (Boucher et al. 2003 ; Puettmann et al. 2009 ; Raymond et al. 2010). Toutefois, dans la littérature on utilise la structure de manière plus large afin de désigner la variabilité des attributs forestiers, la vigueur des arbres, l'abondance de chicots, la présence de débris au sol, la composition, la canopée et la sous-canopée ou encore l'absence d'arbres (trouées) (Schütz 1997 ; Brokaw and Lent 1999 ; Pommerening 2002 ; Newton 2007 ; Ruel et al. 2007 ; Pretzsch 2009 ; Puettmann et al. 2009). Par extension, la structure forestière peut aussi inclure l'organisation interne des arbres comme leur port et leur forme (Martin-Ducup 2017 ; Côté et al. 2018 ; Beland et al. 2019). Dans cette thèse, la structure forestière réfère à *l'organisation des arbres*, ce qui reflète l'usage habituel du terme dans la littérature. On peut ainsi parler de structure d'âge, de structure verticale, horizontale, ou de composition qui seront abordées dans cette thèse.

Dans un contexte d'aménagement écosystémique (Gauthier et al. 2008), l'inventaire forestier fournit l'information nécessaire à l'aménagiste pour qu'il puisse fonder ses décisions sur les particularités des écosystèmes et en maintenir la variabilité (Parker and Russ 2004 ; Côté 2006). Lorsque l'inventaire forestier simplifie les écosystèmes par des valeurs moyennes, il

1. Dans cette thèse, on utilise *aménagement forestier* au sens large, incluant la sylviculture.

en dissimule la variabilité (Pretzsch 2009). Pour que les aménagistes puissent adapter leurs pratiques aux particularités des écosystèmes, il leur faut disposer d'une information exprimant leur complexité.

Pour mieux décrire la structure lors de l'inventaire, une des solutions consiste à collecter davantage d'information en forêt : davantage de placettes-échantillons, de carottes de bois, de mesures de hauteurs, etc. Malheureusement, les efforts investis dans le travail terrain ont bien souvent un coût élevé et une valeur marginale décroissante.

Depuis longtemps, l'aménagement des forêts repose sur la télédétection afin de réduire le fastidieux travail de terrain et d'observer des phénomènes dont la complexité et l'étendue les rendent inaccessibles avec des méthodes traditionnelles. En 1926, le Ministère des Terres et Forêts accordait le premier mandat de photographie aérienne de la péninsule gaspésienne (BANQ 2018), puis en 1970 créait le premier inventaire décennal qui s'appuiera sur l'imagerie aérienne. C'est dans la même région, dans la Réserve faunique de Matane, que le Ministère des Ressources naturelles, de la Faune et des Parcs expérimentera le lidar en 2007 pour en évaluer la pertinence pour l'inventaire forestier.

Le Québec a rapidement adopté le lidar : après un premier projet pilote couvrant une unité d'aménagement forestier (UAF) dans la réserve faunique de Matane en 2007, déjà plusieurs régions et divisions du Ministère des Ressources naturelles et de la Faune réclamaient leur projet pilote. En 2009, on ajoutait des acquisitions ponctuelles qui se sont multipliées, pour culminer en 2015 avec l'annonce par le Ministère de l'Énergie et des Ressources naturelles de l'ajout du lidar aux inventaires forestiers nationaux et la diffusion publique des données. Ainsi, les 529 000 km^2 du Québec méridional auront été couverts à la fin de l'année 2022.

Le lidar aéroporté permet de mesurer la structure de la forêt à l'aide d'un laser balayant embarqué dans un avion. Le capteur enregistre précisément l'origine et l'orientation de l'impulsion laser et en mesure le temps de propagation aller-retour pour localiser le site de réflexion. En accumulant les points de réflexion, le lidar permet de reconstruire un nuage de points qui dresse un portrait tridimensionnel du paysage.

Le lidar aéroporté permet d'étudier la structure de manière extensive et de décrire la complexité des écosystèmes à la fois verticalement et horizontalement, plutôt que de se concentrer sur certains indicateurs moyens. Il offre aussi l'avantage que les mesures sont extraites par des algorithmes, devenant ainsi vérifiables et reproductibles, par opposition à des mesures prises sur le terrain ou par différents photo-interprètes.

Plusieurs applications du lidar aéroporté touchent l'inventaire forestier comme la caractérisation d'habitats (Vierling et al. 2008 ; Seavy et al. 2009 ; Vierling et al. 2010), la mesure de caractéristiques dendrométriques (Korhonen et al. 2011 ; Treitz et al. 2012 ; White et al. 2013a), l'état de succession (Falkowski et al. 2009), la structure verticale de la canopée, la

forme de cime, et la biomasse aérienne (Ellsworth and Reich 1993 ; Magnussen et al. 1999 ; Harding et al. 2001 ; Lefsky et al. 2002 ; Parker et al. 2004 ; Maltamo et al. 2005 ; Mehtätalo 2006 ; Coops et al. 2007 ; Riggins et al. 2009 ; Falkowski et al. 2009 ; Stark et al. 2012 ; Cao et al. 2014 ; Papa et al. 2020). Le lidar est aussi utilisé pour l'identification d'espèces (Heinzel and Koch 2011, 2012 ; Vaughn et al. 2012 ; Palace et al. 2015 ; Hovi et al. 2016 ; Fassnacht et al. 2016 ; Budei et al. 2018 ; Axelsson et al. 2018 ; Fedrigo et al. 2018), mais l'absence de signature spectrale du lidar nécessite généralement qu'il soit combiné à un autre capteur, à tout le moins dans des situations opérationnelles où on retrouve plus d'une espèce (Holmgren and Persson 2004 ; Kim et al. 2011 ; White et al. 2013a ; Fassnacht et al. 2016 ; Budei et al. 2018 ; Budei and St-Onge 2018).

La capacité du lidar de pénétrer la canopée en fait une méthode idéale pour étudier la structure verticale de la forêt (Beland et al. 2019). Son grand avantage par rapport aux mesures terrain seules est sa capacité à produire de manière extensive une multitude de variables à la fois spectrales et géométriques qui permettent d'entraîner des modèles statistiques pour étendre les observations terrain à de grandes aires d'aménagement (White et al. 2013a). Ces approches de prédiction statistique dites par zone (area-based) sont très utilisées avec le lidar et fournissent un cadre flexible dans lequel de multiples variables de structure peuvent facilement être ajoutées. La prédiction par zone est la méthode opérationnelle la plus répandue et fournit un cadre particulièrement bien adapté aux besoins de l'aménagement écosystémique puisqu'elle permet d'intégrer plusieurs sources d'information pour exprimer plusieurs variables sur une même unité de territoire, dont des descripteurs de variabilité.

L'aménagement écosystémique nécessite le maintien des structures d'âge parmi les objectifs des plans d'aménagement forestiers (MRNFQ 2005 ; Gauthier et al. 2008 ; Larson et al. 2008 ; Puettmann et al. 2009). Pourtant, l'âge est une des mesures les plus laborieuses à collecter sur le terrain puisqu'elle nécessite l'insertion d'une sonde dans le tronc de l'arbre pour en extraire une carotte dont les cernes annuels sont ensuite dénombrés. Conséquemment, l'âge est établi de façon très ponctuelle et exprimé par des valeurs moyennes à l'échelle du peuplement forestier. L'absence de mesures par télédétection rend difficile l'amélioration de l'estimation de l'âge autrement que par l'intensification des prélèvement réalisés sur le terrain. Le lidar a été utilisé afin de quantifier des attributs dendrométriques (Treitz et al. 2012), mais la plupart se sont concentrées sur les attributs liés à la hauteur. La prédiction de l'âge à partir du lidar n'a pas beaucoup été explorée, bien que le lien entre l'âge et la structure observée par lidar l'ait été Kane et al. (2010a).

La connaissance des espèces est aussi essentielle pour prendre des décisions d'aménagement. Pour cette raison, l'identification des espèces est depuis longtemps effectuée par interprétation de photographies aériennes. L'interprétation repose sur des propriétés bien connues des espèces comme leur port, leur réflectivité à différentes longueurs d'ondes et leur autécologie (Leboeuf and Vaillancourt 2013a, b). Toutefois, la qualité de l'interprétation réalisée par des humains

peut varier selon leur expérience. De plus, l'opacité du couvert forestier limite l'observation à la strate forestière dominante et les méthodes d'inventaire terrain, comme le lidar terrestre ou les observations in situ, fournissant des portraits plus détaillés de la structure verticale sont limitées dans l'espace. Il demeure que l'utilisation du lidar pour l'étude de la structure est encore relativement peu explorée par rapport à son potentiel.

La structure verticale des peuplements varie selon les espèces et leurs conditions de croissance (MacArthur and Horn 1969 ; Aber 1979 ; Purves et al. 2007 ; Weiskittel et al. 2009 ; Thorpe et al. 2010 ; Power et al. 2012 ; Pretzsch and Dieler 2012 ; Power et al. 2014). Les effets de la structure verticale sur la distribution verticale des retours du lidar (White et al. 2013b ; Beland et al. 2019) ont été utilisés afin de classifier les espèces forestières. En général, les classifications d'espèces à partir du lidar ont opté pour une approche prédictive centrée sur l'identification de la qualité de prédicteurs, avec des résultats mitigés (Fassnacht et al. 2016). De plus, les méthodes centrées sur les prédictions utilisent souvent des méthodes statistiques de réduction de la dimension, comme l'analyse en composante principale, qui rendent très difficile l'interprétation de l'effet des variables (Koenig and Höfle 2016 ; Räty et al. 2016 ; Axelsson et al. 2018). Très peu de publications s'intéressent à la compréhension des mécanismes menant aux variations de distributions verticales des retours du lidar aéroporté (Fassnacht et al. 2016). Pourtant, une meilleure compréhension de la relation entre les retours lidar et les variables de structure pourrait aider à identifier les descripteurs de structure les plus pertinents pour l'aménagement de la forêt, et potentiellement pour la classification des espèces.

La densité de couvert est un indicateur de structure horizontale critique pour l'aménagement. Un estimé stable et juste de la densité du couvert est essentiel à l'estimation de caractéristiques dendrométriques ou pour comparer les mesures de densité dans le temps afin de suivre les effets de l'aménagement sur les forêts. La densité du couvert est particulièrement intensive à mesurer sur le terrain, alors qu'elle est plus facile à observer par photo-interprétation. Elle peut néanmoins présenter une qualité variable selon les photo-interprètes, en plus d'être difficilement reproductible. La densité est couramment estimée par lidar, mais les méthodes varient, sans que leur effet sur la capacité de comparaison des survols ne soit connu (White et al. 2013b). Le changement de paramètres de vol comme l'altitude ou l'angle de balayage conduisent à des différences entre les survols (Roussel et al. 2017), mais l'effet de paramètres post-survol comme la résolution spatiale de la grille utilisée pour l'agrégation des mesures, et le seuil de hauteur utilisée demeure inconnus. Or la comparaison de survols dont certains paramètres sont différents, pourrait mener à l'observation de différences qui sont en fait des artéfacts. Ces différences, qui ne sont pas réelles, peuvent modifier notre compréhension de l'évolution de la structure de la forêt.

But, hypothèses et objectifs

Le but de cette thèse est de valoriser l'information du lidar aéroporté pour décrire la structure forestière à l'échelle du paysage et ainsi contribuer à améliorer la connaissance des écosystèmes forestiers. Nos travaux portent sur la description de la structure par lidar pour améliorer l'évaluation de l'âge, de l'espèce dominante et de la densité. La compréhension de la relation entre le lidar et la structure forestière du peuplement pourrait aider à supporter les décisions d'aménagement. Les trois axes de structure choisis –âge, composition et densité– permettent d'explorer la capacité du lidar dans des tâches très différentes pour l'observation de la forêt.

Le premier chapitre de cette thèse pose l'hypothèse que le lidar peut décrire la structure forestière de manière à refléter l'âge des peuplements forestiers et que l'estimation de l'âge basée sur la hauteur peut être améliorée en incluant des descripteurs de station dérivés également du lidar. Les objectifs méthodologiques sont d'utiliser la distribution verticale des points lidar pour refléter la structure forestière verticale à l'échelle de la placette et d'identifier une méthode qui permette de lier cette structure aux âges qui y sont mesurés. À cet effet, la forêt Montmorency sélectionnée comme site d'étude, est l'un des sites au Québec avec la plus grande densité de carottes d'arbres. La méthodologie repose donc sur des prédictions par zone (*area-based*) où le lidar est calibré sur des mesures d'âges prises sur le terrain dans des placettes-échantillons. Cette méthode a le désavantage de nécessiter un intense travail d'échantillonnage et de localisation des placettes, mais permet d'utiliser des attributs mesurés sur le terrain.

Le deuxième chapitre pose l'hypothèse que la distribution verticale des retours lidar est liée à la composition, l'âge et la densité de couvert à l'échelle du peuplement forestier. Nous utilisons la cartographie aérienne, les données de photo-interprétation, comme données de référence pour caractériser la distribution verticale des retours lidar de cinq espèces forestières et leur relation avec l'âge et la densité du couvert. L'espèce dominante est difficile à établir avec le lidar monospectral, même avec des densités de points très élevées. Nous abordons le problème avec les techniques de lidar par zone. Pour pouvoir bien comprendre la relation entre la composition, l'âge et la densité de couvert, nous appliquons une nouvelle méthode de visualisation et d'analyse qui permet de comprendre ces relations de manière visuelle.

Le troisième et dernier chapitre aborde la comparaison de différentes acquisitions lidar pour la mesure de la densité de couvert, une variable utilisée pour représenter la structure horizontale des peuplements. La densité est couramment estimée par lidar, mais les méthodes varient (White et al. 2013a). Les archives lidar qui s'accumulent rendent possible le suivi de la structure horizontale dans le temps. Or les effets des différents paramètres utilisés pour le calcul de la densité de couvert peuvent créer des distorsions qui ne reflètent pas des changements réels dans l'écosystème. En particulier, les effets de la résolution spatiale de la grille, utilisée pour l'agrégation des mesures, et le seuil de hauteur utilisé demeurent inconnus. Plu-

sieurs méthodes pour calculer la densité de couvert sont disponibles (Holmgren et al. 2003 ; Korhonen et al. 2011 ; White et al. 2013a ; Liu et al. 2018 ; Alain et al. 2019 ; Burkhart et al. 2019 ; ESRI 2019), mais leurs effets n'ont pas été comparés sur des survols différents. Nous posons l'hypothèse qu'il existe une combinaison de paramètres post-survols faisant en sorte que les mesures lidar de densité de couvert sont répétables, c'est-à-dire que deux acquisitions de données lidar indépendantes devraient mener aux mêmes valeurs de densité de couvert. Bien que l'utilisation d'une résolution plus fine puisse permettre de mieux représenter la variabilité des écosystèmes (Pretzsch 2009), nous posons l'hypothèse qu'il existe une limite inhérente au lidar au-delà de laquelle la variabilité observée est un artéfact qui peut conduire à des conclusions erronées sur l'évolution de la densité. Bien que ces effets soient soupçonnés, il demeure qu'ils ont été peu explorés (White et al. 2013a). Nous présentons une méthode de sélection de paramètres post-survols pour maximiser la similarité des mesures de densité de couvert entre les acquisitions lidar permettant ainsi de mieux caractériser la dynamique des changements spatio-temporels.

En résumé, les objectifs de cette thèse sont :

— **Chapitre 1** : Prédire l'âge de placettes-échantillons à partir d'information de structure et de qualité de station dérivée du lidar.

— **Chapitre 2** : Décrire la relation entre la distribution verticale des retours lidar, l'espèce dominante, la densité de couvert et l'âge.

— **Chapitre 3** : Proposer une méthode pour sélectionner les paramètres post-survols qui permettent de mesurer la densité de couvert de manière répétable.

Chapitre 1

Estimating Forest Stand Age from LiDAR-Derived Predictors and Nearest Neighbor Imputation [1]

1.1 Résumé

Les forêts boréales aménagées au Québec (Canada) requièrent le maintien d'une diversité d'âge et conséquemment, l'âge des peuplements forestiers est une variable importante pour les plans d'aménagement forestiers. L'âge de la forêt est un déterminant de la hauteur des peuplements, tout comme d'autres facteurs reliés à la station tels le climat, l'eau et la lumière disponibles qui modifient la hauteur selon les conditions locales. Le lien entre l'âge des peuplements forestiers et leur hauteur est utilisé pour évaluer l'indice de qualité de station, communément utilisé pour mesurer la productivité et servir de critère lors de la prise de décision dans la gestion de la forêt. La détermination *in situ* de l'âge des peuplements est une méthode extrêmement laborieuse et coûteuse, et d'autres technologies sont nécessaires pour permettre d'améliorer la capacité de prédiction, comme le lidar (*Light Detection And Ranging*) qui permet d'observer la structure de la forêt et les caractéristiques de la station. Dans cet article, nous examinons l'intérêt du lidar aéroporté pour estimer l'âge des peuplements de 158 points d'échantillonnage situés à l'intérieur d'une forêt boréale régénérée naturellement au Québec (Canada). Nous avons créé une série d'indicateurs dérivés du lidar pour caractériser la structure de la forêt (hauteur, taux de pénétration des premiers retours, paramètres de la distribution de Weibull) et la station (altitude, pente, orientation, radiation solaire, indice d'humidité, aire de bassin versant et longueur de pente arrière). L'approche des k-plus proches voisins a permis l'imputation de l'âge des placettes sur notre aire d'étude en plus de nous informer sur le pouvoir prédictif des

1. Racine EB, Coops NC, St-Onge B, Bégin J (2014) Estimating Forest Stand Age from LiDAR-Derived Predictors and Nearest Neighbor Imputation. Forest Science 60 :128–136. https://doi.org/http://dx.doi.org/10.5849/forsci.12-088

indicateurs lidar. Les résultats montrent que l'âge peut être bien estimé ($R^2 = 0.83$, EQM = 19%) avec une erreur de prédiction inférieure à 10 ans. Les estimés utilisant uniquement les variables de structure forestière étaient moins bons ($R^2 = 0.74$, EQM = 22%). Les prédicteurs les plus importants étaient la hauteur du peuplement et les paramètres de la distribution de Weibull associés à la forme de la cime. Les caractéristiques de stations les plus importantes, qui avaient relativement moins de pouvoir prédictif, étaient l'altitude, la longueur de pente arrière et l'aire du bassin versant dont l'importance variait de basse à modérée.

1.2 Abstract

Within the managed boreal forest of Quebec (Canada), there is a need to ensure the maintenance of age diversity across the forest resource, and, as a result, forest age has become an important variable in forest management plans. Forest age is a major driver of stand height, with site factors such as climate, water and light availability, modifying height based on local conditions. The link between stand age and height is used to evaluate the site index, a commonly used measure of productivity, which is the basis of many forest management decisions. Stand age is extremely costly and laborious to measure in situ and as a result new technologies are required to provide added predictive power, such as Light Detection and Ranging (LiDAR) which can provide insights into forest structure and site characteristics.

In this paper, we examined the utility of airborne LiDAR data to estimate stand age across 158 sample plots within a naturally regenerated boreal forest in Quebec, Eastern Canada. A suite of forest structure (height, first return penetration rate and corresponding Weibull distribution parameters) and site attributes (elevation, slope, aspect, solar radiation, wetness index, catchment area and flow path length) was derived from the LiDAR data. The *k*-Nearest Neighbor approach allowed imputation of stand age across the forest area, as well as providing key information on the predictive power of LiDAR metrics for estimating age in this forest region. Results indicate that LiDAR-derived predictors can estimate age well ($R^2 = 0.83$, RMSE = 19%) with a predicted error of less than 10 years. Estimations using only forest structure variables were lower ($R^2 = 0.74$, RMSE = 22%). The most important forest structural predictors were stand height and Weibull crown shape parameters. Site predictors, in contrast, which had less predictive power, included elevation, flow path length and catchment area with low to moderate importance.

1.3 Introduction

Forest stand age is a key variable in understanding forest dynamics, growth and ecosystem functioning and, as a result, is an important attribute for sustainable forest management (Kneeshaw and Gauthier 2003). Forest age can be used as an indicator of habitat, as well as provide information on tree growth rates, decay or mortality. Stand age also drives forest

structure, with older stands tending to be more structurally heterogeneous than younger ones (Brokaw and Lent 1999). In addition to age, site elements such as water or nutrient availability, insolation, and temperature can influence the rate of stand development (Assmann 1970). The global effect of variables that determine the stand developmental rate is often referred to as the site index, which is generally expressed as the height of dominant trees within a stand at a given age (Vanclay 1994).

Since forest management activities tend to homogenize forest structure (Puettmann et al. 2009, pp. 48–52), it has been proposed that portions of the managed boreal forest could lack older stands and, thus, alter natural forest stand development processes (Kneeshaw and Gauthier 2003), resulting in ecosystems that are less adaptable to new conditions (Schütz 1997, pp. 35–45 ; Puettmann et al. 2009, pp. 48–52). Accordingly, maintenance of age diversity has become a key objective of regional forest management plans (MRNFQ 2005 ; Larson et al. 2008). Forest stand age, however, is extremely costly to measure in naturally regenerated forests. At a broad management scale, it can be assessed using aerial photographic interpretation or inventory-based coverage of management activities, such as establishment plans. To derive precise tree age information within a stand requires the measurement of a number of representative trees using tree cores, which are time-consuming to extract, process and analyze.

In many forest ecosystems age is directly linked to forest structure and, as a result, vertical forest structural information is often used as a proxy for age. Of the forest structure variables that are most commonly measured, tree height is often the one that is most strongly related to age. This is frequently the case in even-aged stands where the dominant height is extremely well correlated with stand age. However, it is also true that in mixed age stands the age-structure relationship is more ambiguous, especially in stands containing shade-tolerant species (Ung et al. 2001). Forest structure and height, therefore, can be a surrogate of age and can be used as an indicator of the overall site conditions affecting both individual trees and the stand as a whole (Ung et al. 2001).

Light Detection and Ranging (LiDAR), is a relatively new remote-sensing technology, which can provide insights into forest structure and site characteristics (Kane et al. 2010b). LiDAR has been used in a number of forestry applications, including habitat characterization (Vierling et al. 2008) and dendrometry (Treitz et al. 2012) ; however, most studies have focused principally on prediction of height-driven attributes. Limited studies have investigated the capacity of LiDAR to estimate forest age.

Previous research linking age and forest structure using LiDAR successfully demonstrated the strong relationships, not only between height and age, but also with other structure variables. Weber and Boss (2009) used LiDAR-derived vegetation height and site predictors to distinguish three stages of stand evolution. While they identified height as the most important

factor discriminating among stages, additional site predictors such as distance to streams and slope improved estimation. Falkowski et al. (2009) used a random forest classifier to identify seven stages of forest succession in a mixed forest using LiDAR-derived vegetation structure. Using variable importance ranking, they identified stem density as the most important variable, followed by vertical information such as mean or maximum tree height and the proportion of returns in different forest layers. Maltamo et al. (2009) used k-Nearest Neighbors (k-NN) variant, k-Most Similar Neighbors (k-MSN), to predict plot-level stand age using a combination of spectral and LiDAR structural information. Kane et al. (2010b) subsequently used LiDAR in western coastal forest to document increasing vertical structure complexity along development stages. The intermediate development stands exhibited diverse degrees of complexity, revealing non-linear development of stand structure (Lefsky et al. 2005; Kane et al. 2010a). Similarly, Straub and Koch (2011) used LiDAR-derived stand structural and multispectral information to estimate stand age in a European mixed forest. While all of these studies confirmed the link between LiDAR data and derived forest structure, and thus age, quantitative age assessments using LiDAR, and the detailed understanding on the influence of site properties on the development of forest structure, remain to be fully explored.

In this paper, we examine the utility of airborne LiDAR data in estimating plot age across a managed boreal forest in Quebec. To do so we utilize the k-NN approach, which allows imputation of stand age across forest tenures, and provides key information on which LiDAR metrics have the greatest discriminatory power for estimating age in this forest type. This could improve temporal and spatial resolution of age estimates.

1.4 Methods

1.4.1 Study area

The study was conducted in the Montmorency Research Forest, which is located in central Quebec, Canada (47.3°N, 71.1°W), about 70 km north of Quebec City (Figure 1.1). The forest covers 66 km^2 and is situated within boreal forest (Leblanc and Bélanger 2000) that is dominated by balsam fir (*Abies balsamea* (L.) Miller). White or paper birch (*Betula papyrifera* Marshall) and several spruce species (*Picea mariana* (Miller) BSP, *P. glauca* (Moench) Voss) are also common. The region is characterized by high annual precipitation (mean = 1400 mm) and a mean annual temperature of 0°C. Soils are mostly deep, sandy Laurentian tills frequently exhibiting seepage at mid-slope positions (Bélanger et al. 1995).

From 1932-1944, the forest was heavily harvested (Bélanger et al. 1995) and allowed to regrow from advance regeneration. In 1992, an ecosystem-based management approach was introduced and 13% of the forest area was designated as protected. Since the 2000's, the forest has been actively managed for multi-use with both timber harvesting and recreational uses.

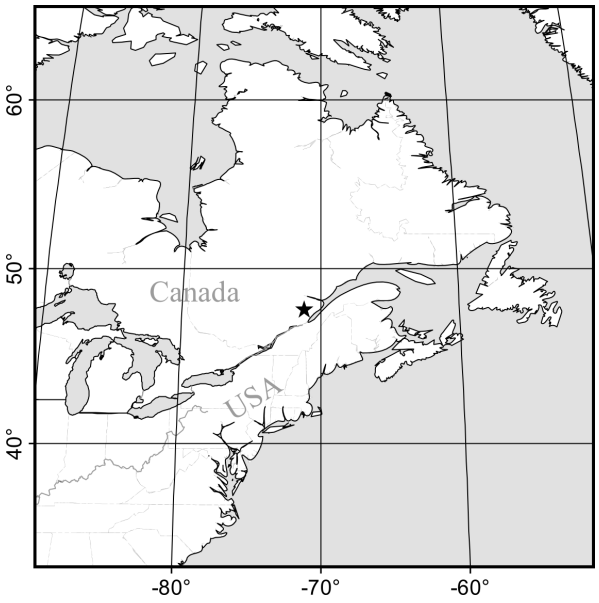

FIGURE 1.1 – Location map of the Montmorency Research Forest (star). Robinson projection (central meridian 70°W), boundaries adapted from openstreetmap.org

While fire is the major non-anthropogenic disturbance that occurs across most of the boreal forest, insect infestations and windthrow are the most common forms of perturbation in the wet climate of the Montmorency research area (Leblanc and Bélanger 2000). The latest major infestation by the spruce budworm (*Choristoneura fumiferana* (Clemens)) occurred between 1981 and 1986 (Leblanc and Bélanger 2000). Other natural disturbances include tree decay (Bélanger et al. 1995) and more localized endemic insect infestations. When combined, these disturbance events have resulted in a highly patchy forest structure with a maximum dominant stand height of about 25 m.

1.4.2 Field data

A network of permanent sample plots have been established in the Montmorency Research Forest that are based on a stratified random design, weighted by the area of the major forest types. In total, 158 circular plots were used in this study. Each plot had a radius of 11.28 m (400 m^2) and was measured between 2005 and 2010 as part of the standard re-measurement cycle of the plots. The center of each plot was marked using aluminum pole and located using a field computer displaying position from an external dual frequency antenna GPS (Trimble Tornado) and identified on the LiDAR canopy height model (described below). All trees within the plot with a dbh over 9 cm were counted and the species were recorded. A suite of basic tree-level inventory data such as dbh (diameter at breast height, cm), height (dm) and health status was also recorded. Within each plot, tree age was assessed following procedures established by the Quebec Ministry of Natural Resources, which were as follows. First, candidate trees within each plot were selected by two methods : (i) random and (ii)

random-within-representative trees (Perron and Morin 2002). Second, a single core was taken from each tree using a Pressler probe (increment corer) at 1 m height. Third, cores were dried and rings were counted to provide accurate estimates of tree age (following procedures in Perron and Morin (2002)). Fourth, mean plot age was then calculated as the average of all cored tree ages within the plot. Last, to provide a consistent comparison for the analysis, the plot age was prorated from the year of measurement to 2011 to produce a standard age database.

1.4.3 LiDAR Data

Airborne LiDAR data were acquired in August 2011 using an Optech ALTM 3100 sensor at a pulse repetition rate of 100 kHz, laser wavelength of 1046 nm, divergence of 0.25 mrad and scan rate between 46 Hz and 56 Hz. The sensor was flown at 1000 m above the terrain at a median first return density of about five returns per square meter with a 50% overlap to improve point density stocking and a maximal scan angle of 17°. The sensor could record up to 4 measurements per pulse. Separation of ground versus non-ground returns was carried out by the provider using the TerraScan application from TerraSolid (Finland). Ground returns were interpolated to create a digital terrain model (DTM) at 5 m spatial resolution and first returns were interpolated to produce a digital surface model (DSM) at 5 m resolution for the sole purpose of computing local insolation. LiDAR point elevations were then normalized by subtracting the underlying ground level TIN elevation to produce estimates of vegetation height. In this study, a gridded resolution of 5 m was judged sufficient to capture the local terrain variations despite that the acquired data density would allow a finer resolution to be derived for additional focused studies.

1.4.4 Site Attributes

Two sets of plot level LiDAR attributes were calculated, i.e., site and structure. A number of terrain attributes were derived from the LiDAR DTM. These included primary attributes such as elevation, slope and aspect, and a number of derived terrain attributes, which characterized water and light availability. These derived attributes included the catchment area, flow path length, and direct potential incoming solar radiation (Böhner and Antonić 2009). Catchment area was defined as the area draining through a cell, divided by the contour width. The flow path designated the trajectory of a water particle falling within the catchment area (Quinn et al. 1991) and direct insolation was average incoming radiation that was intercepted by the canopy surface model each day from 10h00 to 14h00 throughout the growing season (June – August). The topographic wetness index was computed as the natural logarithm of the ratio of the specific catchment area divided by the tangent of the slope, to reflect the relative availability of water (Beven and Kirkby 1979).

To validate the correlation between field data and recent LiDAR data, plots exhibiting strong

TABLE 1.1 – Selected predictive features derived from LiDAR with software which generated them

Feature	Type	Software	Min	Max	Mean
Elevation (m)	Site	LAStools	518	964	750
Slope (%)	Site	gdaldem	1	34	10
Aspect (°)	Site	gdaldem	3	357	195
Direct insolation (kWh/m^2)	Site	SAGA GIS	289	417	366
Wetness Index	Site	SAGA GIS	6	13	8
ln(catchment area)	Site	SAGA GIS	4	11	7
Flow Path Length	Site	SAGA GIS	1	6	5
95% LiDAR return height (m)	Structure	R	1	24	12
First return penetration rate	Structure	R	0	1	0.7
Weibull a	Structure	R	4	22	10
Weibull b	Structure	R	0	8	4
Weibull c	Structure	R	0.0	0.8	0.3

discrepancies between field height and LiDAR height were reviewed using aerial photography or field assessment and removed from the analysis when evidence of an unrecorded recent disturbance such as windthrow, was evident.

1.4.5 Structure Attributes

There are a number of approaches for deriving structural attributes from a normalized LiDAR point cloud. These include (i) the use of plot-level summary statistics, (ii) percentiles (Næsset 2004), and (iii) a curve-fitting method that is applied to the plot-wise vertical profile of binned return counts (Coops et al. 2007). In this study, all three approaches were used, from which the mean, standard deviation, range and penetration rate, the 95% quantile, and a three-parameter Weibull distribution function (Equation (1.1)) were computed. We created the vertical curves by plotting the number of returns above 2 m against height to fit a three-parameter Weibull density distribution by least-squares minimization (Coops et al. 2007; Thomas et al. 2008). With respect to the parameters of the Weibull function, a provides information on the vertical location of the curve and b controls the breadth of the curve, while c scales the curve without affecting its shape. To reduce data redundancy a priori, Pearson product-moment correlations (r) were calculated between all variables and those with an r>0.7 were removed with the exception of the a parameter which exhibited slightly higher correlation with 95% quantile height. The variables used in the analysis are shown in Table 1.1.

$$f(x;a,b,c) = c \cdot \left(\frac{x}{a}\right)^{b-1} \cdot exp\left(-\left(\frac{x}{a}\right)^{b}\right) \tag{1.1}$$

1.4.6 Data analysis

The complex interactions between site conditions and forest structure can be difficult to model using standard regression-based approaches (Puettmann et al. 2009, pp. 56–59; McRoberts 2012). The k-NN method provides an alternative to regression for predicting forest attributes and, consequently, its use is becoming more commonplace around the world (McRoberts 2012). To estimate a variable of a plot, the k-NN method selects the closest k neighbors from a set of training plots. While spatial neighbors can be considered, k-NN generalizes the neighbor concept to a multidimensional space of variables.

Nearest-neighbor methods have several advantages over fitted methods in that for small k, they can retain the distribution shape and variance structure of the original data set (Kim and Tomppo 2006; LeMay et al. 2008; McRoberts 2009), maintain predictions within the bounds of biological reality (Moeur and Stage 1995), can easily be used to create maps (McRoberts 2011), and when compared to other machine-learning methods, generally perform well in real data problems (Hastie et al. 2009, p. 459). However, k-NN is considered as a *black box* prediction method and is limited in providing an underlying understanding of the predictor relationships (Hastie et al. 2009, p. 459). Thus, it exhibits limited inference capacity (McRoberts 2011). Crookston and Finley (2008) introduced a distance metric that is calculated using random forests (Breiman 2001) and which ranks predictor importance. This predictor importance can then be used to identify variables that have discriminatory power (Cutler et al. 2007), thereby providing inference capacity. A discussion regarding the critical differences in random forest distance computation relative to other k-NN metrics can be found in (Hudak et al. 2008).

We developed two approaches to predict age from the LiDAR observations. First, we conducted an analysis of plot age from the available LiDAR structure and site predictors using the k-NN method. However, given the inherent underlying positive relationship between age and height, and the acknowledged ability of LiDAR to measure stand height we developed a second approach, similar to that employed by Hember et al. (2012). This second approach explicitly accounts for the underlying relationship between the two variables using a fitted age-response function and removes this effect from the overall model by estimating residuals from the linear relationship, rather than age. We will refer to this second approach as the *detrended* method.

To produce detrended age, we utilized simple linear model (Equation (1.2)) to fit the observed field age and used the detrended age as a basis for prediction with the LiDAR data.

$$age = \beta_0 + \beta_1 H_d \tag{1.2}$$

where age is mean plot age, H_d is the 95% quantile LiDAR return, β_0 and β_1 are the pa-

rameters that were estimated by mean square error minimization. In addition to the linear model an inverted non-linear model (Chapman-Richards (Pienaar and Turnbull 1973 ; Bi et al. 2012)) was also fitted but did not achieve a satisfying adjustment common to other studies, discussed in detail by (Bi et al. 2012).

In our research, model performance was assessed using leave-one-out cross-validation comparing the models root mean squared error (RMSE) and a pseudo-R^2 for an expected $y = \hat{y}$ relation (Mayer and Butler 1993 ; Seber and Lee 2003), defined as $R^2 = 1 - \frac{SS_{\text{error}}}{SS_{\text{residual}}}$ and where $SS_{\text{error}} = \sum_i (y_i - \hat{y})^2$ and $SS_{\text{residuals}} = \sum_i (y_i - \bar{y})^2$. To estimate the variance of predictor importance, we repeatedly estimated predictor importance and prediction accuracy from the random forest distance metric until a stable value was achieved. We suggest that importance, combined with a variance estimate, can be used for inference, with evident limitations about the nature of the relationship. Importance only reflects the discriminatory ability of a predictor, which is not a concrete quantity to estimate, unlike the parameters of a regression (Archer and Kimes 2008 ; Grömping 2009).

We used the LibLAS open source library for re-projection of LiDAR returns from Universal Transverse Mercator zone 19 North to Modified Transverse Mercator zone 7. LAStools (Isenburg 2012) was used for LiDAR point extraction, gridding and ground correction. Statistical analysis was conducted in R (R Development Core 2012) using yaImpute (Crookston and Finley 2008) for k-NN method with the random forest distance metric (Liaw and Wiener 2002).

1.5 Results

A statistical summary of the Montmorency Research Forest field data is shown in Figure 1.2 and provides information on the number of cored trees per plot, which ranges from four to 14 individuals. On most plots between nine and 13 trees were cored. In total, 1640 trees were sampled with ages ranging from 8 to 179 years, with a mean plot age ranging from 11 to 94 years. The variability of tree age within each plot was relatively constant with 70% of the plots having a standard deviation for age less than 10 years, with a general increasing trend with age.

The fitted linear model of the age-height relationship is shown in Figure 1.3 and, as expected, shows considerable scatter, with an R^2 of 0.60 (Table 1.3). Many plots follow a linear relationship ($\beta_0 = 4.4$, $\beta_1 = 3.156$) between age and height, but we observe that the linear height model offers limited ability to predict plot age.

The predictions of plot age and detrended age, based on the LiDAR-derived terrain and structural features, are shown in Figure 1.4, with predictors summarized in Table 1.2. The capacity of the k-NN method to predict age, solely based on height, is shown in Figure 1.4(a)

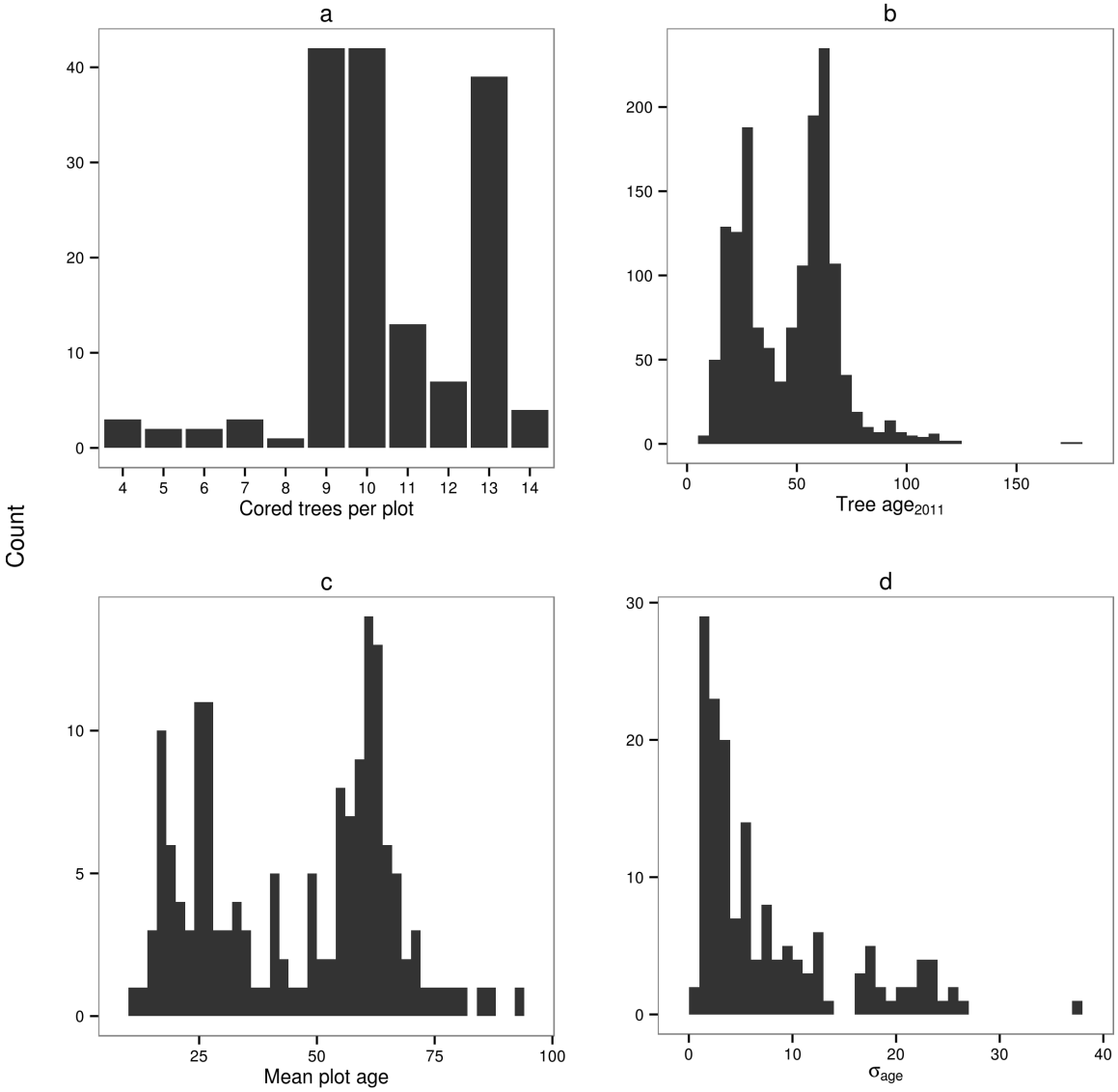

FIGURE 1.2 – Statistical distribution of (a) number of observations per plot, (b) age distribution of trees, (c) mean plot age, and (d) standard deviation of plot age.

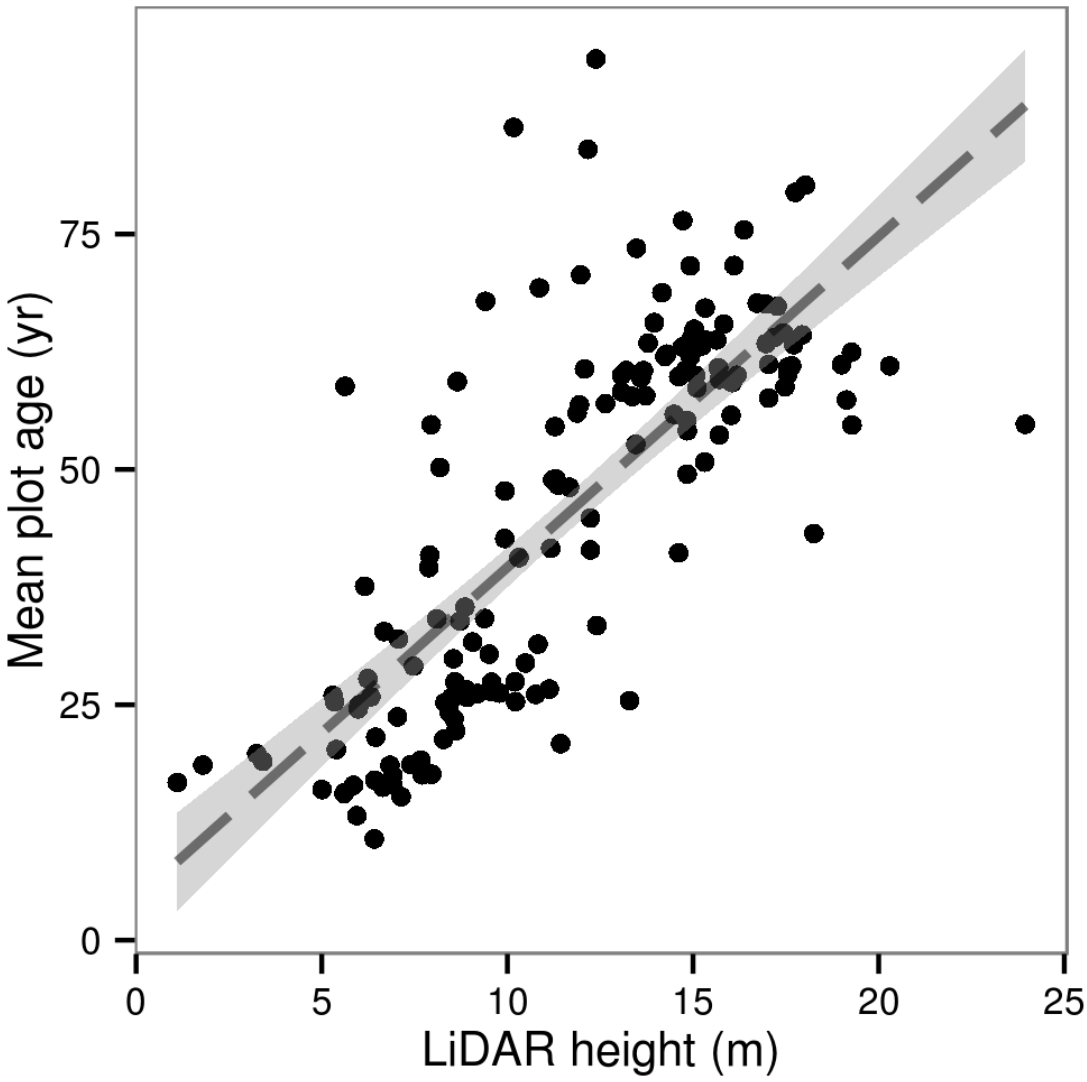

FIGURE 1.3 – Inverted linear growth model (Equation 2), where mean plot age is fitted to the 95% LiDAR return height. Shaded envelope represents standard error.

Table 1.2 – Model specifications

Model	Target	Predictors
Linear	Age	Plot Height
knn_age_h	Age	Plot Height
knn_age_all	Age	All
knn_age_struct	Age	Structure
knn_res_all	Linear model residuals	All
knn_res_site	Linear model residuals	Site only

Table 1.3 – Model performance

Model	R^2 (residuals)*	RMSE (yr)	RMSE (%)
knn_res_all	0.84 (0.60)	8.0	18
knn_age_all	0.83	8.8	19
knn_age_struct	0.74	10.1	22
knn_res_site	0.69 (0.23)	11.0	33
Linear	0.60	12.5	26
knn_age_h	0.48	14.1	31

* R^2 residuals are calculated from linear growth model (Linear)

and is generally poor, with a R^2 of 0.48. When the suite of LiDAR structure and site predictors is added to k-NN, the results are considerably improved, with an $R^2 = 0.83$ (Figure 4b). A model based solely on the structural information offers good performance, with an $R^2 = 0.74$ (Figure 4c).

The detrended model based on a linear growth presents similar predictions than LiDAR-derived site and structural attributes having an $R^2 = 0.84$. The explained variance decreases to $R^2 = 0.69$ when we consider only the LiDAR site predictors. An analysis of the model residuals (not shown) indicated homogeneity of variance across all models. Table 1.3 presents the detailed model performance.

To perform the imputations, importance of each predictor was weighted using the random forest algorithm. Figure 1.5 indicates the importance of each LiDAR site and structural predictor for both the k-NN age model, which was based on all variables (Figure 1.5a), and the detrended age model (Figure 1.5b). The empirical importance distribution provides information on variation in the results from 5000 runs of the random forest. Variable importance expresses the mean square error (MSE) reduction relative to the mean of the ensemble of predictors. For each tree fitted, MSE on the out-of-bag data is noted, predictors are then randomly permuted within the tree and the effect on MSE is noted. Thus, on average an unimportant variable (e.g. random variable) permutation won't affect MSE, while permutation of an important variable will affect it. A variable exhibiting scaled negative importance

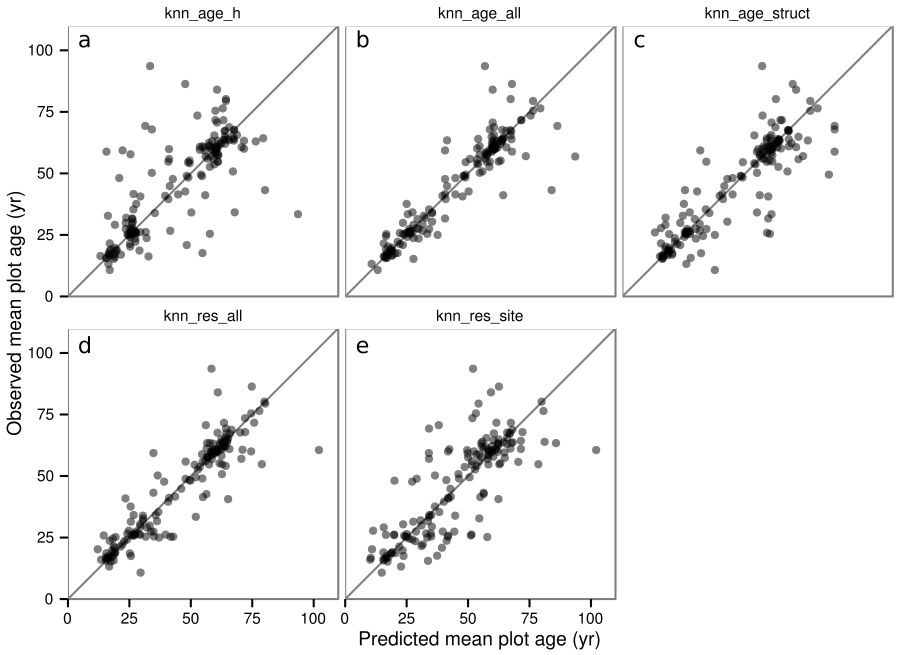

FIGURE 1.4 – Observed vs expected plot age for each model ; points are transparent to show overlay. (a) knn_age_h represents the ability of k-NN to predict age strictly using height ; (b) knn_age_all uses all of the predictors to predict age ; (c) knn_age_struct uses structure only to predict mean plot age ; (d) knn_res_all uses all of the predictors to predict de-trended age, however, the fitted age was added to facilitate comparison ; (e) knn_res_site uses just the site variables to predict de-trended age, and we also added fitted age to facilitate comparison.

can be interpreted as generally exhibiting MSE variation below the mean of the predictors. We observe that vegetation structure is generally more important than site for discriminating age in all models.

As expected, the most important predictor in the age model was LiDAR-derived height (95% quantile). Weibull a and c parameters were also important in model prediction. Of the site predictors, elevation was identified as having the most important effect on imputation for both models. Once the linear height effect was accounted for in the detrended data, all of the LiDAR-derived structure predictors were still important, as were most of site variables such as elevation, flow path length and catchment area.

1.6 Discussion

Age has remained an important indicator in forest management, especially when it is evaluated on small units such as plots. Combining LiDAR-derived site and structural information within k-NN provided an approach for both improving the prediction of plot age and providing insights into factors that influenced tree growth.

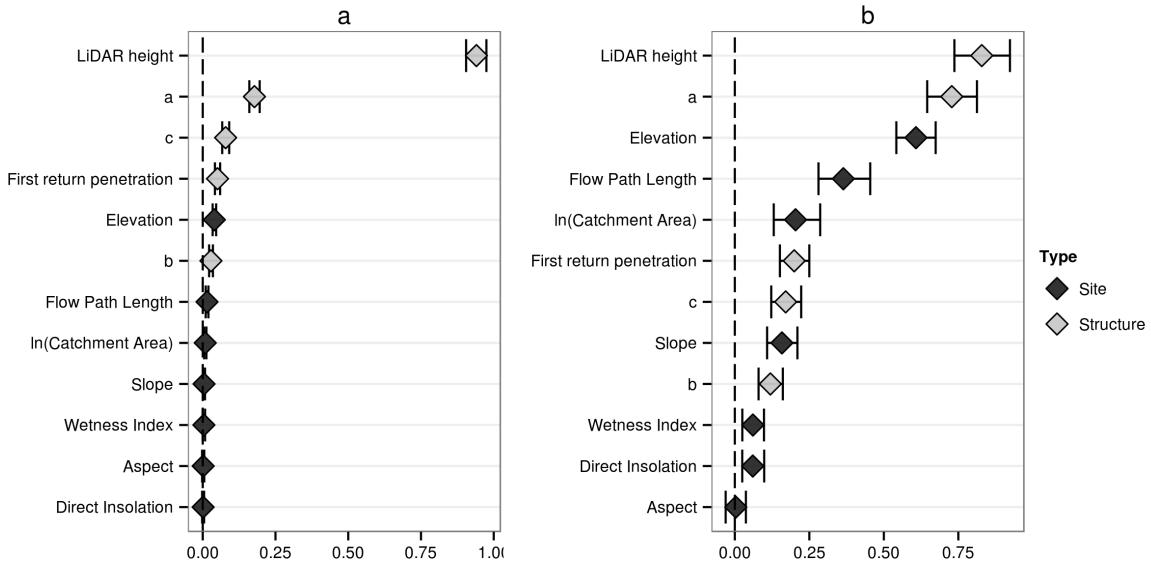

FIGURE 1.5 – Predictor mean importance for (a) complete, and (b) de-trended models. Variables are sorted by their degree of importance. Marks indicate mean (diamond) and 95 % interval (black tick) of the empirical importance distribution. Color indicates if the predictor is structural (grey) or site (black). The dashed lines indicate the average scaled importance.

1.6.1 Structure predictors

Forest structure has been shown to be related to growth and age, which is particularly true within the boreal forest biome (Pothier and Savard 1998 ; Ung et al. 2001). The importance of structure was also apparent in this study, with results indicating that all structural variables that had been derived from the LiDAR data were important in predicting stand age. When all LiDAR structural predictors were included in the k-NN method, height, which is a key vertical structure indicator, was the predictor with the most importance. This was not surprising given it is well established that LiDAR returns can be used to predict stand height (Lim et al. 2003) and that height is strongly linked to age (Oliver and Larson 1996).

To minimize the inherent link between height and age, we applied a linear model explicitly accounting for the age-height relationship. This allowed expression of the discriminatory abilities of other vertical structure predictors, especially in the form of the Weibull distribution, which had previously been related to crown shape (Coops et al. 2007). For both models, all three Weibull parameters were important, with the a parameter being the most important. As discussed by Coops et al. (2007), this is likely due to the a parameter providing information on the vertical position of the crown, which is strongly related to height. The least important parameter was b, which generally describes crown depth. We also observed that first return penetration rate had moderate importance in discriminating ages. This predictor has been shown to be a good descriptor of structure in both western coastal (Kane et al. 2011) and

Bavarian temperate forests (Bässler et al. 2010).

Our selection of structural predictors did not present explicitly the horizontal structure of the forest. However, horizontal structure could potentially improve predictive power even if we believe that such a small unit (400 m^2) horizontal differentiation is hard to assess.

1.6.2 Site predictors

While LiDAR predictors of forest structure were important for the predictive models, our results indicated that the site indicators made a small contribution to the complete model, yet was amplified in the de-trended model. The R^2 difference (0.09) between the structure-only and the complete model revealed that inclusion of the site predictors improved prediction by accounting for a part of the non-linear structural development of the forest. The inclusion of the linear model slightly improved predictions by potentially forcing linear extrapolation, which appears as a reasonable hypothesis for the range of values of our study. This not only reduced the relative importance of height and Weibull a (both closely related), but also allowed the expression of more site information and slightly improve performance.

Whilst elevation in Montmorency Research Forest present a limited range of variability (460 m) compared to other mountainous regions, elevation still represent an important degree-days and soil depth gradient which are two important factors known to influence growth. Accordingly, elevation was the most important site predictor in both models. This is likely reflecting the vegetation variation described by (Bélanger et al. 1995) for our study area. Aspect had no importance, while slope exhibited importance in the detrended model.

Hydrology importance ranking increased from the complete model to the de-trended model. In the case of the age model, hydrologically related predictors exhibited low importance. In the case of the age-detrended model, catchment area and flow path length exhibited higher importance. The importance of hydrology predictors better reflect the expectations for Montmorency Research Forest that was shown to be influenced substantially by underlying water relations (Bélanger et al. 1995).

The effect of insolation on the predictions was also low, which is likely indicative of the low degree of variation in radiation across the entire research forest rather than insolation as a limiting factor in the fir-dominated plots. (Bässler et al. 2010) also observed that radiation did not provide good classification accuracy of habitats compared to penetration rate, mean vegetation height and altitude. Low importance of direct insolation could also be explained by the grid resolution (5 m) of the computation that might have been too coarse and a sub-crown resolution (e.g. 0.2 m) might provide better information.

1.6.3 Nearest-neighbor imputation

Our results indicated that k-NN methods can be successfully combined with the random forest distance metric to better understand the importance of both site and structural predictors on forest plot age. While the random forest variable importance provided some indications of the predictors driving forest structure, it did not provide detailed insights into underlying, often complex, mechanisms and could not provide estimates of the effect. For example, interactions within forest stands such as shade-tolerant growth dynamics, and the role of occasional disturbances such as infestations will influence stand structure evolution (Ung et al. 2001), yet they were not modeled explicitly by this approach. The use of classical inference methods like regression would not have allowed the observation of the importance of a predictor, without stating on the functional nature of its relationship with age.

Combining k-NN and random forest, and plot-level imputation in part may explain our improved predictions compared to other studies predicting age using LiDAR data (Maltamo et al. 2009 ; Straub and Koch 2011). It is also possible that the addition of multispectral data for these two studies was not as important as the addition of site variables in our case, however this was not tested due to the lack of available multispectral data. The k-NN and random forest approach also yielded lower RMSE than k-MSN for (Hudak et al. 2008).

Furthermore, the advantages of using k-NN imputation were the limits it imposed on the range of observed credible values (Archer and Kimes 2008). With the large number of plots used in this study (158), the results had reduced RMSE variability. However, it was likely that k-NN predictions with fewer plots would still yield, on average, the same RMSE while variability would be greater. Moreover, k-NN imputation can exhibit a lack of fit when interpolation distances are too long (McRoberts 2012). This was particularly true for plots that were less than 20-years-old and greater than 65-years-old, since these plots had limited numbers of neighbors, potentially requiring extrapolation. In addition, it can be difficult to assess the productivity of younger stands (Ung et al. 2001). Furthermore, understory seedlings and saplings are hard to distinguish from shrubs, downed woody debris or other components using LiDAR (Falkowski et al. 2009 ; Richardson and Moskal 2011).

1.6.4 Implications for forest management

The results of this research have provided additional insights into the relationships between site characteristics and productivity, given that most existing studies have been conducted without the added benefit of LiDAR measurements. The capacity of LiDAR data to directly measure forest structure was a significant benefit (Zimble et al. 2003 ; Falkowski et al. 2005), when compared to correlative optical approaches such as classification of satellite imagery or aerial photographic interpretation, and permitted a range of predictor variables to be assessed.

Airborne LiDAR and the k-NN method could be used to improve regional forest maps by

increasing both the spatial resolution and timeliness of data acquisition, thereby improving forest managers' knowledge of current forest age distributions. Additional modeling will be required, however, to ensure that the models being developed are robust to interpolation across the entire land base. More specifically, while usual maximum age of balsam fir in the Montmorency Research Forest is 100 years (Bélanger et al. 1995), plot ages were higher than this in some cases, due to the presence of other older species such as paper birch and black spruce. Predicted plot age did not necessarily represent the age of the dominant species. Yet, the oldest plot in the analysis was still less than 100-years-old. Given the long fire return period, older forests exist in the region and, as a result, extremes in height variability and gappiness in these older stands may not be captured very well by the approach, especially given the constraints of the k-NN method. Nevertheless, the flexible framework provided by k-NN led us to believe that prediction of other plot statistics such as median or dominant age would be possible.

The integration of LiDAR into forest inventory assessments is particularly timely since LiDAR has made the transition from an experimental development phase to serving as a production-ready tool for many forest applications around the globe. In the Province of Quebec, for example, some 315 900 ha were overflown in 2011 alone (Maurice Massé, Quebec Ministry of Natural Resources, personal communication). Despite its higher acquisition cost compared to that of traditional aerial photographs, LiDAR can provide many more metrics (e.g. Treitz et al. (2012)).

Since variance reduction is a problem in extensively managed ecosystems (Puettmann et al. 2009, pp. 48–52), combining k-NN and LiDAR can aid in representing the landscape more accurately and improve forest management by refining the decision scale and increasing our understanding of forest variability.

1.7 Conclusion

Our study showed that LiDAR can effectively be used to produce quantitative estimates of plot mean age by combining vegetation structure and site indicators. We identified important contributions of structure to age estimation and lesser contributions by site characteristics such as elevation, catchment area and flow path length. The k-NN method proved to be effective at estimating plot age, while permitting the analysis of variable importance through the use of the random forest distance metric. The direct application of our results will provide forest managers with a within-stand age estimate that considers the variability of the forest and which will refine the spatial dimension of the stands.

Chapitre 2

Tree species, crown cover, and age as determinants of the vertical distribution of airborne LiDAR returns [1]

2.1 Résumé

L'information détaillée fournie par le lidar (*Light Detection And Ranging*) sur la structure verticale des peuplements permet d'étudier en détail les écosystèmes. Toutefois, la structure verticale étant complexe, elle est souvent résumée par des caractéristiques scalaires et des techniques de réduction de la dimension des données qui limitent l'interprétation des résultats. Au lieu de cela, nous avons quantifié l'influence de trois variables : l'espèces, la densité de couvert et l'âge, sur la distribution verticale des retours lidar aéroportés des peuplements forestiers. Nous avons étudié 5 428 peuplements réguliers équiennes au Québec (Canada) dont les espèces dominantes étaient : le sapin baumier (*Abies balsamea* (L.) Mill.), le bouleau à papier (*Betula papyrifera* Marsh), l'épinette noire (*Picea mariana* (Mill.) BSP), l'épinette blanche (*Picea glauca* Moench) et le peuplier faux-tremble (*Populus tremuloides* Michx.). Nous avons modélisé la distribution verticale des données obtenues par lidar pour chacune des trois caractéristiques en utilisant un modèle linéaire généralisé fonctionnel (fGLM) et un nouveau test de signifiance non paramétrique graphique. Les résultats indiquent que les retours LiDAR des peuplements de peuplier faux-tremble avaient la distribution verticale la plus uniforme ; les peuplements de sapin baumier et de bouleau à papier sont semblables, avec une distribution centrée autour de 50% de la hauteur de peuplement ; les distributions dans les peuplements dominés par les épinettes blanche et noire avaient une distribution décentrée

1. Racine EB, Coops NC, Bégin J, Myllymäki M (2021) Tree species, crown cover, and age as determinants of the vertical distribution of airborne LiDAR returns. Trees. https://doi.org/10.1007/s00468-021-02155-2

vers le tiers inférieur de la hauteur du peuplement ($p<0.001$).
Une augmentation de la densité de couvert concentrait la distribution autour de 50% de la hauteur du peuplement. L'augmentation de l'âge déplaçait la distribution dans la partie supérieure du peuplement jusqu'à 50–70 ans, puis se stabilisait et redescendait à 90–120 ans. Le modèle complet présentait un R^2 de 0.47 à environ 10% de la hauteur du peuplement. Les résultats suggèrent que la distribution verticale des retours lidar dépend des caractéristiques étudiées. Cette compréhension peut servir à classifier les espèces et à étudier l'évolution de la structure de la forêt en fonction des conditions environnementales changeantes.

2.2 Abstract

Light detection and ranging (LiDAR) provides information on the vertical structure of forest stands enabling detailed and extensive ecosystem study. The vertical structure is often summarized by scalar features and data-reduction techniques that limit the interpretation of results. Instead, we quantified the influence of three variables, species, crown cover, and age, on the vertical distribution of airborne LiDAR returns from forest stands. We studied 5,428 regular, even-aged stands in Quebec (Canada) with five dominant species : balsam fir (*Abies balsamea* (L.) Mill.), paper birch (*Betula papyrifera* Marsh), black spruce (*Picea mariana* (Mill.) BSP), white spruce (*Picea glauca* Moench) and aspen (*Populus tremuloides* Michx.). We modeled the vertical distribution against the three variables using a functional general linear model and a novel nonparametric graphical test of significance. Results indicate that LiDAR returns from aspen stands had the most uniform vertical distribution. Balsam fir and white birch distributions were similar and centered at around 50% of the stand height, and black spruce and white spruce distributions were skewed to below 30% of stand height ($p<0.001$). Increased crown cover concentrated the distributions around 50% of stand height. Increasing age gradually shifted the distributions higher in the stand for stands younger than 70-years, before plateauing and slowly declining at 90–120 years. Results suggest that the vertical distributions of LiDAR returns depend on the three variables studied.

2.3 Introduction

The distribution of vegetation within canopies varies with tree allometry and competition strategies, leading to variations in canopy structure and ultimately, in environmental conditions (Purves et al. 2007 ; Thorpe et al. 2010 ; Pretzsch and Dieler 2012). Species-specific canopy structures create different microhabitats, light conditions, and microclimates, which in turn influence the rates at which stands sequester carbon. Species have different carbon allocation strategies that evolve during the growth season, relative to above and below-ground carbon allocation. Examples include growing fruits, deploying leaves, and growing roots for better access to nutrients and water (De Pury and Farquhar 1997 ; Lacointe 2000 ; Stark et al.

2012). These growth and allocation strategies result in distinct species-specific tree shapes.

Traditionally, the characterization of stand vertical distribution of aboveground biomass required either on-site estimation of biomass per vertical layer (often requiring destructive measurements), scaffolding, or tree climbing, all of which are time-consuming and limit surveys to small areas (MacArthur and Horn 1969 ; Aber 1979 ; Bassow and Bazzaz 1997 ; Tackenberg 2007).

2.3.1 Forest remote sensing

The increasing availability of data collected remotely from airborne, spaceborne and terrestrial sensors has improved our understanding of forest dynamics (Wulder et al. 2012 ; White et al. 2013a ; Beland et al. 2019). Among these sensors, light detection and ranging (LiDAR) has the ability to penetrate the canopy and provide information on the spatial location of reflective material. LiDAR is increasingly used to perform both extensive and highly detailed imaging of forest. It uses a laser, at a precisely known location and orientation, to sample a 3D scene. A discrete LiDAR pulse is reflected back to the sensor by the vegetation as it penetrates the canopy. The sensor then records the total travel time of the pulse and its energy to deduce the distance from the sensor to the location of reflection. LiDAR can be used from both the ground, and an aircraft to provide different perspectives on the forest. Terrestrial LiDAR provides highly detailed structural information about individual trees, but its extent is limited to a few hundreds of meters (Beland et al. 2019 ; Crespo-Peremarch et al. 2020). Airborne LiDAR, on the other hand, is typically less detailed than terrestrial LiDAR but can be used for extensive landscape measurements.

Airborne LiDAR has been used to characterize vertical canopy structure, crown shape, and aboveground biomass for entire ecosystems (Ellsworth and Reich 1993 ; Harding et al. 2001 ; Lefsky et al. 2002 ; Parker et al. 2004 ; Coops et al. 2007 ; Stark et al. 2012 ; Cao et al. 2014 ; Papa et al. 2020). It has also been used to identify tree species (Heinzel and Koch 2011, 2012 ; Vaughn et al. 2012 ; Hovi et al. 2016 ; Fassnacht et al. 2016 ; Budei et al. 2018 ; Axelsson et al. 2018 ; Fedrigo et al. 2018) and to study stand characteristics such as age, crown cover, and basal area (Korhonen et al. 2011 ; White et al. 2013a ; Racine et al. 2014 ; Karna et al. 2019). Airborne LiDAR is an important tool for biomass quantification, and offers the opportunity to explore large-scale phenomena that could only be observed on the field (Vierling et al. 2008 ; Seavy et al. 2009 ; Vierling et al. 2010 ; Karna et al. 2020).

One limitation of the airborne LiDAR data is its inability to distinguish differences in foliage condition or in species spectral variation. This is because it lacks the spectral information commonly used to classify species such as variations in red, green, and blue or near-infrared multispectral imagery. In response, the most common strategy for distinguishing species using LiDAR has been to differentiate individual tree shapes and texture (Holmgren and Persson

2004 ; Kim et al. 2011 ; Fassnacht et al. 2016), and add spectral information from multispectral imagery. More recently multispectral LiDAR has also been used to distinguish stand species (Budei et al. 2018 ; Budei and St-Onge 2018).

2.3.2 Individual tree-crown vs area-based methods

Most studies on species classification using aerial LiDAR have focused on species identification based on individual tree crowns. However, tree crown delineation requires a large number of LiDAR returns and highly accurate registration of ground observations (Ørka et al. 2009 ; Muss et al. 2011). Using a small observation area such as an individual tree crown causes a loss in the shape of the vertical distribution of LiDAR returns. This is due to a decrease in the number of LiDAR returns, causing the distribution to become a collection of random variates. Thus, although the accuracy of species identification would be improved by a very high point density in excess of 10 pt/m^2 (Fassnacht et al. 2016), it is difficult to apply and validate these approaches for use over large areas and with less-dense LiDAR datasets.

An alternative to individual tree-crown extraction approaches is the application of area-based approaches (see e.g. White et al. (2013a)). This approach generally uses a pixel or a stand on which LiDAR returns are aggregated and predictors are derived before being used in a model to predict forest attributes. Predictors are often derived from the vertical distribution of LiDAR returns : the number of LiDAR returns per height slice. The vertical distribution of LiDAR returns is often presented as quantiles, projections of quantiles (such as principal component analysis), or parametric functions (such as a Fourier, beta or Weibull functions), which are used to predict stand attributes (Magnussen et al. 1999 ; Maltamo et al. 2005 ; Mehtätalo 2006 ; Coops et al. 2007 ; Riggins et al. 2009 ; Falkowski et al. 2009 ; Racine et al. 2014 ; Palace et al. 2015). The area-based method can be effective with a point density as low as 1 pt/m^2, which reduces cost and require less processing compared to tree-crown approaches (White et al. 2013a).

Lowering the minimum LiDAR point density threshold for species classification would increase the number of potential surveys where this method could be applied, and at the same time reduce the cost of acquisition. The species information could then be used for extensive forest management, or landscape-scale studies. One way to achieve area-based species mapping is to increase our understanding of the interaction between LiDAR and stand-level vegetation. However, the vertical distribution of LiDAR returns is difficult to analyze without resorting to dimension reduction, a method that generally limits the interpretability of results.

We hypothesize that using functional general linear models (GLM) and a novel non-parametric graphical test of significance (Mrkvička et al. 2019) would allow us to link the forest attributes to the vertical distribution of returns from low-density LiDAR surveys. The test provides a framework to compare a function (i.e. the vertical distribution of LiDAR returns) against

categorical and continuous variables, as well as a visual understanding of the effects of the variables on the function. Versions of non-parametric graphical tests have been applied to economical data (Mrkvička et al. 2020), and non-parametric inference is commonly used in neuroimaging (Winkler et al., 2014). However, to our knowledge, our study is the first to use a functional GLM combined with a non-parametric graphical test of significance in the field of ecology or remote sensing.

2.3.3 Forest vertical structure determinants

The information contained in the vertical distribution of LiDAR returns is closely related to the distribution of the vegetation. Reduced crown cover [the proportion of area covered by vegetation ; Gonsamo et al. (2013)] typically increased the probability for the LiDAR returns to reach lower vegetation (Hilker et al. 2010), while age influences the vertical position of the crown within a stand (Coops et al. 2009 ; Racine et al. 2014). Using direct foliage measurements, Aber (1979) observed that the vertical concentration of the foliage evolved with stand age, and that the end point of forest succession seemed to reach an equilibrium where the foliage was relatively evenly distributed within the canopy. Martin-Ducup et al. (2016) noted that crown cover and stand maturity affected the shapes of the crown of sugar maples when measured using terrestrial LiDAR.

The shapes of different species influence the distribution of LiDAR returns, but the interpretations from most studies are limited and hard to generalize across ecosystems or LiDAR surveys (Fassnacht et al. 2016). Some studies explicitly compared the vertical distribution of LiDAR returns between species. For example, Ørka et al. (2009) found that the first and last returns were more dispersed in Birch (*Betula* spp.) stands than in Norway spruce (*Picea abies* (L.) Karst.). The vertical distribution of first returns were also skewed toward the top of the canopy, and increased stand height was shown to influence the overall return distribution (Ørka et al. 2009).

In this study, we verify that we can differentiate the distinct patterns for individual species in the vertical distribution of LiDAR returns from a low-density area-based survey. We hypothesize that the use of a functional GLM combined with a non-parametric graphical test of significance makes it possible to identify these inter-species differences in the vertical distribution patterns after stand crown cover and age effects are accounted for.

2.4 Method

2.4.1 Study area

The study was conducted in Matane Wildlife Reserve (Quebec, Canada, 48°41'N, 66°58'W) and covering 1,600 km^2 (Figure 2.1). The reserve is a mixed forest dominated by balsam fir

FIGURE 2.1 – Location of Matane Wildlife Reserve (left panel) and selected stands within the study area (right panel, dark patches).

(*Abies balsamea* (L.) Mill.), paper birch (*Betula papyrifera* Marsh), and black spruce (*Picea mariana* (Mill.) BSP). Other species in the reserve include white spruce (*Picea glauca* Moench), aspen (*Populus tremuloides* Michx.), Norway spruce (*Picea abies* (L.) Karst.), jack pine (*Pinus banksiana* Lamb.), and other non-commercial deciduous species. Most of the reserve is subject to active commercial logging. Logging activities in that area have been documented since 1962 ; 27% of the area has been harvested (mostly total harvesting) and half of that has been replanted. Two percent of the stands originated from natural perturbations (e.g. windthrow, insect epidemic, fire) and the remaining 71% was undocumented.

2.4.2 Data

Airborne imagery and LiDAR were acquired during the summer of 2007. All data were collected by the Quebec Ministry of Natural Resources as part of their decennial forest mapping program. The LiDAR survey used a nominal point density of 3 points/m^2 with an Optech ALTM 2050 sensor that recorded the first and last returns at 40kHz. The survey was flown at 1,200 m above ground, with a flight overlap of 30% and a maximal scan angle of 15° from nadir and a footprint diameter of 25 cm.

Airborne photography was conducted using a Leica ADS–40 pushbroom camera at a resolution of 0.2 m for panchromatic, and 0.5 m for near-infrared, green, and blue bands (NIR, G, B respectively centered on 860, 560, and 460 nm) ; the side overlap was 40% to ensure complete coverage of the area. This imagery was used to partition the territory into stands following provincial guidelines adapted from MRNQ (2007) by expert photo-interpreters. Using digital stereopsis (virtual 3D vision) from the forward and nadir-facing ADS–40 sensor images, the expert photo-interpreters identified tree species by integrating information on landscape positions, crown shapes, textures, and colors. Every photo was segmented into homogeneous stands using species, crown cover, height, and geomorphic criteria. Each stand was classified based on species composition, crown cover, age, height, and other ecological variables using

a combination of photography, ground-control points and historical data, which was used as a reference. Stand age was estimated using ground control plots where trees were cored. This information was then combined with available archives, height, and ecology to estimate age from aerial photography. Stand age was divided in six regular classes : 10 (0–20), 30 (21–40), 50 (41–60), 70 (61–80), 90 (81–100), and 120 (101, ∞), and irregular age classes (such as uneven-aged and multi-stratum stands). Crown cover was also estimated by visually comparing the proportion of open ground with the space occupied by the mature tree crowns. Crown covert was categorized in 9 classes : 10 (5–14), 20 (15–24), 30 (25–34), 40 (35–44), 50 (45–54), 60 (55–64), 70 (65–74), 80 (75–84), and 90 (85–100). Species were identified by their distinctive features in the composite images of near-infrared, green and blue (NIR+G+B) mapped onto red, green, and blue (R, G, B) channels, and their frequent associations in forest stands (Table 2.1). Finally, the interpretation of the aerial images relied on the ground-control points and the ecological knowledge of the photo-interpreters. We used this photo-interpreted forest map as our reference data for species, crown cover, and age.

TABLE 2.1 – Description of tree shapes, associated species, preferred conditions, and colors

Species	Silhouette	Description[1, 2]	Associated species[2]
Abies balsamea		Mesic sites. Narrow conic crown with a sharp and thin summit that is frequently pale due to accumulated cones that are more reflective than foliage. Brown, slightly pink tint. Browner and pinker than white spruce.	Trembling aspen, white birch, white spruce, black spruce, red spruce, and eastern hemlock

Betula papyrifera		Avoids sites with poor drainage. Flat half-sphere shape. Crown is highly mingled with neighbors and exhibits an irregular texture that makes it hard to identify individual crowns even at higher resolutions. Dark pink tint between yellow birch and maples.	Various species including other birches, pines, spruces, hemlocks, poplars, maples, balsam fir, northern red oak, and pin cherry
Picea mariana		Sites with poor drainage. Crown is thin and narrow, spirelike, with sharp summit and compact foliage. When located on well-drained upland sites, principal branches are shorter than other spruces. Lower branches droop and tips are upturned. Upper part of the crown is often very dense and oddly shaped with many cones. Brown, slightly pink when young. Paler than white spruce.	Tamarack in the southern part of the range. Jack pine, white spruce, balsam fir, white birch, trembling aspen in the northern part of the range

Picea glauca		Mid slope sites with good to moderate drainage. Broad conical crown is star-shaped, ragged, irregular, densely foliated, and spirelike in northern parts of its range. Principal branches are bushy, generally horizontal, and sometimes sloping downward in the lower part of the crown, with tips gradually upturned. Brown, slightly pink when young. Darker than black spruces.	Trembling aspen, white birch, black spruce, and balsam fir
Populus tremuloides		All sites except those with poor drainage. Short, rounded, light bulb-shaped crown. Usually taller than surroundings when mixed. Crown surface looks blurred and smooth because of its small leaves. Orange-tinted pink.	White spruce, black spruce, balsam fir, white birch, balsam poplar and jack pine

[1] Colors are based on (NIR+G+B mapped to R, G, B channels).

[2] Adapted from Farrar (1995) ; Leboeuf and Vaillancourt (2013a, 2013b)

Even-aged stands are less complex than irregular stands when analyzed from a vertical structure point of view. Therefore, we focused our analysis on even-aged stands where clearly dominant species represented at least 50% of the stand cover. Using a low threshold for species dominance increased the number of usable observations for the analysis. This improved

the ability of the analysis to detect effects, but also increased the noise from other co-dominant species.

2.4.3 LiDAR Data Processing

The steps required to prepare LiDAR data for processing are summarized in Figure 2.2. We excluded stands with average LiDAR sampling rates below 2 pt/m^2 or an area of less than 4 ha to ensure a sufficient number of LiDAR returns. From the remaining stands, we kept only those with a dominant species that was observed at least in 100 stands : aspen, balsam fir, black spruce, paper birch and white spruce. From the 22,365 stands on the original forest map, we reduced our dataset to 5,428 stands representing 35% of the study area (Figure 2.1). Stand area distributions were similar for all selected species (median of 9 ha, minimum of 4 ha, maximum of 137 ha).

We registered the LiDAR returns by scaling their height between 0 and 1 to allow comparisons across stands of different heights. We subtracted the ground elevation from the absolute point cloud elevation (Muss et al. 2011). For each stand, LiDAR returns were binned into a vertical distribution histogram of 39 height slices from their highest LiDAR return (Harding et al. 2001 ; Coops et al. 2007). We then divided each slice count by the total number of points in the stand, so the vertical distribution of each stand summed to one, regardless of their inconsistent shapes, areas, and LiDAR point densities.

2.4.4 Statistical Analysis

We used a novel method that builds on the functional data analysis field (Ramsay and Silverman 2005) to compare the complete vertical distribution of LiDAR returns. Most studies of species classification have focused on the accuracy of classifiers and the value of predictors for species identification (Fassnacht et al. 2016), often using dimension reduction to decrease and decorrelate the number of predictors. Some of these reduction methods include linear discriminant analysis and principal component analysis (Koenig and Höfle 2016 ; Räty et al. 2016 ; Axelsson et al. 2018). However, dimension reduction diminishes the ability to understand the effect of individual variables and interpret the results of the model.

To compare inter- and intraspecific variations in the distribution of LiDAR returns and the effect of three variables, we used a nonparametric graphical test of significance (Mrkvička et al. 2019 ; Myllymäki and Mrkvička 2020). We modeled the vertical distributions of LiDAR returns as a function of dominant species, crown cover, and age using the general linear model

$$d(h) = \beta_0(h) + X_{sp} \cdot \beta_{sp}(h) + X_{cc} \cdot \beta_{cc}(h) + X_{age} \cdot \beta_{age}(h) + \varepsilon(h) \tag{2.1}$$

where, for every scaled height h, $d(h)$ is the $N \times 1$ vector of observed LiDAR distributions at

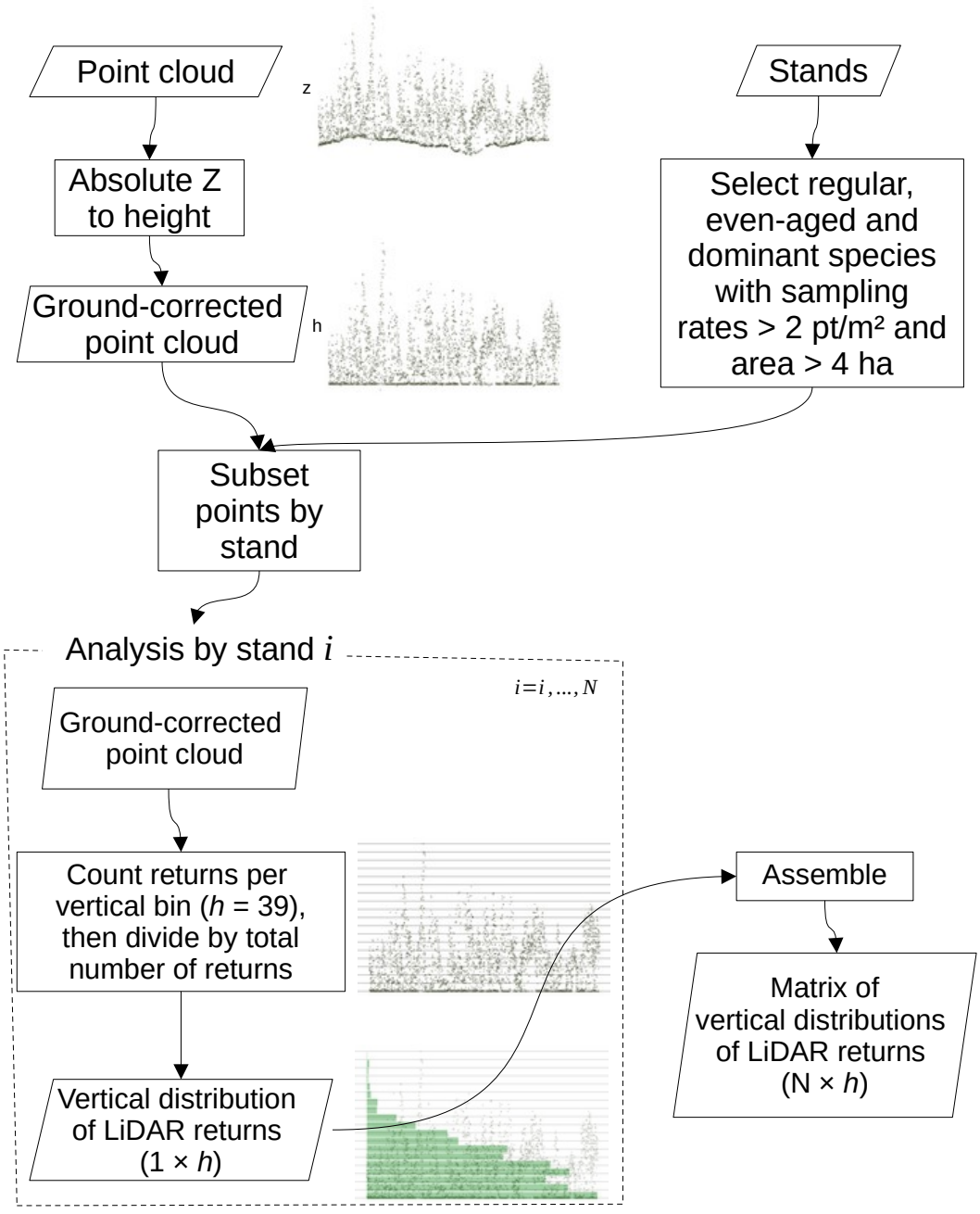

FIGURE 2.2 – Step-by-step preparation of the LiDAR data

scaled height h, and $\beta_{sp}(h)$, $\beta_{cc}(h)$, and $\beta_{age}(h)$ are the parameter vectors related to species in X_{sp}, crown cover in X_{cc}, and age in X_{age} ; $\varepsilon(h)$ is the vector of random errors with mean zero and finite variance $\sigma^2(h)$. The crown cover was considered a continuous variable, while species and age were considered categorical variables (given that the last age class was open). This model that incorporates all three variables is referred to as the full model.

We studied the effect of each variable after accounting for the other variables (also called the nuisance factors by Freedman and Lane -Freedman and Lane (1983)) using the methodology illustrated in Figure 2.3. We tested the effect of each three variables using the following null hypothesis : $\beta_{sp,m}(h) = 0$ for all m and h, $\beta_{cc}(h) = 0$ for all h, and $\beta_{age,l}(h) = 0$ for all l and h, where m and l refer to the elements of the parameter vectors $\beta_{sp}(h)$ and $\beta_{age}(h)$ for each species and age groups, respectively. The β coefficients of the discrete factors were constrained to sum to zero. The corresponding three null models were obtained by removing the studied variable from the full model (Equation (2.1)) :

$$d(h) = \beta_0(h) + X_{cc} \cdot \beta_{cc}(h) + X_{age} \cdot \beta_{age}(h) + \varepsilon(h) \tag{2.2}$$

$$d(h) = \beta_0(h) + X_{sp} \cdot \beta_{sp}(h) + X_{age} \cdot \beta_{age}(h) + \varepsilon(h) \tag{2.3}$$

$$d(h) = \beta_0(h) + X_{sp} \cdot \beta_{sp}(h) + X_{cc} \cdot \beta_{cc}(h) + \varepsilon(h) \tag{2.4}$$

We used the coefficients of the variable of interest (the left-out β in Equations (2.2)–(2.4)) for the statistical test as suggested by Mrkvička et al. (2019). For the continuous crown cover variable, the test statistic we used was the vector $\beta_{cc}(h)$ for all h ; and for age, the test was based on the values of the effect $\beta_{age,l}(h)$ of all the age groups l for all h. To examine species differences, the test was based on all differences $\beta_{sp,m}(h) - \beta_{sp,n}(h)$ for species m and n with $1 \leq m < n \leq 5$.

The test we used relies on two procedures : 1) the Freedman-Lane algorithm (described in details by Winkler et al. 2014, p. 385) to permute the residuals of the null model and create the reference distribution of the coefficients under the null hypothesis, and 2) the global extreme rank length envelope test to build a null global envelope for the above-mentioned test statistics and correct for the multiple tests conducted along h (Myllymäki et al. 2017). The Freedman-Lane algorithm includes all the steps ranging from the simulation under the null hypothesis to the final estimation of the chosen test statistic (Figure 2.3). We used 2,999 random permutations to build the distributions under the null hypothesis. The global extreme rank length envelope test (Myllymäki et al., 2017, Mrkvička et al., 2020) was then constructed from the test statistics calculated from the empirical vertical distribution of LiDAR returns and the 2,999 permuted data sets.

The null hypothesis was rejected if the empirical test vector left the 98% global envelope at any point. To account for the three variables tested (species, crown cover, and age), we used a Bonferroni adjusted significance level $\alpha = 0.05/3$ in addition to the inherent correction applied within the global extreme rank length envelope test to account for multiple h. We observed that the variances of the model residuals were heterogeneous for all the variables (Winkler et al. 2014). Following Mrkvička et al. (2020), we transformed the matrix of vertical LiDAR returns distribution (Figure 2.3) by scaling the functions d_i of each group j according to their variance dispersion. The initial $d_{i,j}$ function was transformed into a $S_{i,j}$ (scaled) function by

$$S_{i,j}(h) = \frac{d_{i,j}(h) - \bar{d}_j(h)}{\sqrt{Var(d_j(h))}} \cdot \sqrt{Var(d(h))} + \bar{d}_j(h) \tag{2.5}$$

where the group sample variance $Var(d_j(h))$ is used to correct for unequal variance among groups. The group sample mean $\bar{d}_j(h)$ and overall variance $Var(d(h))$ are used to preserve the original scale of the mean and variability of the functions.

Our experiments with simulated data showed that transforming all groups at once (by combining all group levels) removed the heterogeneity of the variance. However, this required there to be sufficient observations in all categories, which was not the case for our data. We therefore relied on the successive application of the transformation (Equation (2.5)) for each of the three variables, and we found that the order in which the transformation is applied can reintroduce heterogeneity of variance. We settled on the successive transformation of crown cover, age, and species which provided the best results and reduced heterogeneity. We verified the importance of the correlation by running Breusch-Pagan test of heteroscedasticity (Breusch and Pagan 1979) using the squared residuals $(d(h) - \hat{d}(h))^2$ on the left-hand side of the reduced equations (2.2)–(2.4). While the test indicated significant heteroscedasticity in some areas of the curves, the coefficient of determination was less than 4% for all variables and all h, which confirmed that no further adjustments were required.

We performed the analysis using R version 3.6.3 (R Core Team 2020), the GET package (Mrkvička et al. 2019 ; Myllymäki and Mrkvička 2020), and Lastools (Isenburg 2012) to correct and extract the LiDAR data.

2.5 Results

The comparisons from the nonparametric graphical test of significance confirm that the differences between all species, after accounting for age and crown cover, were significant ($p < 0.001$) (Figure 2.4). We observed two groups of species where differences were significant but small : balsam fir–paper birch, and black spruce–white spruce. Differences between balsam fir and paper birch were small and localized at 65–70% and below 12% of stand height. White

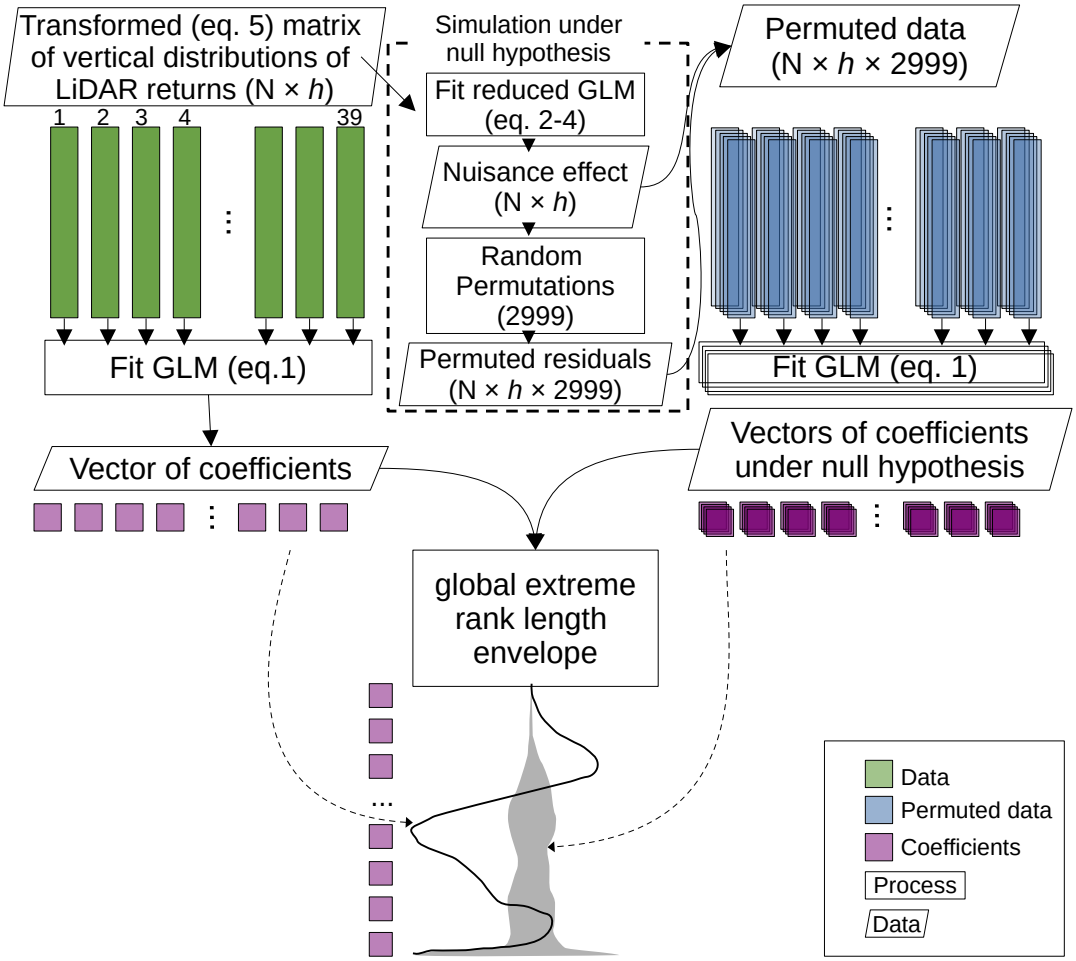

FIGURE 2.3 – Description of the steps of the graphical test of significance of a variable (e.g. species) on the vertical distribution of LiDAR returns.

spruce and black spruce also had small localized differences at 22–30% and 5–8% of stand height. However, some differences between groups of species were larger (indicated by the bold lines in Figure 2.4) : black and white spruces had the lowest distribution of LiDAR returns when compared to other species. Black spruce had fewer returns than balsam fir between 38–62% of stand height (40–57% for paper birch), while it had more returns below 28% of stand height (30% for paper birch). The vertical distribution of LiDAR returns for aspens had a distinctive shape when compared to every other species : it did not display a prominent peak, which made the distribution more uniform than for other species (Figures 2.5 and 2.6). Aspen was significantly different from other species ($p<0.001$) except in the areas between 57–60% of height, and 8–18% for balsam fir and paper birch specifically. Overall, the areas with the largest differences between species were located at around 5, 25, 50, and 70% of stand height.

An increase in crown cover was associated with a decrease in the density of LiDAR returns below 33% of stand height, while the density of LiDAR returns above 38% increased (Figure 2.7). The largest increase was concentrated around the middle height (50%), while the largest reduction effect occurred closer to the ground (around 3% height). Figure 2.5 displays the vertical distribution of LiDAR returns for each species per crown cover (including the effect of age). The increased crown cover concentrated the returns at around 50% of the stand height, except in the case of aspen, where the peak was higher in the stand (around 80% of stand height), and white spruce, where the peak was lower (around 20%). Although the black spruce peak was centered at 50% of the stand height for high values of crown cover, the observed variability was skewed toward the lower stand heights. Some species were more widely represented in younger or older age classes, which inflated the variation envelopes. The model from Figure 2.7 accounted for this effect.

Increased age was associated to a gradual upwards shift in LiDAR return distribution (Figure 2.8). This shift occurred until 70 years of age, when a plateau was reached. The effect of age was significant at most stand height between 10 and 70 years of age.
Stands that were in the 10- and 30-year age groups had an abundance of returns below 28% and 41% of stand height, respectively, and fewer returns above 33% and 49%, respectively. However, the effect is reversed in stands in the 50- and 70- year groups, where age inflated the distribution between 38–97% of stand height (44–100% for 70 yr), and deflated it below 31% of stand height (38% for 70 yr). The significant age effects for stands in the 90- and 120-year age groups were smaller, and occurred below 69% and 44% of the stand height, respectively ($p<0.001$). These stands also had an abundance of returns in the middle and upper part of the stand (38–68% for 90 yr ; 33–44% for 120 yr). For stands that were in the 90- and 120-year groups, there were reduced numbers of returns below 28% and 23% of stand height, respectively.

Overall, the rate of change in the vertical distribution of LiDAR returns gradually decreased

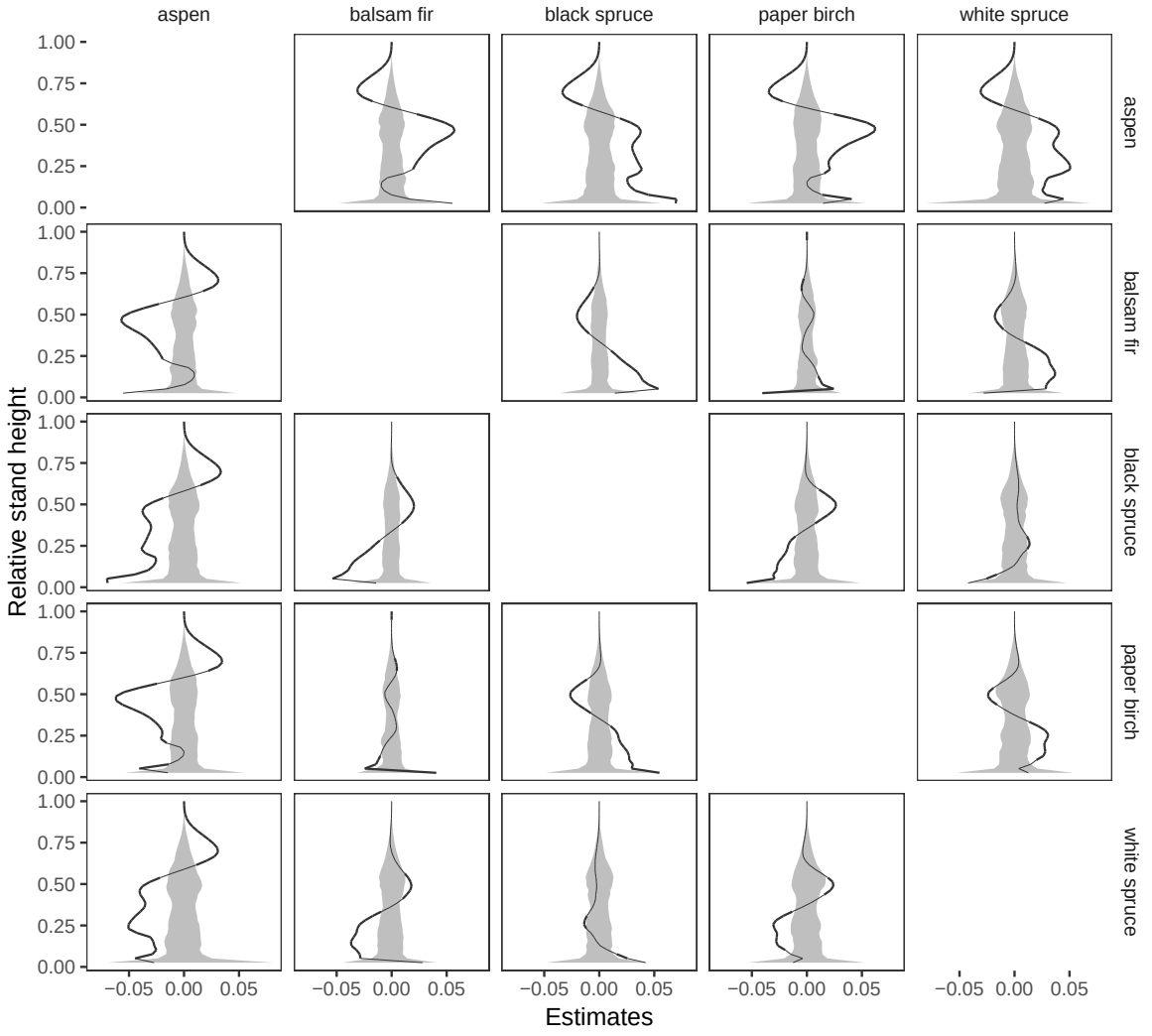

FIGURE 2.4 – Nonparametric graphical tests of significance comparing species using contrasts : the observed difference between the coefficients of two species (black curve), where the species in the rows are subtracted from the species in the columns (e.g. first column, second row is the aspen − balsam fir contrast). The 98% global envelope (grey bands), shows the area of acceptance of the null hypothesis (no effect, $p<0.001$) obtained from the permutations of the residuals of the null model (Equation 2.2). The observed curve that is outside the envelope is in bold. Panels above the diagonal are the reflection of the observed functions and the global envelope from the lower part (the tests were performed only once).

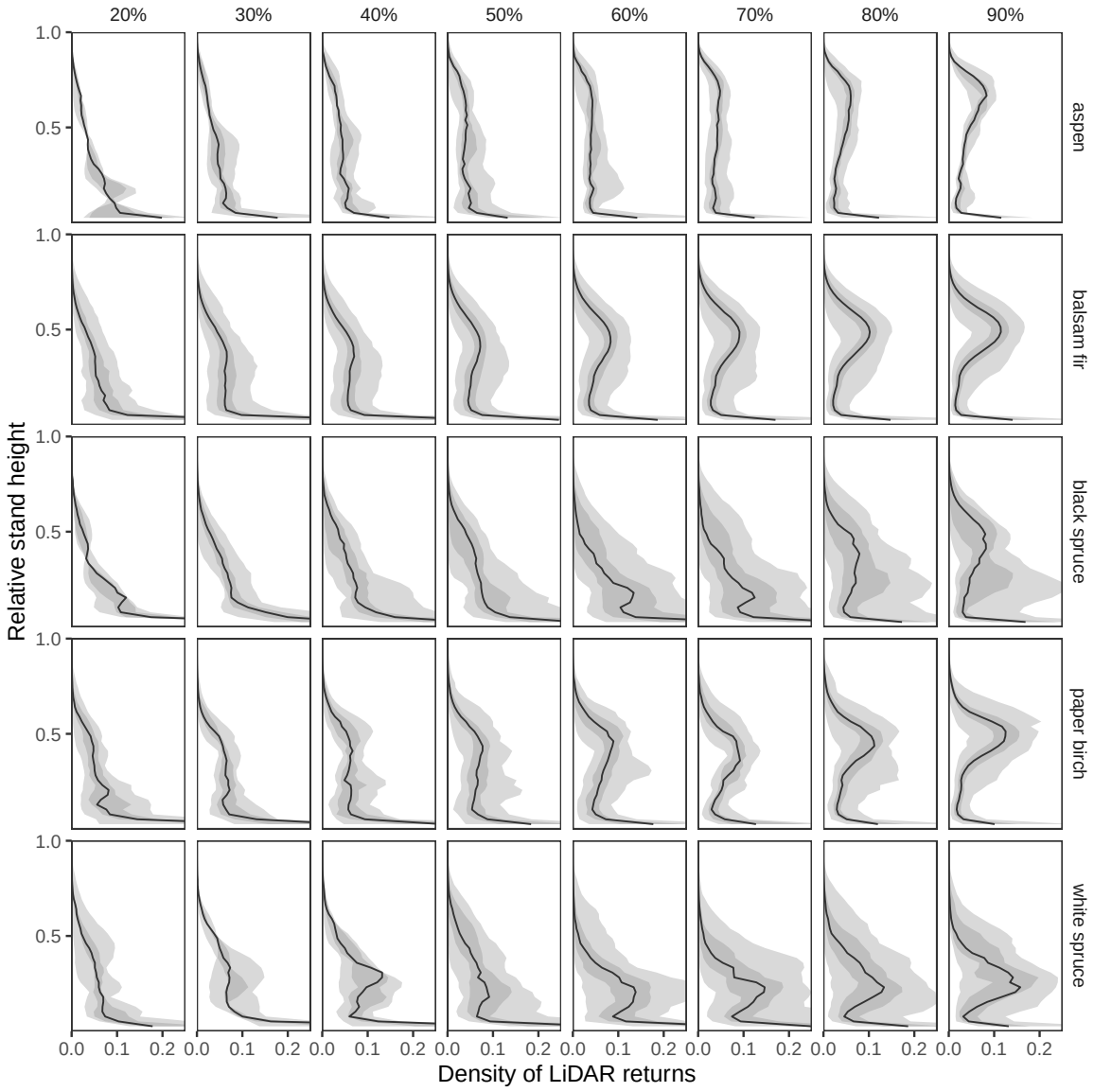

FIGURE 2.5 – Vertical distribution of LiDAR returns as a function of crown cover (columns) and species (rows). Black lines represent the median distribution ; shaded areas represent 95% and 50% local variation envelopes.

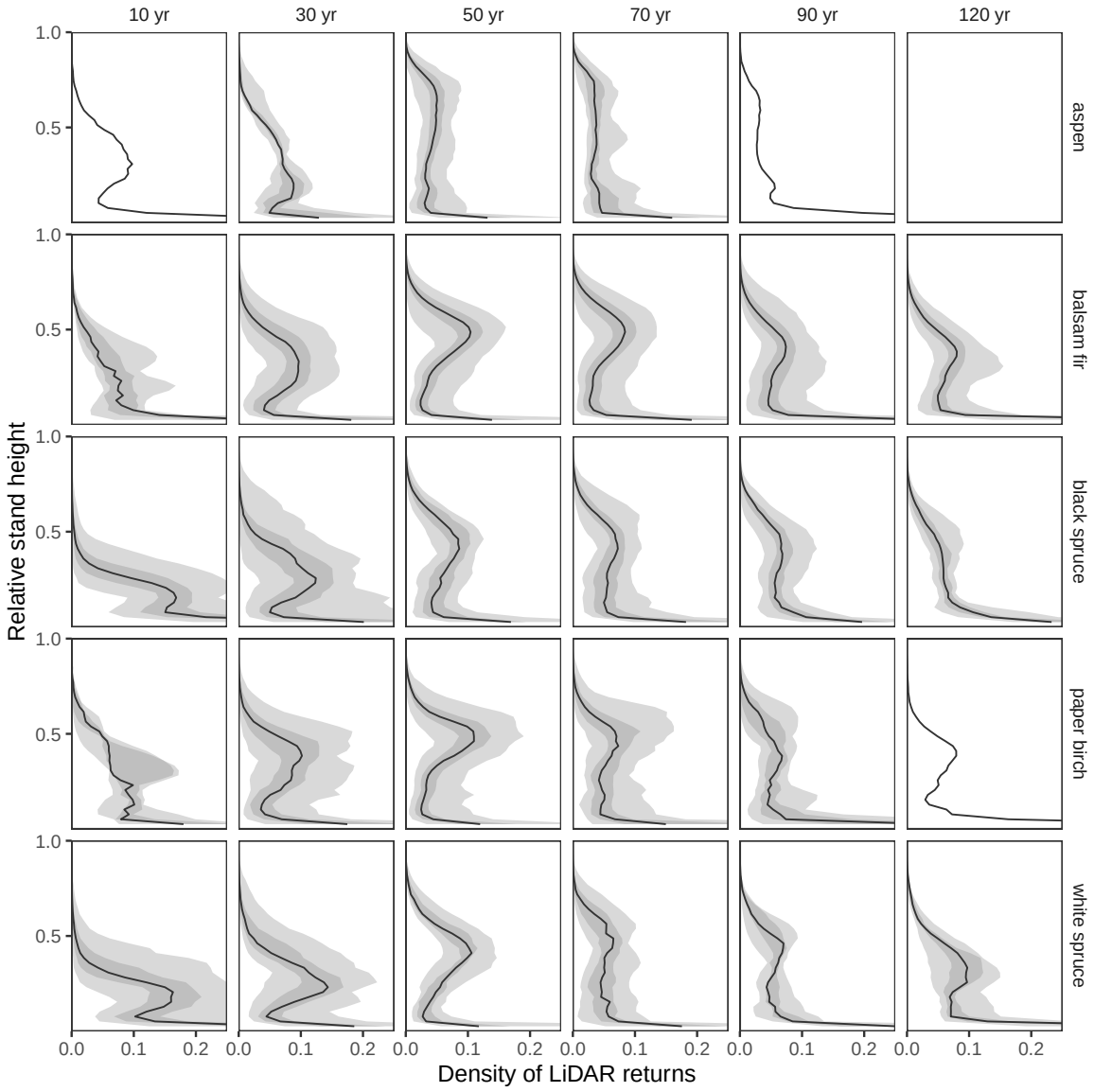

FIGURE 2.6 – Vertical distribution of LiDAR returns as a function of age (columns) and species (rows). Black lines represent the median distribution ; shaded areas represent 95% and 50% local variation envelopes.

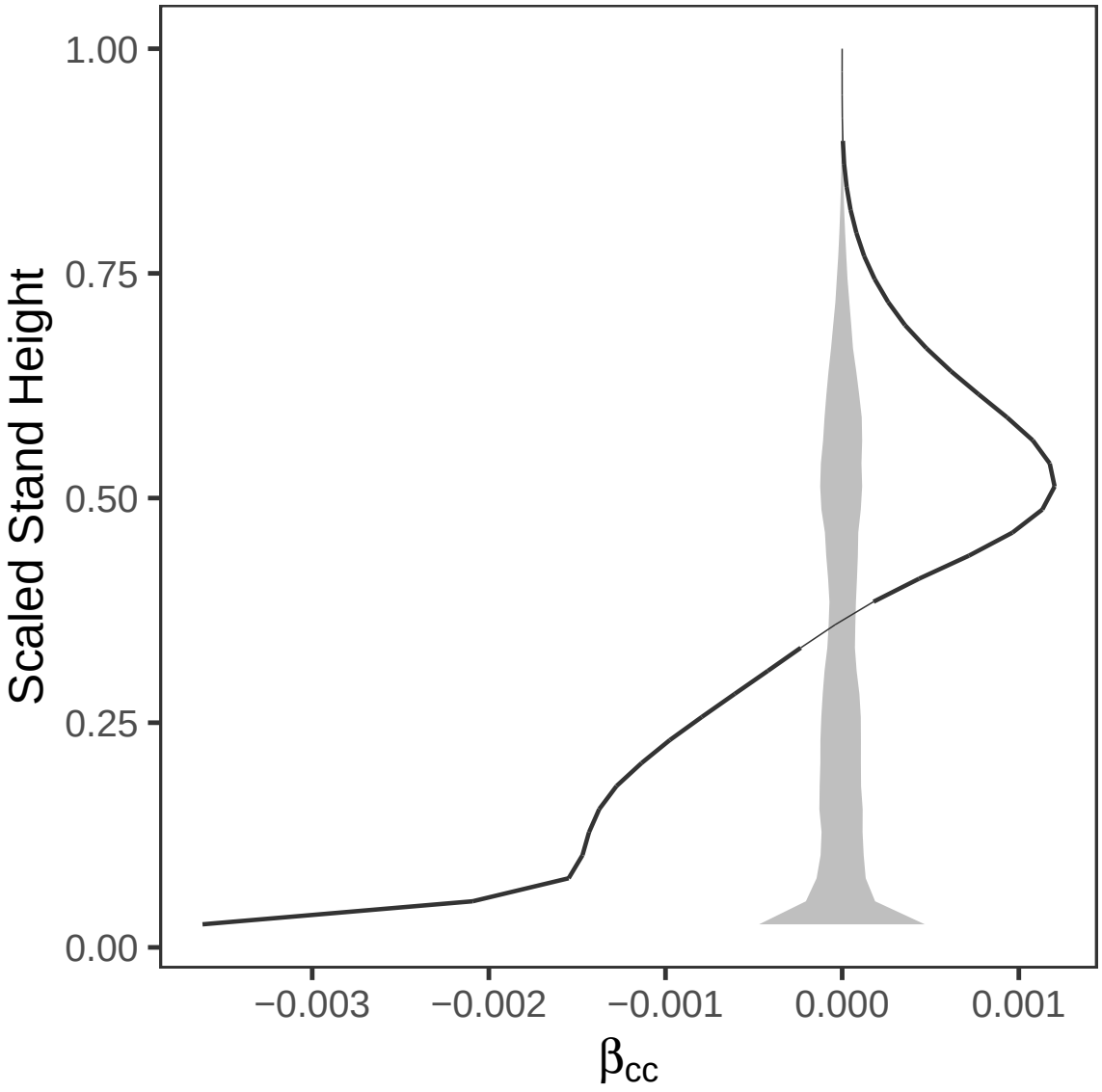

FIGURE 2.7 – Nonparametric graphical tests of significance for crown cover. The observed coefficient (black curve) and the 98% global envelope (grey band) that shows the area of acceptance of the null hypothesis (no effect, $p<0.001$) obtained from permutations of the residuals of the null model (Equation 2.3). The observed curve that is outside the envelope in bold.

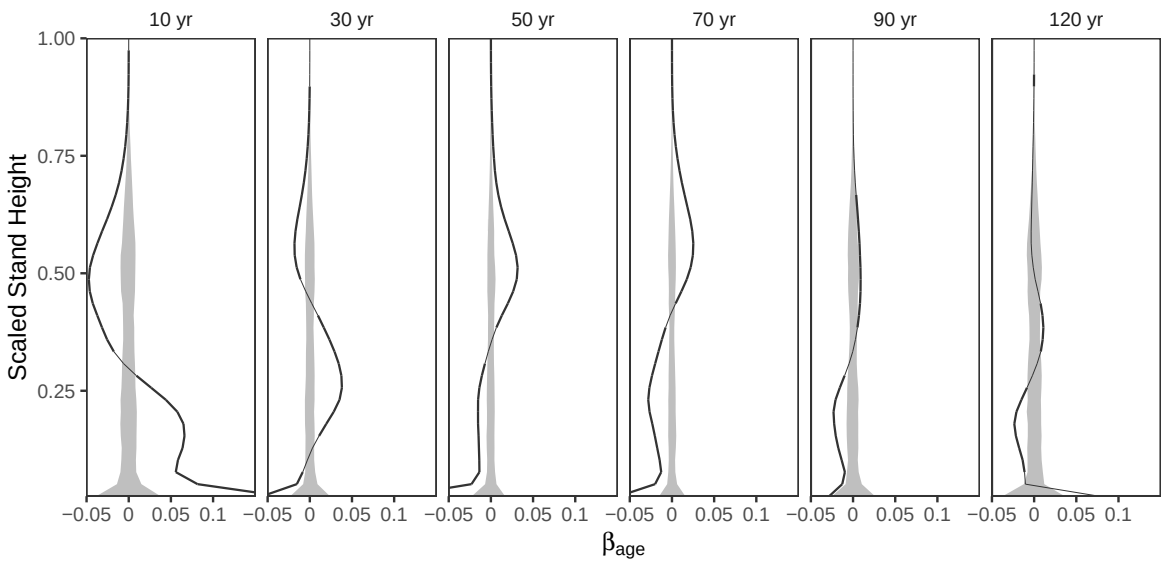

FIGURE 2.8 – Nonparametric graphical tests of significance for age. The observed coefficients of the six age groups (black curves), and the 98% global envelope (grey bands below the diagonal) that shows the area of acceptance of the null hypothesis (no effect, $p<0.001$) obtained from the permutations of the residuals of the null model (Equation 2.4). The observed curve outside the envelope is in bold.

as the age increased. For example, changes in the distribution between 10 and 30 years were larger than the changes between 70 and 90 years. Areas of higher variability for age groups were located around 5%, 20%, and 50% of stand height. Figure 2.6 displays the median vertical distribution of LiDAR returns for each species, by age class (including the crown cover effect). The young white spruce and black spruce stands displayed a high degree of asymmetry toward the lower part of the stand that disappeared in older stands.

The coefficient of determination for the models varied across stand heights (Figure 2.9). The most correlated areas for every model were around 5–15% and 46–54% of stand height. All models displayed a sharp decline between 28–40%. The highest R^2 was for the full model at 0.47 (at 10–13% of stand height) and 0.42 (at 49–51% of stand height). The model that excluded the species variable (Equation (2.2)) produced a difference in R^2 of more than 0.10 for 72–92% stand height compared to the full model. When the crown cover variable was excluded from the model (Equation (2.3)) for between 0–21% and 46–67% of stand height, there was a difference in R^2 of more than 0.10 with the full model. The model that excluded the age variable (Equation (2.4)) produced a difference in R^2 of more than 0.10 with the full model at 18–38% and 62–64% of stand height.

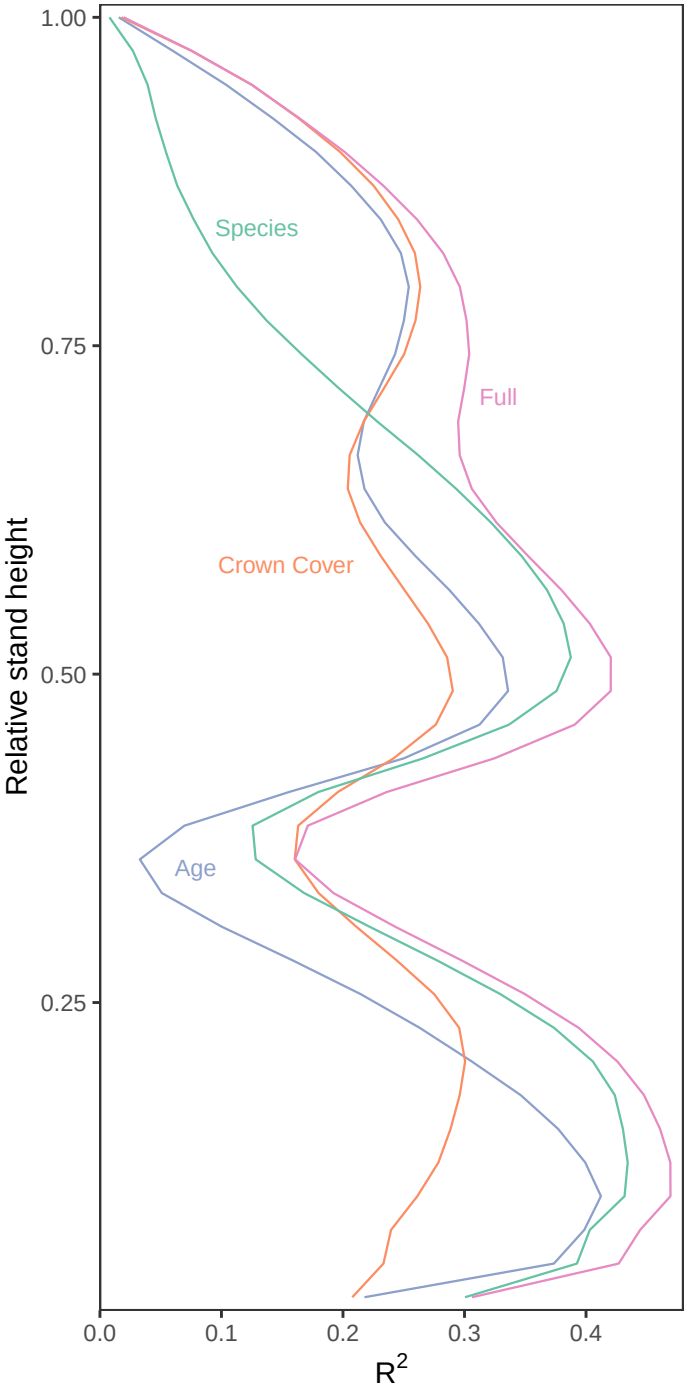

FIGURE 2.9 – Comparison of $R^2(h)$ of the full model (Equation 2.1), and the three reduced models (Equations 2.2–2.4) where one variable (either Species, Crown Cover, or Age) was excluded.

2.6 Discussion

Our objective was to study the influence of species, crown cover and age on the vertical distribution of LiDAR returns. We found that even-aged stands exhibit species-specific patterns that predictably evolve with crown cover and age. We observed two groups of species : the first, balsam fir and paper birch had more symmetrical vertical distributions of LiDAR returns that were centered between 40% and 60% of stand height, and the second, white spruce and black spruce, had distributions of LiDAR returns that were generally skewed lower in the stand (below 30% of the stand height). Aspen displayed a more even distribution of LiDAR returns with a higher proportion of returns higher in the stand compared to other species.

While individual trees are plastic and can adapt to various light and environmental conditions, we found that stands of the same species share similar vertical characteristics. These characteristics distinguish them from other species. This observation is consistent with previous field observations that were conducted over a smaller area using different measurement methods (Purves et al. 2007). However, we expected clearer vertical distribution patterns along shade-tolerance gradients or between conifer and deciduous trees ; we found that patterns of paper birch were more similar to those of balsam fir (a shade-tolerant) than aspen, another shade-intolerant deciduous. Since we used the dominant species to classify each stand, the similar vertical distribution patterns could be the result of frequent occurrence of balsam fir and paper birch within the same stand. The effect of species associations could be controlled by using a higher dominance threshold than the 50% we used. However, we found that using a 60% dominance made little difference to the conclusions, whereas a higher threshold removed too much data for some species.

The results in this paper demonstrate that vertical LiDAR return distribution can be useful for species classification. Based on these findings, models could be trained to link these vertical distributions to species and then used to estimate species occurrence over the landscape. Many studies performing species classification with LiDAR use the vertical distribution of LiDAR returns (Fassnacht et al. 2016), however the approach developed here allows the drivers of cover and age to also be integrated into the estimation, thereby making the species prediction more robust when applied more broadly.

Additional evidence is required in order to establish whether the relationships between vertical density of LiDAR returns and the species, crown cover, and age are specific to our study area. Including other variables, such as LiDAR scan angle and abiotic factors, might improve the model, making it more applicable to other study areas or complex stand structures.

Increased crown cover led to an increased concentration of the vertical distribution of LiDAR returns to higher in the stand. In turn, stands with decreased crown cover exhibited a vertical distribution of LiDAR returns that was more dispersed and lower to the ground, with fewer returns higher in the stand. The gradual displacement of LiDAR returns from below 33%

to above 38% associated to crown cover was also apparent when we compared the variance explained by the models in Figure 2.9 where crown cover appeared to explain at least 25% of the variance of the full model below 21% and between 46–67% of stand height.

Increased age was associated with the vertical distribution of LiDAR returns being displace higher in the stand for up to 70 years, followed by a plateau or decline in the 90- and 120-year-old groups. The rate of change between age groups decreased as the age increased. Vertical distribution of LiDAR returns from younger stands appeared to undergo a rapid transformation in the 10-year group, which gradually decelerated and stabilized in the 70-year-old group. The 90- and 120-year-old groups displayed the least amount of change. While it is well established that absolute stand height varies predictably with age, the changes we observed here are relative to the maximal height of the stand.

The effect of age was akin to that of crown cover : as the age or crown cover increased, there was an increased concentration of points in the upper part of the stand. However, age explained the variation slightly higher in the stand than crown cover (between 18–38% and 62–64% of stand height). Unlike Aber (1979) who observed a stable distribution of foliage at the end point of forest succession, the vertical distribution of LiDAR returns of the 120-year group displayed a small concentration of returns at 33–44% of stand height and a small decrease below 23% of stand height.

The most pronounced differences in vertical distributions of LiDAR returns occurred below 80% of stand height. The upper sections of the stand often yielded very small differences in distribution while the lower section yielded large variations. The distribution of LiDAR returns in the upper and lower sections of the stand can heavily dependent on the LiDAR survey parameters and species crown shape (Roussel et al. 2017 ; Roussel et al. 2018). This might make these sections more variable across different surveys. Nonetheless, the full model (Equation (2.1)) still explained 20% of the variability from the ground up to 90% of the stand height. The difference in variability explained by the species model compared to the full model was greatest at heights above 72%, and peaked at around 80% of the stand height (Figure 2.9). One possible explanation for this is that the section encompassing 74–90% of stand height exhibited considerable differences between aspen and all other species.

A common challenge associated with functional data analyses is making functions comparable, a process called registration (Ramsay et al. 2009). We registered the vertical distributions of LiDAR returns by using the highest measured LiDAR return of each stand. However, this registration makes the distributions potentially more affected by extremely high LiDAR returns and could explain, in part, why the upper section of the stands had a lower R^2. For example, in young stands where there might only be a single remaining mature tree, the vertical distribution of LiDAR returns could be compressed. Using a height quantile as a registration point, such as 95% height rather than the highest return, could reduce the

chances of compression and improve the vertical distributions. In addition to compression, the vertical distribution of LiDAR returns can be distorted by strong slopes (Liu et al. 2017). Furthermore, the occlusion of vegetation in lower stand parts underestimates the density of vegetation. Some of the noise in the vertical distribution can be mitigated by using correction methods such as voxels, or partly accounting for laser incidence angle, footprint size and pulse density (Wilkes et al. 2016 ; Roussel et al. 2017 ; Roussel et al. 2018).

There was a decline in R^2 between 31% and 46% of the stand height, where age explained most of the variance of the full model (Figure 2.9). While the reasons for the decline are unknown, this section of stand height is associated with an increase in LiDAR returns in the 120-year-old group. This vertical section of the stands also seems to be a transition for the spruce group and the balsam fir–paper birch group between lower distributions and distributions centered around 50% of the stand height. The decrease in R^2 might be attributed to the intersection of these two distributions.

The nonparametric graphical test of significance that we used is slightly liberal because is based on the Freedman-Lane algorithm which uses an approximation from permutations (Mrkvička et al. 2019). However, this permutation method is regarded in the literature as one of the best methods when there are confounding variables (Anderson and Robinson 2001 ; Winkler et al. 2014). The graphical output from our analyses is advantageous, especially for identifying the sections of rejection. This graphical interpretation allowed us to determine the relative heights at which the differences in species, crown cover, and age occurred. When interpretability is desired, we think that this method could complement, and in some cases replace other methods of analysis for the vertical distribution of LiDAR returns, such as the principal component analysis or linear discriminant analysis (Fedrigo et al. 2019).

In a review of tree species classification using remote sensing, Fassnacht et al. -Fassnacht et al. (2016) noted that most studies pursued the optimization of classification accuracy and provided little information on the causal understanding of species discrimination. Using nonparametric graphical tests of significance can help us understand the evolution of forest structure by highlighting the association of variables with the distribution of reflective material. In our study, we applied this method to a selection of simple stands (that are even-aged with clear species dominance) to visually understand the effect of each of these factors. Further work is necessary in order to apply this method to multi-species or irregular stands.

The median stand area in our study area was 9 ha, which is large compared to other area-based approaches. This allowed for the aggregation of LiDAR returns to identify specific patterns. Stands are by design the most homogeneous unit of the forest landscape, and vertical LiDAR distributions are more reliable for identifying species when there is a sufficient number of aggregated returns grouped together. To determine the optimal area for observing these patterns will require additional research.

2.7 Conclusion

Light detection and ranging (LiDAR) vertical distributions can provide an understanding of the interplay between tree species, crown cover, and age. The use of functional generalized linear models combined with graphical tests of significance enabled us to interpret the differences in distributions caused by multiple variables. Using airborne LiDAR surveys makes it is possible to identify ecosystems that are at multiple evolutionary stages. Vertical LiDAR distribution patterns variations can be observed and eventually linked to structural and functional dynamics. Our results show that individual species feature distinctive vertical distributions of LiDAR returns that concentrate with crown cover and rise with age. Balsam fir and paper birch had similar vertical distributions of LiDAR returns, as did white spruce and black spruce. Aspen was the most unique species, yielding a more uniform distribution of LiDAR returns and a peak in the upper part of the stand. The balsam fir and paper birch group exhibited a peak centered at around 50% of stand height, while the distributions from the white spruce and black spruces groups were skewed to below 30% of the stand height. Increases in crown cover concentrated the distributions of all species at around 50% of the stand height and deflated the distribution below 33%. The effect of age was more diffuse across the whole stand height. Age increase was associated to a gradual displacement of the vertical distribution higher in the stands up to the 70 years. The distribution of the 90– and 120-year-old groups then plateaued and slowly declined. These results could improve our understanding of the evolution of the forest structure in changing conditions and could be used for LiDAR stand-level species classification.

Chapitre 3

Optimal Height Threshold and Grid Resolution to Maintain Repeatability of Crown Cover Estimation by Airborne Laser Surveys

3.1 Résumé

Le suivi de l'évolution de la densité de couvert en utilisant des relevés lidar (*Light Detection and Ranging*) à différents moments est une méthode appelée à être de plus en plus adoptée, compte tenu de la disponibilité des capteurs lidar et de l'accumulation des données d'archives. Toutefois, peu d'attention a été consacrée à comparer les estimations de la densité de couvert effectuées lors de relevés indépendants. Bien que les paramètres lors des relevés ne puissent être modifiés après l'acquisition, nous pensons que l'erreur associée à la comparaison des estimés de densité de couvert peut être réduite en choisissant de meilleurs paramètres post-relevés. Dans la présente étude, nous comparons les estimations des densités de couvert de trois relevés lidar aéroportés réalisés en 2018 ($40\,\mathrm{pt/m^2}$), qui nous sert de référence, et deux autres relevés de faible densité réalisés en 2016 ($4.5\,\mathrm{pt/m^2}$) et 2018 ($2\,\mathrm{pt/m^2}$). Nous avons étudié l'effet de la hauteur seuil à partir de laquelle les points de la canopée sont séparés et celui de la résolution de la grille en utilisant l'asymétrie et la variance des différences décalées des fermetures de cimes. Les estimés de densité de couvert utilisant des hauteurs seuils basses affichaient plus de différences entre les relevés, produisant ainsi une racine des écart-quadratique moyen (RMSE), des biais plus élevés, et des variogrammes plus différents. Les résultats montrent que les paramètres suivants étaient optimaux : hauteur seuil de 3 m,

résolution de grille de 25 m (RMSE de 7% et 5%, biais de 4% et 0% pour les relevés à basse densité de 2016 et 2018), bien qu'il y avait une marge de décision.

3.2 Abstract

Monitoring crown cover evolution using multi-temporal Light Detection and Ranging (LiDAR) surveys is a method that we expect to be increasingly adopted given the availability of LiDAR sensors and the accumulating survey archives. However, little attention was devoted to comparing crown cover estimates from independent surveys. Although survey parameters cannot be modified after the data collection, we speculate that the error associated with crown cover estimates comparison can be reduced by selecting optimal post-survey parameters. In this study, we compared crown cover estimates of three airborne LiDAR surveys from 2018 (40 pt/m^2) used as a reference, and two lower-density surveys from 2016 (4.5 pt/m^2) and 2018 (2 pt/m^2). We studied the effect of the height threshold used to separate canopy points and the grid resolution, using skewness and variance of lagged difference of crown cover. Crown cover estimates using low height thresholds were more different across surveys, resulting in higher root mean squared error (RMSE), bias, and more different variograms. Results show that optimal height threshold was 3 m and grid resolution was 25 m (RMSE of 7% and 5%, and bias of 4% and 0% for 2016 and 2018 low-density surveys), although there was room for decision.

3.3 Introduction

Airborne Light Detection and Ranging (LiDAR) measures of stand crown cover are frequently among the most important variables to predict stand attributes and describe the forested habitats (FAO 2015). Monitoring crown cover across time through repeated LiDAR surveys is a method that should increasingly be adopted given the availability of LiDAR sensors and the accumulating archives. However, comparing LiDAR surveys across time and space is difficult when parameters change (Roussel et al. 2017).

Comparing surveys is challenging because often multiple parameters vary simultaneously in addition to the evolution of the vegetation that is to be observed. It is therefore difficult to establish how much of the differences between two LiDAR surveys are due to vegetation evolution only.

In the absence of reference ground data, it can be difficult to confirm the validity of a remotely sensed observation. Practitioners such as forest managers are especially likely to face this dilemma when forest management objectives change, or questions are added to a follow-up survey. While it is difficult to measure the precision of a metric estimated by two LiDAR surveys without ground observations, it is still possible to compare surveys conducted in a

short time interval that did not allow for significant changes to understand the factors that can impact the results of the survey.

3.3.1 Crown Cover

We noted several tree density descriptors in the literature : crown cover, crown closure, stand density, vegetation density, canopy density, (vertical, fractional) canopy cover, gap fraction, and LiDAR penetration. They essentially refer to the proportion of horizontal space occupied by tree stems or tree crowns depending on whether the survey is terrestrial or airborne (Holmgren et al. 2003 ; Korhonen et al. 2011 ; White et al. 2013a ; Liu et al. 2018 ; Alain et al. 2019 ; Burkhart et al. 2019 ; ESRI 2019). In our study, we defined crown cover as the proportion of a surface covered with vegetation (Gonsamo et al. 2013), measured as the ratio of first LiDAR returns above a threshold on the total number of first returns on an area. We further detail this definition in the methods section.

3.3.2 LiDAR Measurement

Crown cover can be difficult to measure on the ground because unlike observations of individual tree mensuration, crown cover requires a large area of observation. Furthermore, ground plot locations are often registered within three to five meters, while LiDAR surveys can be matched within less than a meter using standard LiDAR survey protocol (Frazer et al. 2011 ; Muss et al. 2011). As a result, comparison between field estimates and LiDAR surveys can be biased or display inflated error.

Lidar was found to provide measures that matched ground observations of crown cover. Korhonen et al. (2011) reported an RMSE of 3.7–7.0% and an overestimation of 4.6–3.7% of LiDAR estimates when compared to ground measurements. However, in the absence of repeated measures, it was not established which method, LiDAR or ground measurements, provided the most accurate estimates. In a study of the impact of LiDAR scan angles on crown cover estimates against ground measurements, Liu et al. (2018) found an R^2 of 0.74, and 0.87 for measurements using a scan angle of 0–7°, and 7–23° respectively ; they reported no difference in crown cover estimates for surveys with point densities higher than 5 pt/m^2.

LiDAR bias for crown cover estimates can be mostly attributed to four elements : (1) the absence of LiDAR pulse due to sensor design, sampling rate, scan patterns, scan angles, and aircraft altitude ; (2) the topography which can induce bias in height and distort crowns ; (3) the interaction of LiDAR pulses with different vegetation, and canopy architectures such as leaf and needle or canopy shape and angle ; and (4) survey post-processing, such as ground point classification, height threshold, and area (Chasmer et al. 2006 ; Wasser et al. 2013 ; Roussel et al. 2017 ; Liu et al. 2018 ; Moudrý et al. 2020). Our study concentrates on the impact of post-processing to increase the repeatability of LiDAR surveys, especially in areas where no ground measurements are available.

3.3.3 Post-Survey Parameters

Many parameters of a LiDAR survey are decided before the survey, set during the acquisition, and cannot be changed subsequently (e.g. flight altitude). However, some parameters that we will call post-survey can be modified after the realization of the survey. The choice of the grid resolution or the height threshold used to estimate crown cover can be decided based on the results of the survey. We used combinations of height thresholds and grid resolutions to quantify their impact on crown cover estimates. We set two objectives for the optimization of the crown cover : the distribution of crown cover values should span the full range of possible values (0–100%) and describe the variation found in the study area.

Height Threshold

The height threshold is used to separate canopy returns from non-canopy, and its value should be adapted to the environment studied (White et al. 2013a). The height threshold can be calibrated using ground data (Nyström et al. 2012) or taken as the same height used during field observations (Korhonen et al. 2011). Some studies used the ground points directly (no height threshold, or 0 m)(Woods et al. 2008 ; Woods et al. 2011 ; Liu et al. 2018). While using a height threshold too high decreases the overall crown cover, conversely a height threshold too low can artificially increase the overall crown cover. For that reason, finding the optimal height threshold might in turn provide a more balanced distribution of crown covers throughout the landscape and cover the full range of possible values : 0–100%.

Grid Resolution

Crown cover estimates can change depending on the area used to compute it—often a raster grid composed of cells. A small spatial resolution (i.e. small grid cell size) artificially inflates the variability because they are subject to the idiosyncratic trajectory of the LiDAR reflections and tree location. Conversely, using a large area regresses values to the mean and hides the natural variation occurring in the study area. In both extreme grid resolutions, the information cannot be used to discriminate ecosystems. For that reason, there must be an optimal grid resolution to balance volatility, stability, and bias (Hengl 2006).

Methods to estimate the optimal cell size for LiDAR surveys vary. For example, ESRI (2019) state that the grid resolution should be at least 4 times the point spacing : a survey with $0.5\,\mathrm{pt/m^2}$ yields a point spacing of 1.4 m/point and would require a minimal cell size of 5.7 m. The disadvantage of this method is that it evacuates the biological component of the crown cover and does not depend on species, crown size, nor vegetation height. White et al. (2013a) suggest that the cell size for forest inventory should generally be close to plot size and adapted to the average crown size, with typical sides of square cells of 20–25 m. Increased plot size provides a more uniform distribution of pulses, minimizes within-pixel edge effect, and improved the estimates by asymptotically increasing the overlapping area between the LiDAR

data and the field observations (Naesset 2004 ; Frazer et al. 2011 ; White et al. 2013a). On the other hand, comparing vector data such as forest stand polygons to large grid resolutions amplifies the edge effect (i.e. pixelization). Smaller cell size also better reflects the variability of the study area, which is important for forest management (Pretzsch 2009). For crown cover, the grid size has to be large enough to collect enough vegetation and ground points, even in a very closed cover, to reflect the local crown cover. Hengl (2006) suggested using a variogram to select an appropriate cell size for point interpolation. Indeed, crown cover estimation can be seen as the interpolation of a highly sampled binary variable across space. The variogram can thus be used to observe the range of spatial autocorrelation and guide the decision of grid size, especially to provide an upper bound for the grid size. However, computing the variogram for an aggregate measure such as crown cover requires deciding on an aggregation measure before the calculation of the variogram, which can lead to a distorted understanding of the data.

3.3.4 Objectives

While LiDAR survey parameters are crucial for crown cover estimates, we have found that little attention was shed on the post-survey parameters that impact crown cover : the height threshold to separate canopy returns from non-canopy returns, and the area on which crown cover is calculated. In this study, we compare the crown cover estimates from three independent LiDAR surveys and propose a method to facilitate the comparison of crown cover across surveys by the optimization of the post-survey parameters. We look at the impact of these two parameters on crown cover using RMSE and bias between surveys as well as the spatial autocorrelation over the study area to propose a method for the selection post-acquisition parameter.

3.4 Methods

The study area partially overlaps the Grands-Jardins National Park, Québec, Canada (Figure 3.1). The forest is dominated by coniferous species, such as *Abies balsamea*, *Picea mariana*, and some deciduous such as *Betula papyrifera* and *Populus tremuloides*. The site is representative of a wide range of boreal forest conditions, from open black spruce to closed mixedwood forests. The growing seasons are short, between 80 and 100 days (Pedlar et al. 2014).

3.4.1 LiDAR

Three LiDAR surveys were used for this study : one conducted in 2016 and two conducted in 2018. The 2016 low-density (LD) survey (June 26 to August 15) nominal point density was 4.5 $\mathrm{pt/m^2}$, the 2018LD survey (August 21 to October 5) was 2 $\mathrm{pt/m^2}$, and the high-density (HD) 2018 survey (August 24 to October 23) was 40 $\mathrm{pt/m^2}$ (Table 3.1). The 2016LD survey

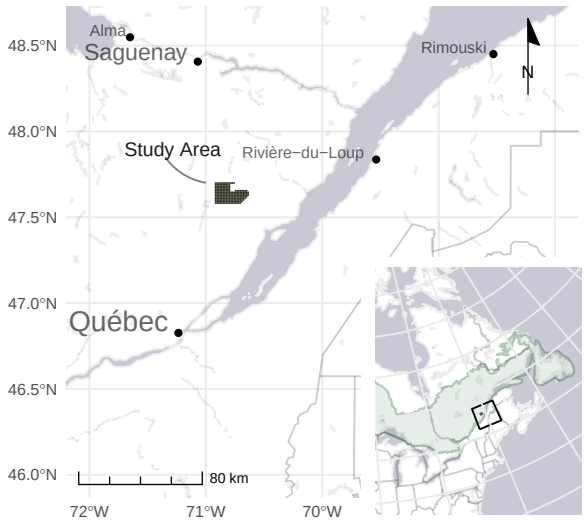

FIGURE 3.1 – Study area is located in the Boreal Shield ecozone (light green area) within the Grands-Jardins National Park, Québec, Canada.

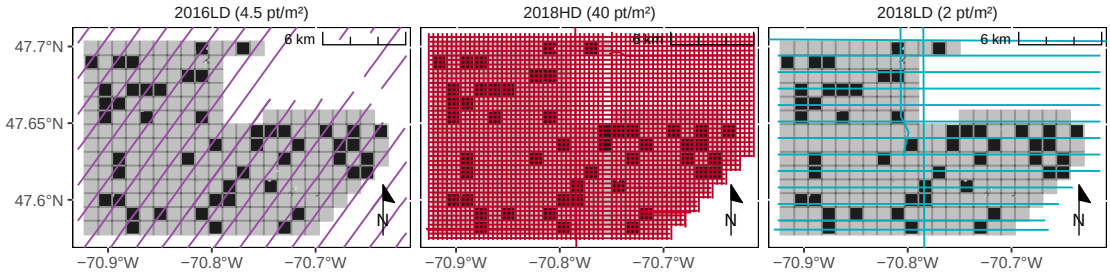

FIGURE 3.2 – Flight lines (colored) of each survey over the study area (light gray), 1 km tiles holdout data for validation are in black.

had a northeast azimuth while the 2018LD survey has an east azimuth with a north crossing flight line for registration. The 2018HD survey has a crossing flight lines pattern with both north and east azimuths (Figure 3.2). Apart from the point density, one of the most notable differences of the 2016 survey is that it was conducted earlier in the growing season than the 2018 surveys, and used a higher maximal scan angle, which can impact crown cover estimation (Roussel et al. 2018). Our study area is the intersection of the three independent LiDAR surveys. All points were classified with *lasground* (LAStools 2019) using default settings for the forest environment.

Sampling

We randomly sampled 5000 observation points within the study area to extract LiDAR metrics. We excluded two observations that presented insufficient LiDAR returns because they

Table 3.1 – LiDAR survey parameters

Year	Nominal density	Altitude	Speed	Sensor	Freq	Angle	Over	Divergence	Footprint	Median density
2018	40.0	1150	66.8	RIEGL VQ-780i	1000	20	50	0.25	0.1	38.9
2016	4.5	1932	92.6	RIEGL LMS Q-1560	800	30	30	0.25	0.3	4.6
2018	2.0	2300	66.9	RIEGL VQ-780i	350	20	30	0.25	0.4	2.1

Year : year flown
Nominal density : nominal first return density (pt/m^2)
Altitude : average sensor altitude above ground (m)
Speed : Flying speed (m/s)
Sensor : sensor model
Frequency : scan frequency (kHz)
Angle : maximal scan nadir angle (°)
Over : Flight line overlap (%)
Divergence : Laser beam divergence (mrad)
Footprint : Average laser footprint diameter on the ground (⌀m)
Median density : median first return density (pt/m^2)

were either on the edge of at least one survey or included in a water body.

To minimize the impact of spatial autocorrelation on the estimation of the performance, we used random block sampling to create a spatially independent holdout (Roberts et al. 2017a). We divided the study area into 1 km tiles to group observations : 1037 observations in the holdout tiles were selected to compute performance metrics (Figure 3.2).

Data Preparation

We computed the crown cover as the total number of first returns above the height threshold divided by the total number of first returns (Figure 2.7). Using only first returns was found to be more stable than using all returns or a canopy height model (Korhonen et al. 2011 ; Frazer et al. 2011 ; Bater et al. 2011), although (Liu et al. 2018) used a weighting to use all returns. For each sample point, we used eleven height thresholds (0 to 10 m) and 36 resolutions (1–20 m by 1 m increment, then 25–100 m by 5 m increment) on a squared pixel centered on the sampling point of observation.

Skewness

We needed to select a height threshold that is neither too high nor too low. In order to select the right height threshold, we compared the crown cover distribution to maximize the symmetry of the crown cover distribution across our observations. Given that our study area was representative of the boreal forest conditions with closed mixed stands and open coniferous stands, we speculate that a symmetric distribution of crown cover should lead to a more representative indicator because it avoids clustered crown covers around 100% (threshold too low) or 0% (threshold too high).

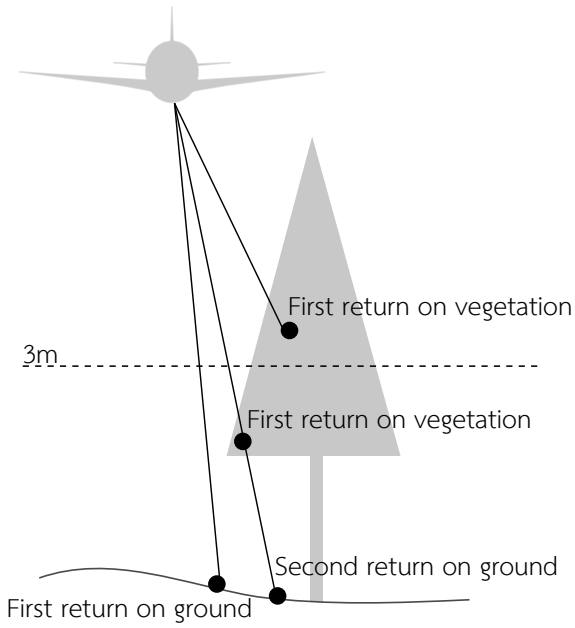

FIGURE 3.3 – Illustration of crown cover. Each dot represents a LiDAR return and each stroke represents a pulse. The dashed line indicates a height threshold at 3 m. Crown cover is the ratio of the number of first returns above the threshold by the total number of first returns. In this example, crown cover above 3 m is : 1 first return above 3 meters / 3 first returns = 33%.

Variance of Lagged Difference in Crown Cover

The size of the observation unit was found to be an important driver of accuracy and variability. To find the optimal plot size, Frazer et al. (2011) recommended increasing it gradually until measurements stabilized ; given the large number of parameters combinations and observations, we propose a formal indicator based on their suggestion.

One of our objectives was to reflect the variability of the forest cover, while still removing the noise from the individual tree measurements. We chose to use the variance of lagged difference in crown cover as an indicator of crown cover stability. For each pair of consecutive pixels at observation i and resolutions r in $\delta = 5\,m$ increment, we computed the crown cover $Z_i(r)$ difference $d_i(r)$ between the increased pixel area. Then for each pixel resolution r, we computed the variance of the lagged differences

$$d_i(r) = Z_i(r) - Z_i(r - \delta) \tag{3.1}$$

The variance V of the lagged difference at each resolution r is

$$V(r) = \frac{1}{n}\sum^{n}(d_i(r) - \bar{d}(r))^2 \tag{3.2}$$

with $\bar{d}(r)$ the average $d_i(r)$ of all i. We expected the variance to be rapidly decreasing as the pixel size increased and then stabilized close to 0 once the pixel size was sufficiently large to encompass enough area. It would mean that increasing the pixel by δ would not change crown cover $Z_i(r)$. We deliberately used a notation close to the one typically used in variography (see e.g. Dale and Fortin (2015), §6.2.3).

3.4.2 Performance Metrics

We compared LiDAR surveys crown cover estimates on the holdout data with the exact same post-survey parameter values using root mean squared error (RMSE) and mean bias :

$$RMSE = \sqrt{\frac{\sum^{n}(\hat{y_i} - y_i)^2}{n}} \tag{3.3}$$

$$Bias = \frac{\sum^{n}(\hat{y_i} - y_i)}{n} \tag{3.4}$$

Where y_i is the observation i of n from the reference 2018 HD survey, $\hat{y}_i$ is the observation from the low-density survey.

We performed an analysis of variance on the difference $(\hat{y_i} - y_i)$ for each combination of resolution and height threshold. To protect from Type I error, we used a Bonferroni-corrected $\alpha \approx 0.0001$ (0.05 / 11 height thresholds $\times$ 36 resolutions) to detect differences between surveys. The null hypothesis was that the differences between surveys were zero, meaning the estimated crown cover from low-density surveys was not different from the reference survey.

3.4.3 Spatial autocorrelation

We also looked at the spatial autocorrelation of crown cover by computing a variogram for each combination of height threshold and grid resolution on the holdout data. The empirical variogram expresses the average variance of pairs of points in a given range of distance. Typically, in the presence of spatial autocorrelation, the variance is lower for nearby points and stabilizes once it reaches a distance at which no correlation is observed. Since crown cover is driven in part by spatial processes, we can expect to observe spatial autocorrelation in the variogram. The variogram can be described using three parameters : the *nugget*, which is the variance at 0 m, a combination of the local variability and measurement error ; the practical *range* is the distance at which we cannot detect any spatial autocorrelation ; the *sill* is the semivariance reached by independent pairs of points once the semivariance reaches a plateau

(Bivand et al. 2008 ; Dale and Fortin 2015). An empirical variogram of spatially decorrelated values does not increase with distance ; semivariance moves randomly and the trend is flat.

We approximated the empirical variogram as a spherical model using a damped least square approximation from the gstat package (Pebesma 2004 ; Pebesma and Heuvelink 2016). We used an initial seed range of 250 m and adjusted a few seeds when the algorithm failed to converge to reasonable values.

We used the R software (R Core Team 2020) and the *lidR* R package (Roussel et al. 2020) for our analysis and the extraction of lidar metrics. Type 3 skewness was computed using the *e1071* R package (Meyer et al. 2019).

3.5 Results

The height threshold modified the skewness of the crown cover distribution (Figure 3.4A). Lower height thresholds of 0–3 m were associated with a negative skew of the crown cover in the study area (more observations toward closed cover), while higher thresholds of 4–10 m were associated with a positive skew (more observations toward open cover). The 3–4 m height thresholds minimized the absolute skewness of the crown cover distribution for all surveys, even if we excluded the non-forested areas. Increased grid resolution reduced the absolute skewness of crown cover, especially for extreme thresholds (0 m and 7–10 m), except for the 2018HD and 2016LD surveys at 0 m height threshold. The effect of an increased grid spatial resolution (hereinafter referred to grid resolution) on skewness was larger for height thresholds that were more skewed, such as the 0 and 10 m thresholds. For thresholds that produced the most symmetrical distributions (3–4 m), the effect of grid resolution appeared linear for resolutions larger than 6 m.

Most surveys' skewness were similar at a given threshold and grid resolution, but the 0 m height threshold created notably large differences across surveys compared to other threshold values. The 2018LD survey skewness was systematically higher than the two other surveys for all height thresholds. The difference between surveys was more apparent for more extreme height thresholds (0 m, and 7–10 m), while all surveys seemed to reach an asymptotic difference at larger grid resolutions.

Increased grid resolution reduced the variance of lagged difference of crown cover across the study area (Figure 3.4B). The difference in variance declined rapidly by increasing the grid resolution until 25 m where variance stabilized near zero. The height thresholds that had the highest symmetry (lowest absolute skewness, i.e. 3–4 m) captured the highest variance and were more impacted by the grid resolution, while extreme height thresholds (0 and 10 m) presented smaller changes in variability.

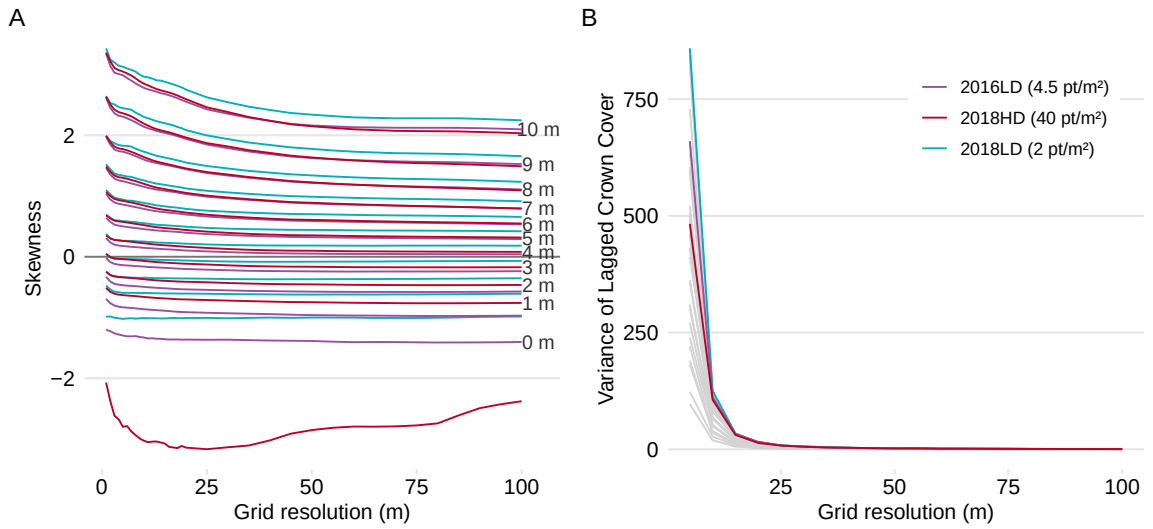

FIGURE 3.4 – Effect of post-survey parameters. A : effect of resolution on crown cover skewness for 10 height thresholds. B : effect of grid resolution on variance of lagged crown cover difference with 3 m threshold (other thresholds are displayed in gray).

3.5.1 Comparison With 2018 HD

Using the same post-survey parameter values for each comparison, we found that maximal bias between surveys was at 0 m threshold (Figure 3.5 top row). At 1 m height threshold, both survey biases decreased to 5.6 and -0.5% for the 2016LD and 2018LD respectively. The 2016LD survey was significantly different from the 2018HD survey ($p < \alpha$), except for resolution 2 m with height threshold 5 m. Using the 0 m height threshold reversed the bias for the 2016LD survey, which became negative. Overall, the resolution had little impact on the bias especially for resolutions larger than 7 m. The bias slightly changed for small resolutions and stabilized at around 7 m resolution. The 2018LD survey was not statistically different from the 2018HD survey for height thresholds 1 m ($p < \alpha$).

Higher height thresholds were associated with a lower RMSE, with an important decline between the 0–1 m (Figure 3.5 bottom row). For grid resolutions smaller than 7 m, the RMSE remained above 10% for thresholds <2 m. The increased grid resolution reduced the RMSE with a steep decline in 1–7 m resolutions.

3.5.2 Spatial Autocorrelation

The empirical variogram of crown cover was influenced by the grid resolution and the height threshold selection (Figure 3.6). Small grid resolutions displayed a weak structure of spatial correlation on crown cover, increased variance, and larger differences between surveys, especially when combined with low height thresholds of 0–1 m. The 2018LD survey exhibited a

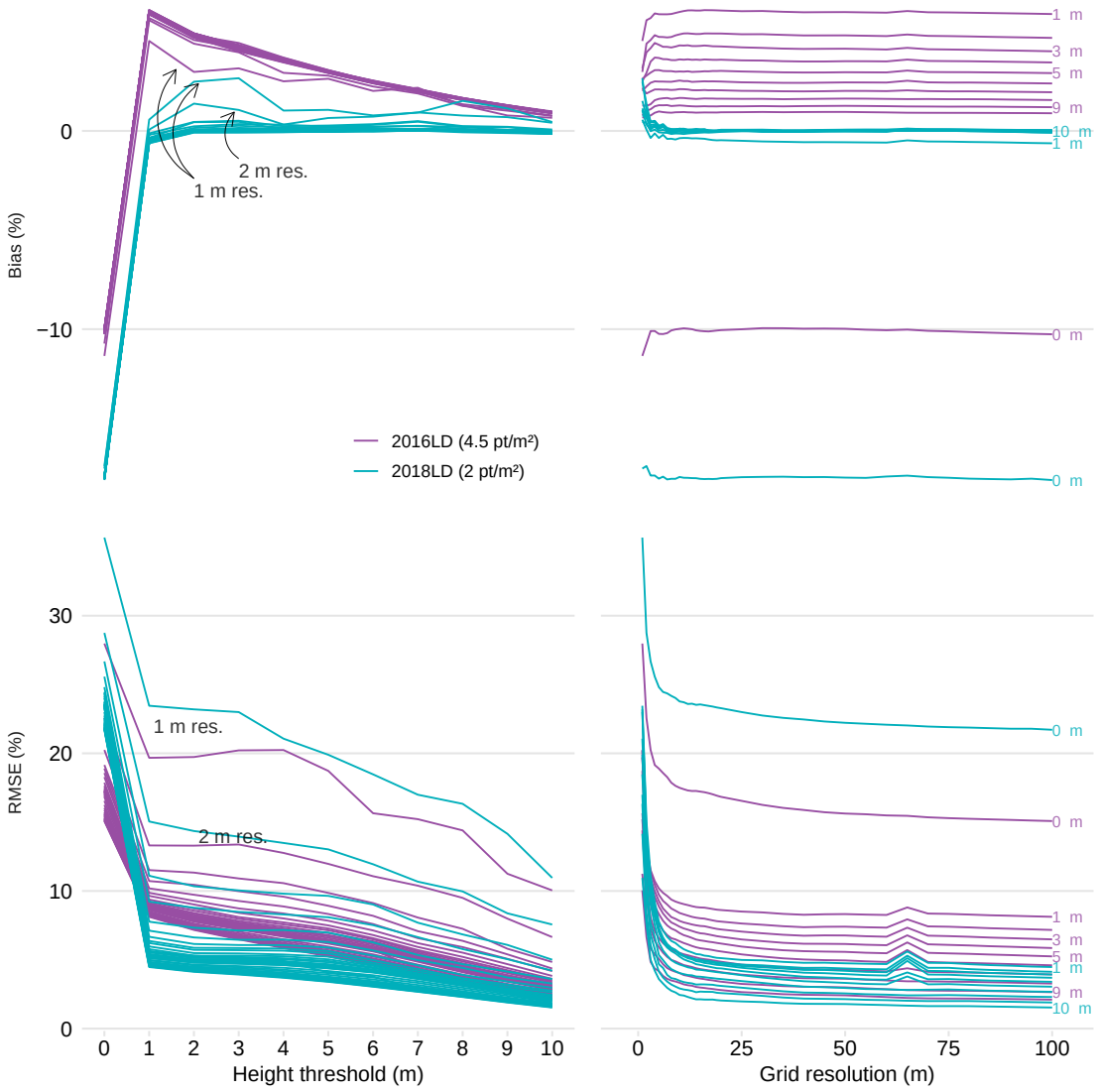

FIGURE 3.5 – Effect of post-survey parameters on the difference between surveys. Left : Effect of height threshold on bias (top) and RMSE (bottom) against the 2018 HD survey. Right : Effect of grid size on bias (top) and RMSE (bottom) against the 2018 HD survey. Resolutions of 1 and 2 meter and identified to facilitate the interpretation of the figure.

variogram similar to the 2016LD at lower height thresholds and gradually shifted toward the 2018HD as the threshold was raised. The 2018HD survey semivariance (sill and nugget) was generally lower, especially at resolutions 2 m, or 0 m height threshold. Furthermore, the 0 m height threshold also amplified differences between surveys and decreased the observed sill and nugget of spatial autocorrelation.

Using damped least squares fitting of a spherical variogram, we observed ranges of 100–350 m excluding the 0 and 10 m height thresholds. Surveys had mostly similar ranges for identical combinations of parameters (global $R^2 = 0.85$), however, resolutions >50 m had a much lower correlation between ranges. The mean absolute difference of range between surveys stabilized at around 12 m (not shown).

3.5.3 Parameter Selection

The selection of the grid resolution and height threshold must generally be performed without a reference survey. For that reason, we evaluated the relevance of the skewness and lagged variance of crown cover difference to select a combination of parameters that produced comparable crown cover estimates across surveys.

Given our study area and the objective we set for our crown cover estimators, we selected the 3 m height threshold (Figure 3.4A). It provides a balanced crown cover distribution and captures the most natural variance of the crown cover within the study area. The 4 m height threshold would also have been a good choice, but considering that the vegetation height rarely exceeds 20 m, we favored a lower threshold.

The 25 m grid resolution was the smallest unit that achieved complete stabilization of the crown cover (Figure 3.4B). Practically, it is often convenient to select a grid resolution that divides evenly into 100 (White et al. 2013a), so resolutions of 20 and 25 m seemed good choices and could have been matched to ground plot area or preexisting grid resolutions.

With a 3 m height threshold and a 25 m grid resolution, we observed for the holdout data that the 2018HD and LD surveys were very similar with an R^2 of 0.98, RMSE of 5%, and no bias (Figure 3.7). The 2016LD survey was more different with R^2 of 0.97, RMSE of 7%, and bias of 4%, which might be interpreted as cover opening between 2016 and 2018.

3.6 Discussion

We found that the selection of a height threshold and grid resolution can improve the repeatability of the crown cover measurements in multi-temporal LiDAR surveys. While the grid resolution had a very large impact on performance indicators, it was mostly limited to small resolutions (<7 m) that are less common in area-based approaches. It is, however, more

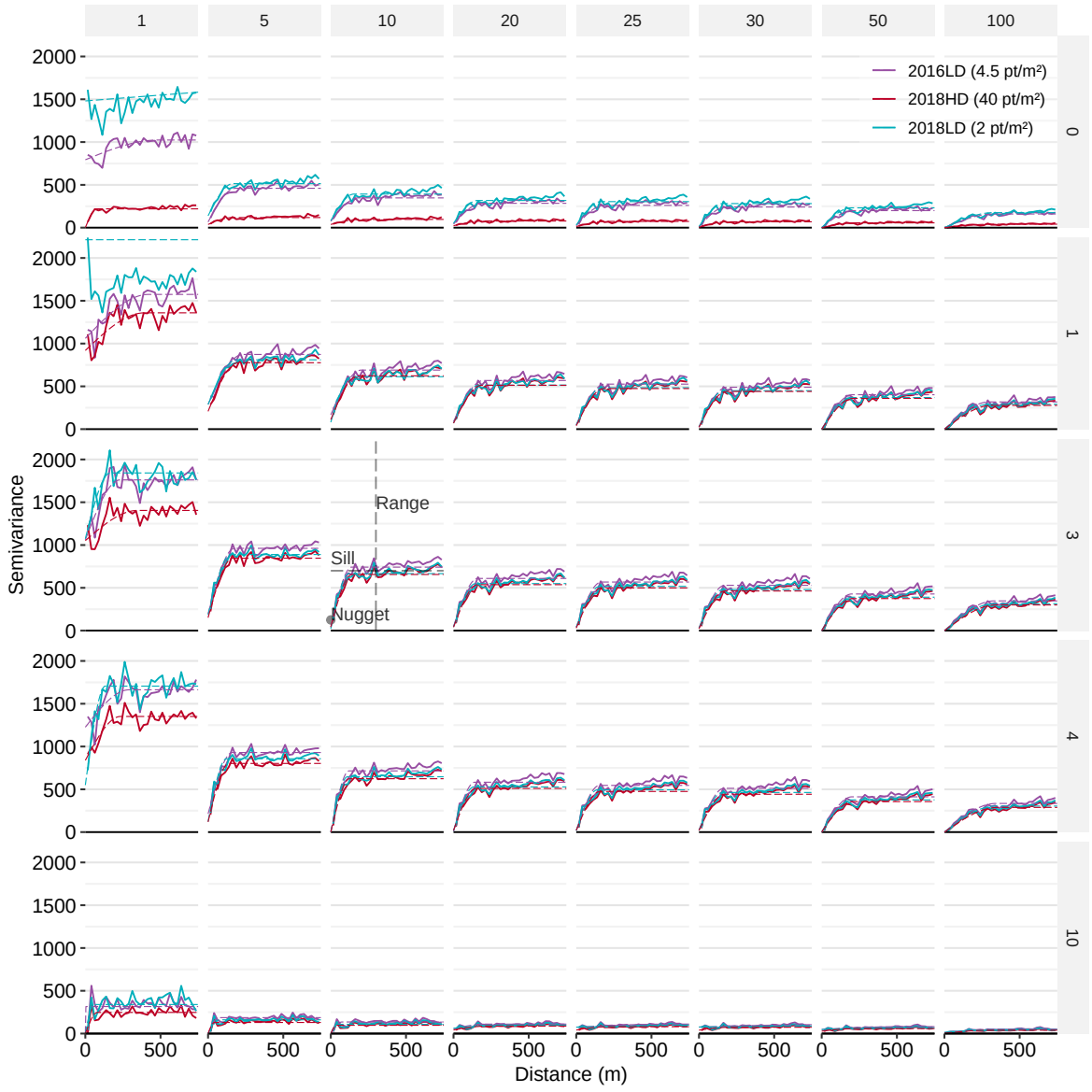

FIGURE 3.6 – Experimental variogram of crown cover for selected grid resolutions (columns) and height thresholds (rows) using holdout data. The dashed lines show the corresponding fitted theoretical spherical variogram. Range, sill, and nugget are illustrated for reference.

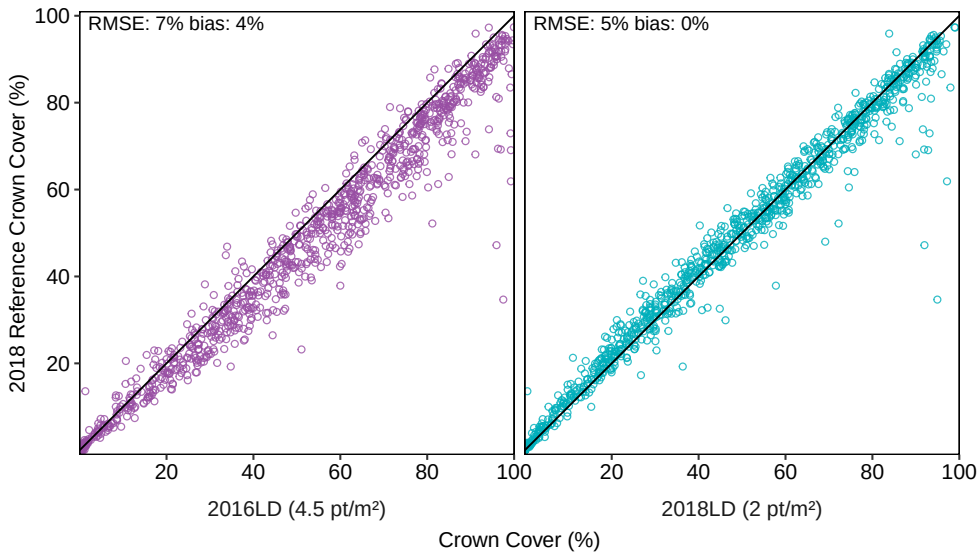

FIGURE 3.7 – Comparison of crown cover from the holdout data against the 2018HD LiDAR survey using a 3 m height threshold and 25 m grid resolution.

common to use low height thresholds (<3 m) which produced volatile crown cover estimates, especially when only ground returns were used (0 m height threshold).

3.6.1 Repeatability

The error between the 2018 surveys was 5% RMSE and 0% bias, while 2 years-apart surveys had a 7% RMSE and 4% bias by using a height threshold of 3 m and a grid resolution of 25 m. The decision of using a slightly different grid resolution or the 4 m height threshold had an impact on bias and RMSE of less than 1% but using a much smaller grid (e.g. 1 m), or a much lower height threshold (e.g. 0 m) made the survey much less comparable because it inflated the bias beyond 10% and the RMSE close to 30%. We conclude that multi-temporal LiDAR surveys can provide a repeatable measurement of crown cover, but the selection of the appropriate post-survey parameters is an important decision.

The general 4% decrease in crown cover between the 2016LD and 2018HD suggested that the forest opened, which we doubted. Forest openings can be attributed to individual or group mortality, epidemics, windthrow, logging, or other non-replacing stand disturbances (Kneeshaw and Bergeron 1998 ; Coops et al. 2020). While these processes take place in the area, a general opening of the forest cover does not seem to correspond to the ecological processes in place and we did not observe any important logging activity. Furthermore, while some non-replacing stand disturbances can be small, most of them would have affected the complete area of the grid (1/16 ha). However early insect infestation, such as the spruce budworm known to be endemic in the area, could have reduced the foliage. The 2016LD survey

was also conducted earlier in the growing season than the 2018 surveys. A different timing could lead to measuring different canopy and understory leaf development and modify the crown cover measurement. Higher maximal scan angles can also result in the overestimation of crown cover in the 2016LD (Korhonen et al. 2011 ; Liu et al. 2018 ; Roussel et al. 2018). While transformations can be applied to the raw point cloud to correct for biased crown cover estimates (Liu et al. 2018 ; Roussel et al. 2018), the relation with the post-survey parameters remains to be studied.

The differences in the variograms (Figure 3.6) illustrated that the choice of parameters also impacted how each survey reflected the spatial structure of crown cover. Low thresholds or small resolutions were more likely to produce structures of spatial correlation that were less repeatable across LiDAR surveys. Using a 0 m threshold created differences in the observed spatial organization of crown cover that remained even at 100 m resolution.

Korhonen et al. (2011) reported an R^2 of 0.73 when they compared one-year apart crown covers using a height threshold of 1.3 m and resolutions between 20 and 40 m (to match ground plot sizes). In comparison, the R^2 for the 2016LD and 2018LD at 1 m height threshold were 0.96 and 0.97 respectively. These differences could be explained by vegetation growth, disturbances, and lidar parameters.

3.6.2 Height Threshold

The height threshold had an impact on the repeatability of crown cover measurements across surveys. The absence of a threshold (0 m) produced volatile estimates of crown cover. As a result, low height thresholds, especially when computed on small grid size, produced crown cover estimates with a higher bias, RMSE, and semi-variance when compared to the reference LiDAR survey.

The height threshold skewed the distribution of crown covers for the study area. Lower height threshold produced more closed cover observations, but more importantly, they almost never produced open areas. While in itself this could reflect the lack of open areas, it overrepresented closed- canopy stands and prevented the use of the full range of possible crown cover values. When modeling forest attributes, for forest volume estimates, for example, the selection of variables that can contribute to a prediction is central, and most methods from generalized linear models to machine learning models generally greatly benefit from variables that span a wider range.

We hypothesize that one of the reasons for the volatility of crown cover measurements with a low height threshold is that the ground classification algorithm might have an increasingly large effect as the threshold approached the ground, especially at 0 m, where the points reaching 0 m are strictly those identified by the algorithm. This could explain the very large differences between the three surveys at 0 m, although they were all classified using the same

algorithm. In addition to the inherent sensor errors, the identification of ground points can add around 15–20 cm of error (RMSE) depending on the slope of the terrain and the algorithm used (Moudrý et al. 2020).

3.6.3 Grid Resolution

Grid resolution did not modify bias between surveys except at resolutions smaller than 10 m. RMSE was inflated for grid resolutions smaller than 7 m and generally decreased with larger grid resolutions. Extending grid resolutions beyond 25 m did not change the crown cover estimates as observed with the variance of the lagged crown cover difference. There were no formal indicators to constrain the grid resolution beyond the reduction of variation that we could rely on. All our indicators improved when the grid resolution increased, which could lead to the selection of larger resolutions and reduce the expression of variation on the landscape. Hengl (2006) suggested Shannon's information criteria to balance pixel variability and information, but further work would be required to adapt it to crown cover measurements.

3.6.4 Skewness and Variance of Lagged Difference

Using the variance of lagged difference and skewness can guide the selection of a height threshold and grid resolution. They present the advantage of being available in the absence of a reference survey. This is not the case of bias and RMSE, which is convenient when comparing archived LiDAR surveys that do not have common reference ground data. While other indicators could be used to decide on optimal height threshold and grid resolution, we think these indicators are well suited to predictive methods, such as volume estimation.

3.6.5 Practical Implications

The influence of the height threshold on the resulting crown cover should prompt a discussion and ideally an evaluation of the optimal selection of crown cover height threshold and criteria for which to optimize. Further work is required to compare the effect of post-survey parameters on field observations and assess the practicality of raising the height threshold to 3 m or increasing the grid resolution, for example.

The ecology of the study area should also influence the selection of the post-survey parameters. For example, the dimensions of the crowns and the maximal height of the vegetation should probably affect how surveys can be compared. Larger crowns could impose a larger grid resolution ; areas with taller canopy and understory could require a higher height threshold. The ground point classification algorithm performance can depend on the environment where it is used. For example, Moudrý et al. (2020) found that low vegetation could be classified as ground points in steppes. Furthermore, the height threshold might be established in function of the season and phenology : a thicker understory in the summer and sparser in spring and fall

might require an adapted height threshold. We should also consider the possibility that post-survey parameters could have a larger impact in different study areas with different crown size and vegetation height, for example. The parameters selected in this study (3 m height threshold and 25 m grid resolution) could potentially apply to similar ecosystems within the boreal forest, and beyond.

Given the impact of small grid size on the error induced between surveys, we recommend a grid size of at least 10 m and a height threshold of at least 2 m to provide reliable crown cover estimates in ecosystems comparable to this study, although we found 3 m height threshold and 25 m grid resolution best suited our objectives. When in need of a smaller grid resolution, for compatibility with other data, for example, the use of a moving window could be explored.

In this study, crown cover estimates benefited from a raised height threshold : it made the measurement more comparable to other surveys. Increased grid resolution also provided more repeatable estimates, but decreased the variability of the territory as illustrated by the variograms (Figure 3.6). When comparing the 2016LD survey to the 2018HD survey, the conclusions on crown cover evolution would have been completely different had we chosen a 0 m or 1 m height threshold. Using a 0 m height threshold, the negative bias indicated that vegetation cover closed, while other thresholds rather had a positive bias that showed that the vegetation was opening (Figure 3.5). This study shows the importance of both grid resolution and height threshold parameters for the repeatability of the crown cover measurements.

3.7 Conclusion

Comparing crown cover from multi-temporal LiDAR surveys introduces additional sources of error : different survey and post-survey parameters. Finding an optimal height threshold and grid resolution can minimize the impact of changing LiDAR survey parameters. We found that using a 3 m threshold and 25 m grid resolution provided the right balance to describe the variability of the study area and reduced crown cover to 7–5% RMSE and bias to 4–0%. These parameters could be reused in comparable ecosystems within the boreal shield ecozone.

Conclusion générale

Cette thèse vise à contribuer à l'aménagement écosystémique des forêts en améliorant l'inventaire de la structure forestière par lidar aéroporté. Un meilleur inventaire forestier permet de constater l'écart entre la forêt naturelle et la forêt aménagée, ce que l'aménagement écosystémique vise à réduire. Une meilleure connaissance de l'état de la forêt permet aussi de sélectionner les traitements sylvicoles adaptés aux particularités des écosystèmes, ce qui peut contribuer à réduire les changements induits par l'aménagement forestier. Les chapitres présentés se concentrent sur la caractérisation d'indicateurs de la variabilité forestière, puisqu'il s'agit d'un aspect négligé de l'inventaire.

Le premier chapitre confirme que le lidar peut être utilisé pour prédire l'âge moyen à l'échelle des placettes-échantillons. L'âge est une variable importante pour décrire les écosystèmes, quantifier les stocks ligneux et établir les prescriptions sylvicoles. Rappelons que l'âge est actuellement imputé à partir d'un petit nombre d'échantillons ou encore interprété visuellement à partir de photographies aériennes. Ces deux méthodes tendent à homogénéiser notre perception de l'âge à travers le territoire, en plus de ne pas fournir d'estimés d'erreur.

La méthode k-NN, combinée à des descripteurs associés à la structure forestière et à la qualité de station estimés par lidar aéroporté, nous a permis de prédire l'âge avec une erreur absolue de 8.8 ans ($R^2 = 0.83$, RMSE = 19%), ce qui n'avait jamais été rapporté. En utilisant uniquement les descripteurs de la structure forestière, la performance diminuait légèrement avec une erreur absolue de 10.1 ans ($R^2 = 0.74$, RMSE = 22%). À l'échelle de la placette, le 95^{e} centile de la hauteur et les paramètres de la distribution de Weibull modélisés sur tous les retours, étaient les descripteurs de structure les plus importants, alors que les descripteurs de station étaient l'altitude, la longueur de pente arrière et l'aire du bassin versant. Ces résultats montrent l'intérêt d'associer des variables issues du lidar pour prédire l'âge localement.

Prédire l'âge sur de plus petites superficies permet de mieux représenter la variabilité et la diversité des âges sur le territoire. En améliorant la disponibilité de cette variable à l'échelle du territoire sur des pixels d'une grandeur équivalente à celle d'une placette-échantillon, l'aménagiste serait en mesure de faire des prescriptions plus fines, adaptées à l'ensemble de la variabilité de la forêt. Par exemple, une cartographie de l'hétérogénéité de l'âge des pixels pourrait servir à cibler et prioriser les peuplements où il est nécessaire de maintenir une

structure d'âge irrégulière.

Une estimation plus raffinée de l'âge peut améliorer la sélection de traitements sylvicoles et permet aussi de mieux refléter l'état des écosystèmes ou une sélection d'habitat pour certaines espèces fauniques. Toutefois, comme nous le montrons dans le chapitre 3 pour la densité de couvert, il existe une limite à la résolution utilisable avec le lidar pour une densité de points donnée. Conséquemment, faire une prédiction de l'âge par arbre ou encore par petits bouquets nécessiterait probablement des densités de points allant au-delà de ce qui est techniquement possible à l'échelle de la province.

Alors que l'inventaire de l'âge par les méthodes traditionnelles est optimisé pour le calcul de volume et des considérations terrain, il serait intéressant de vérifier s'il est possibe d'optimiser la sélection des placettes-échantillon afin d'en augmenter la représentativité pour le lidar. Par exemple, utiliser des indicateurs de structure comme Weibull pour sélectionner les sites de mesure d'âge sur le terrain ou encore concentrer le nombre d'échantillons mesurés sur certaines placettes afin d'avoir un meilleur portrait de la variabilité de l'âge à l'intérieur de la placette. La sélection du nombre d'arbres à échantillonner à l'intérieur d'une placette pourrait en fait être déterminée par apprentissage actif (Settles 2009). L'apprentissage actif permet de maximiser l'apprentissage d'un modèle en déterminant, au fur et à mesure de la collecte de données, quelles sont les zones les plus incertaines pour l'algorithme de prédiction de l'âge et de privilégier ces zones pour la collecte de données.

Plusieurs éléments méthodologiques ont évolué depuis la publication de ce premier chapitre. Par exemple, la méthode k-NN ne permet pas de tirer des conclusions sur l'effet des variables du modèle sur l'âge. Nous avions donc utilisé la méthode de bootstrap pour générer la distribution de l'importance des variables. Des méthodes comme *Local Interpretable Model-Agnostic Explanations* (LIME) ou encore *SHapley Additive exPlanations* (SHAP) sont maintenant plus courantes pour faire de l'inférence sur des méthodes non-paramétriques (Ribeiro et al. 2016 ; Lundberg and Lee 2017). La réduction à 400 m^2 de la superficie sur laquelle l'âge est estimé permet de mieux refléter la variabilité de la forêt, d'autant que 70% des placettes présentaient un écart-type de moins de 10 ans. Toutefois, pour les placettes les plus variables dans lesquelles on peut soupçonner une structure irrégulière, on pourrait suggérer de faire l'imputation d'indicateurs de variabilité comme l'écart-type de l'âge ou encore d'autres indicateurs d'intérêt comme l'âge dominant, d'autant plus que la méthode k-NN se prête bien à l'imputation de plusieurs variables simultanées. Il serait aussi intéressant de vérifier si la précision de 8.8 ans, qui semble suffisante pour des objectifs opérationnels, est maintenue sur des grands territoires plus hétérogènes avec une plus faible densité d'échantillons, ce qui semble être confirmé par Maltamo et al. (2020). Une approche permettant de généraliser le modèle dans l'espace devrait maintenant inclure la validation croisée par blocs (Roberts et al. 2017b) pour tenir compte de l'autocorrélation spatiale, comme on l'utilise dans le troisième chapitre.

Une revue récente des références à l'article montre que les résultats sont utilisés par la communauté scientifique pour soutenir la capacité du lidar à prédire des attributs forestiers et aussi pour développer des méthodes applicables à des densités de mesures d'âges inférieures. À ce jour, la méthode a peut-être été utilisée pour la prédiction d'âges dans d'autres juridictions, mais cette situation n'est pas apparente dans les articles scientifiques consultés.

Le second chapitre associe pour la première fois la distribution verticale de retours lidar à des caractéristiques du peuplement grâce à des méthodes de modélisation de données fonctionnelles. Cette méthode permet de confirmer le lien entre la distribution verticale du lidar aéroporté et la composition, la densité de couvert et l'âge, ces variables expliquant jusqu'à 47% de la variabilité de la distribution verticale des retours lidar. Nous avons ainsi discriminé trois groupes de distributions verticales des retours : les peuplements dominés par le sapin baumier et le bouleau à papier présentaient des distributions centrées autour de 50% de la hauteur, alors que les épinettes blanche et noire, présentaient des accumulations de leur distribution autour de 30% de la hauteur du peuplement. Les peuplements dominés par le peuplier faux-tremble affichaient la distribution verticale la plus uniforme. Un couvert plus dense était associé à une concentration des retours lidar autour de 50% de la hauteur des peuplements. Une augmentation de l'âge était associée à une distribution des points lidar proportionellement plus élevée dans le peuplement jusqu'à 50–70 ans, puis la distribution se stabilisait et redescendait à 90–120 ans.

Le modèle du chapitre 2 est une première étape vers une compréhension plus profonde de la relation entre les espèces et la distribution verticale de leurs retours. Les résultats obtenus démontrent l'intérêt d'approfondir l'étude de la signature du peuplement (la distribution verticale des retours lidar) à la fois pour la compréhension, l'interprétation et plus largement de la prédiction des signatures. Pour développer la méthode, nous avons limité notre analyse à des peuplements de structure régulière dont la composition était dominée par une seule espèce, ce qui en limite pour l'instant l'intérêt opérationnel. Pour rendre les résultats utilisables de manière opérationnelle, nous devrions pouvoir reproduire les conclusions avec d'autres espèces, dans des peuplements d'espèces mélangées, de structure irrégulière, dans d'autres conditions environnementales et d'acquisition. Les conditions de croissance des espèces ont une influence variable sur la structure verticale de la végétation (Power et al. 2012 ; Power et al. 2014), ce qui devrait se refléter dans les signatures lidar.

Le potentiel d'utilisation apparaît grand puisqu'une meilleure compréhension de l'association entre la signature verticale et les caractéristiques du peuplement pourrait contribuer à l'identification d'espèces. On pourrait ainsi utiliser le lidar pour assister le photo-interprète lors de l'identification des espèces forestières dominantes, comme on le fait déjà pour les hauteurs d'arbres et de la densité de couvert.

Cette compréhension améliorée suggère aussi que les modèles de prédiction basés sur des

métriques lidar, comme les diagnostics sylvicoles et les calculs de volume, pourraient être améliorés s'ils incluaient de l'information sur les espèces et l'âge puisque des structures similaires peuvent être expliquées par des valeurs bien différentes. En effet, des espèces différentes d'âge différents pourraient présenter des caractéristiques très similaires lorsque les peuplements sont décrits avec un nombre limité de variables. Par exemple, un jeune peuplement de sapin baumier pourrait présenter des caractéristiques plus similaires à celles d'un peuplement d'épinette noire mature qu'à un autre peuplement de sapin baumier plus âgé. Ces résultats laissent ainsi à penser que l'utilisation d'indicateurs de structure comme le ratio de la hauteur moyenne sur la hauteur maximale des premiers retours, ou encore la variance sur la hauteur moyenne des premiers retours (Bégin et al. 2020) pourraient être améliorés et possiblement généralisés si on les considérait notamment en fonction de la composition et de la densité de couvert qui en sont présentement exclus. Ces résultats suggèrent également de vérifier si les prédictions dendrométriques basées sur des quantiles de distribution comme la hauteur (White et al. 2013a) ne seraient pas sensibles aux variations de la composition, de l'âge et de la densité de couvert.

Certaines des limites du chapitre 1 sont adressées au chapitre 2. Par exemple, la représentation de la distribution verticale des retours lidar avec la distribution de Weibull à trois paramètres nécessite le retrait des deux premiers mètres sans quoi la distribution ne peut être ajustée convenablement par la méthode des moindres carrés. Par ailleurs, la méthode k-NN permet d'identifier l'importance relative des variables, mais pas d'en connaître l'effet direct sur l'âge. Le chapitre 2 permet l'interprétation complète de la distribution par la combinaison des GLM fonctionnels et du test graphique de signifiance. La distribution verticale du coefficient de détermination (R^2) nous donne la proportion de variance expliquée par chacun des modèles, ce qui permet de confirmer l'importance (ou l'absence) de contribution des variables et d'identifier des hauteurs plus discriminantes.

Le troisième chapitre porte sur la mesure de densité de couvert, la principale variable de structure horizontale et la plus importante, après la hauteur, pour le calcul du volume ligneux. Les résultats démontrent que la sélection des paramètres pour la mesure de la densité de couvert joue un rôle dans la capacité à répéter des mesures entre les acquisitions lidar. En sélectionnant une hauteur seuil de 3 m et une résolution de grille de 25 m, nous avons trouvé que la RMSE de la densité était de 5% et 7% et le biais de 0% et 4% entre des relevés conduits la même année et deux ans plus tôt, respectivement. Certaines valeurs de seuil de hauteur et de résolution de grille étaient mieux adaptées à refléter l'ensemble de la variabilité du couvert et d'autres combinaisons pouvaient détériorer les valeurs de densité de couvert estimées par lidar au point de modifier la manière dont l'évolution de la structure pouvait être interprétée. Ces résultats indiquent que les estimations et les comparaisons de densité de couvert entre deux acquisitions lidar, qu'elles soient à des moments différents ou sur des territoires différents, nécessitent de s'attarder à la sélection des paramètres post-survol, en

plus des paramètres du survol. Ces résultats constituent une étape vers la régularisation des estimés de densité de couvert.

Le chapitre 3 documente l'effet de deux paramètres post-survol et propose des indicateurs d'aide à la décision qui sont indépendant d'un survol de référence. L'effet du seuil de hauteur avait peu été étudié et aucune étude, à notre connaissance, ne permettait d'aider à prendre une décision sur le paramètre optimal. On observe d'ailleurs dans la littérature une diversité de seuils de hauteurs (White et al. 2013), incluant le très volatile seuil de 0 m tel que nous l'avons aussi utilisé dans le premier chapitre pour le calcul de la pénétration du lidar (la distribution de Weibull utilisait un seuil de 2 m). Le troisième chapitre touche aussi aux limites de résolution du lidar puisqu'on voit qu'une trop petite grille élimine la structure de corrélation spatiale à l'échelle du paysage et introduit une variabilité qui n'est pas reproductible entre les survols et qui est donc due à des idiosyncrasies du survol. Il pourrait s'agir de la limite d'observation de notre outil de mesure, le lidar, du moins pour la densité de couvert. Par contre, on observe que si l'on choisit les bons paramètres, par exemple en optimisant la symétrie de la distribution à travers le territoire, alors les mesures sont davantage reproductibles entre les survols avec un minimum d'erreur et de biais. Il est probable que l'utilisation des corrections, en particulier de l'angle de balayage, puisse aussi réduire les effets du survol et rendre les mesures plus comparables. L'effet de la phénologie limite probablement la répétabilité des survols puisque la synchronisation exacte de l'état de la végétation est difficile, voire impossible. Aussi, si les conditions phénologiques affectent les mesures de densité de couvert, on peut penser qu'elles peuvent avoir un impact sur les métriques lidar utilisées dans les méthodes de prédictions comme les modèles de volume forestier. Il y aurait probablement lieu de considérer la période de vol dans les modèles dendrométriques et non seulement les paramètres de survols, mais cette question nous a semblé peu étudiée.

Il serait aussi intéressant de confirmer les résultats du chapitre 3 sur de plus grands territoires et de les appliquer à la prédiction de volume. En particulier, pour vérifier si les objectifs de symétrie et de variance que nous avons utilisés peuvent être transférés à d'autres écosystèmes et si l'utilisation de toute l'amplitude de variation de la densité de couvert peut améliorer l'estimation du volume.

Cette thèse présente quelques avenues pratiques pour utiliser le lidar afin de caractériser des indicateurs de la variabilité des écosystèmes forestiers. Nous avons montré le potentiel de l'agrégation des retours lidar à l'échelle du peuplement pour décrire la structure forestière en associant la distribution verticale des retours lidar à l'espèce, l'âge et la densité (chapitre 2). Le lidar permet aussi de réduire l'unité de prédiction et ainsi mieux refléter la variabilité des écosystèmes forestiers (chapitres 1 et 3). Toutefois, les trop petites unités d'inventaire tendent à être plus volatiles et sujettes à la variabilité idiosyncratique du lidar, qui masque alors la variabilité intrinsèque des écosystèmes (chapitre 3). Une meilleure compréhension de la structure verticale et de la variabilité des écosystèmes devrait permettre de mieux suivre

l'évolution de la forêt et aider la prise de décision pour l'aménagement forestier écosystémique.

Références

10 Aber JD (1979) Foliage-Height Profiles and Succession in Northern Hardwood Forests. Ecology 60 :18–23. https://doi.org/10.2307/1936462

Alain D, Boudreault J-F, Brochu M-A, et al (2019) Norme d'inventaire écoforestier - placettes-échantillons temporaires. Ministère des Forêts, de la Faune et des Parcs, Secteur des forêts, Direction des inventaires forestiers

Anderson MJ, Robinson J (2001) Permutation Tests for Linear Models. Australian & New Zealand Journal of Statistics 43 :75–88. https://doi.org/10.1111/1467-842X.00156

Archer KJ, Kimes RV (2008) Empirical characterization of random forest variable importance measures. Computational Statistics & Data Analysis 52 :2249–2260. https://doi.org/10.1016/j.csda.2007.08.015

Assmann E (1970) The principles of forest yield study : studies in the organic production, structure, increment, and yield of forest stands. Pergamon Press

Axelsson A, Lindberg E, Olsson H (2018) Exploring Multispectral ALS Data for Tree Species Classification. Remote Sensing 10 :183. https://doi.org/10.3390/rs10020183

BANQ (2018) Les premières photographies aériennes du Québec. https://www.banq.qc.ca/archives/entrez_archives/branche_histoire/documents_iconographiques/photographies-aeriennes/index.html. Accessed 9 Jan 2021

Bässler C, Stadler J, Müller J, et al (2010) LiDAR as a rapid tool to predict forest habitat types in Natura 2000 networks. Biodiversity and Conservation 20 :465–481. https://doi.org/10.1007/s10531-010-9959-x

Bassow SL, Bazzaz FA (1997) Intra- and inter-specific variation in canopy photosynthesis in a mixed deciduous forest. Oecologia 109 :507–515. https://doi.org/10.1007/s004420050111

Bater CW, Wulder MA, Coops NC, et al (2011) Stability of Sample-Based Scanning-LiDAR-Derived Vegetation Metrics for Forest Monitoring. IEEE Transactions on Geoscience and

Remote Sensing 49 :2385–2392. https://doi.org/10.1109/TGRS.2010.2099232

Bégin J, Ruel J-C, Leboeuf A, et al (2020) Valorisation de l'information structurale du LiDAR aéroporté des points de vue sylvicole et dendrométrique. Université Laval

Beland M, Parker G, Sparrow B, et al (2019) On promoting the use of lidar systems in forest ecosystem research. Forest Ecology and Management 450 :117484. https://doi.org/10.1016/j.foreco.2019.117484

Bélanger L, Paquette S, Morel S, et al (1995) Indices de qualité de station du sapin baumier dans le sous-domaine écologique de la sapinière à bouleau blanc humide. The Forestry Chronicle 71 :317–325. https://doi.org/10.5558/tfc71317-3

Beven KJ, Kirkby MJ (1979) A physically based, variable contributing area model of basin hydrology. Hydrological Sciences Bulletin 24 :43–69. https://doi.org/10.1080/02626667909491834

Bi H, Fox JC, Li Y, et al (2012) Evaluation of nonlinear equations for predicting diameter from tree height. Canadian Journal of Forest Research 42 :789–806. https://doi.org/10.1139/x2012-019

Bivand RS, Pebesma EJ, Gómez-Rubio V (2008) Applied Spatial Data Analysis with R. Springer New York, New York, NY

Böhner J, Antonić O (2009) Chapter 8 Land-Surface Parameters Specific to Topo-Climatology. In : Geomorphometry Concepts, Software, Applications. Elsevier, pp 195–226

Boucher D, Grandpré LD, Gauthier S (2003) Développement d'un outil de classification de la structure des peuplements et comparaison de deux territoires de la pessière à mousses du Québec. Forestry Chronicle 79 :318–328

Breiman L (2001) Random Forests. Machine Learning 45 :5–32. https://doi.org/10.1023/A:1010933404324

Breusch TS, Pagan AR (1979) A Simple Test for Heteroscedasticity and Random Coefficient Variation. Econometrica 47 :1287–1294. https://doi.org/10.2307/1911963

Brokaw NVL, Lent RA (1999) Maintaining Biodiversity in Forest Ecosystems. In : Hunter Jr. ML (ed). Cambridge University Press, pp 373–399

Budei BC, St-Onge B (2018) Variability of Multispectral Lidar 3D and Intensity Features with Individual Tree Height and Its Influence on Needleleaf Tree Species Identification. Canadian Journal of Remote Sensing 44 :263–286. https://doi.org/10.1080/07038992.2018.1478724

Budei BC, St-Onge B, Hopkinson C, Audet F-A (2018) Identifying the genus or species of individual trees using a three-wavelength airborne lidar system. Remote Sensing of

Environment 204 :632–647. https://doi.org/10.1016/j.rse.2017.09.037

Burkhart HE, Avery TE, Bullock BP (2019) Forest measurements

Cao L, Coops NC, Hermosilla T, et al (2014) Using Small-Footprint Discrete and Full-Waveform Airborne LiDAR Metrics to Estimate Total Biomass and Biomass Components in Subtropical Forests. Remote Sensing 6 :7110–7135. https://doi.org/10.3390/rs6087110

Chasmer L, Hopkinson C, Treitz P (2006) Investigating laser pulse penetration through a conifer canopy by integrating airborne and terrestrial lidar. Canadian Journal of Remote Sensing 32 :116–125. https://doi.org/10.5589/m06-011

Coops NC, Shang C, Wulder MA, et al (2020) Change in forest condition : Characterizing non-stand replacing disturbances using time series satellite imagery. Forest Ecology and Management 474 :118370. https://doi.org/10.1016/j.foreco.2020.118370

Coops NC, Varhola A, Bater CW, et al (2009) Assessing differences in tree and stand structure following beetle infestation using lidar data. Canadian Journal of Remote Sensing 35 :497–508. https://doi.org/10.5589/m10-005

Coops N, Hilker T, Wulder M, et al (2007) Estimating canopy structure of Douglas-fir forest stands from discrete-return LiDAR. Trees - Structure and Function 21 :295–310. https://doi.org/10.1007/s00468-006-0119-6

Côté G (2006) Élaboration d'une typologie forestière adaptée à la forêt boréale irrégulière. Mémoire de M. Sc., Faculté de foresterie et de géomatique, Université Laval

Côté J-F, Fournier RA, Luther JE, van Lier OR (2018) Fine-scale three-dimensional modeling of boreal forest plots to improve forest characterization with remote sensing. Remote Sensing of Environment 219 :99–114. https://doi.org/10.1016/j.rse.2018.09.026

Crespo-Peremarch P, Fournier RA, Nguyen V-T, et al (2020) A comparative assessment of the vertical distribution of forest components using full-waveform airborne, discrete airborne and discrete terrestrial laser scanning data. Forest Ecology and Management 473 :118268. https://doi.org/10.1016/j.foreco.2020.118268

Crookston NL, Finley AO (2008) yaImpute : An R Package for kNN Imputation. Journal of Statistical Software 23 :1–16

Cutler DR, Edwards TC, Beard KH, et al (2007) Random Forests for Classification in Ecology. Ecology 88 :2783–2792. https://doi.org/10.1890/07-0539.1

Dale MRT, Fortin M-J (2015) Spatial analysis : a guide for ecologists. Cambridge University Press, Cambridge

De Pury DGG, Farquhar GD (1997) Simple scaling of photosynthesis from leaves to canopies without the errors of big-leaf models. Plant, Cell & Environment 20 :537–557. https://doi.org/10.1111/j.1365-3040.1997.00094.x

Ellsworth DS, Reich PB (1993) Canopy structure and vertical patterns of photosynthesis and related leaf traits in a deciduous forest. Oecologia 96 :169–178. https://doi.org/10.1007/BF00317729

ESRI (2019) Estimating forest canopy density and height—Help | ArcGIS Desktop. https://desktop.arcgis.com/en/arcmap/latest/manage-data/las-dataset/lidar-solutions-estimating-forest-density-and-height.htm. Accessed 11 Dec 2020

Falkowski MJ, Evans JS, Martinuzzi S, et al (2009) Characterizing forest succession with lidar data : An evaluation for the Inland Northwest, USA. Remote Sensing of Environment 113 :946–956. https://doi.org/10.1016/j.rse.2009.01.003

Falkowski MJ, Gessler PE, Morgan P, et al (2005) Characterizing and mapping forest fire fuels using ASTER imagery and gradient modeling. Forest Ecology and Management 217 :129–146. https://doi.org/10.1016/j.foreco.2005.06.013

FAO (2015) Knowledge reference for national forest assessments. 152

Farrar JL (1995) Trees in Canada. Fitzhenry & Whiteside Ltd., Ottawa

Fassnacht FE, Latifi H, Stereńczak K, et al (2016) Review of studies on tree species classification from remotely sensed data. Remote Sensing of Environment 186 :64–87. https://doi.org/10.1016/j.rse.2016.08.013

Fedrigo M, Newnham GJ, Coops NC, et al (2018) Predicting temperate forest stand types using only structural profiles from discrete return airborne lidar. ISPRS Journal of Photogrammetry and Remote Sensing 136 :106–119. https://doi.org/10.1016/j.isprsjprs.2017.11.018

Fedrigo M, Stewart SB, Roxburgh SH, et al (2019) Predictive Ecosystem Mapping of South-Eastern Australian Temperate Forests Using Lidar-Derived Structural Profiles and Species Distribution Models. Remote Sensing 11 :93. https://doi.org/10.3390/rs11010093

Frazer GW, Magnussen S, Wulder MA, Niemann KO (2011) Simulated impact of sample plot size and co-registration error on the accuracy and uncertainty of LiDAR-derived estimates of forest stand biomass. Remote Sensing of Environment 115 :636–649. https://doi.org/10.1016/j.rse.2010.10.008

Freedman D, Lane D (1983) A Nonstochastic Interpretation of Reported Significance Levels. Journal of Business & Economic Statistics 1 :292–298. https://doi.org/10.1080/07350015.1983.10509354

Gauthier S, Vaillancourt M-A, Kneeshaw D, et al (2008) Aménagement forestier écosystémique. PUQ

Gonsamo A, D'odorico P, Pellikka P (2013) Measuring fractional forest canopy element cover and openness – definitions and methodologies revisited. Oikos 122 :1283–1291. https ://doi.org/https://doi.org/10.1111/j.1600-0706.2013.00369.x

Grömping U (2009) Variable Importance Assessment in Regression : Linear Regression versus Random Forest. The American Statistician 63 :308–319. https://doi.org/10.1198/tast.2009.08199

Harding DJ, Lefsky MA, Parker GG, Blair JB (2001) Laser altimeter canopy height profiles : methods and validation for closed-canopy, broadleaf forests. Remote Sensing of Environment 76 :283–297. https://doi.org/10.1016/S0034-4257(00)00210-8

Hastie T, Tibshirani R, Friedman J (2009) The elements of statistical learning : data mining, inference, and prediction : Trevor Hastie, Robert Tibshirani, Jerome Friedman., 5th printing. Springer, New York

Heinzel J, Koch B (2011) Exploring full-waveform LiDAR parameters for tree species classification. International Journal of Applied Earth Observation and Geoinformation 13 :152–160. https://doi.org/10.1016/j.jag.2010.09.010

Heinzel J, Koch B (2012) Investigating multiple data sources for tree species classification in temperate forest and use for single tree delineation. International Journal of Applied Earth Observation and Geoinformation 18 :101–110. https://doi.org/10.1016/j.jag.2012.01.025

Hember RA, Kurz WA, Metsaranta JM, et al (2012) Accelerating regrowth of temperate-maritime forests due to environmental change. Global Change Biology 18 :2026–2040. https://doi.org/10.1111/j.1365-2486.2012.02669.x

Hengl T (2006) Finding the right pixel size. Computers & Geosciences 32 :1283–1298. https://doi.org/10.1016/j.cageo.2005.11.008

Hilker T, Leeuwen M van, Coops NC, et al (2010) Comparing canopy metrics derived from terrestrial and airborne laser scanning in a Douglas-fir dominated forest stand. Trees 24 :819–832. https://doi.org/10.1007/s00468-010-0452-7

Holmgren J, Nilsson M, Olsson H (2003) Simulating the effects of lidar scanning angle for estimation of mean tree height and canopy closure. Canadian Journal of Remote Sensing 29 :623–632. https://doi.org/10.5589/m03-030

Holmgren J, Persson Å (2004) Identifying species of individual trees using airborne laser scanner. Remote Sensing of Environment 90 :415–423. https://doi.org/10.1016/S0034-

4257(03)00140-8

Hovi A, Korhonen L, Vauhkonen J, Korpela I (2016) LiDAR waveform features for tree species classification and their sensitivity to tree- and acquisition related parameters. Remote Sensing of Environment 173 :224–237. https://doi.org/10.1016/j.rse.2015.08.019

Hudak AT, Crookston NL, Evans JS, et al (2008) Nearest neighbor imputation of species-level, plot-scale forest structure attributes from LiDAR data. Remote Sensing of Environment 112 :2232–2245. https://doi.org/10.1016/j.rse.2007.10.009

Isenburg M (2012) LAStools - efficient tools for LiDAR processing. Version 120301URL http://lastools.org

Kane VR, Bakker JD, McGaughey RJ, et al (2010a) Examining conifer canopy structural complexity across forest ages and elevations with LiDAR data. Canadian Journal of Forest Research 40 :774–787. https://doi.org/10.1139/X10-064

Kane VR, Gersonde RF, Lutz JA, et al (2011) Patch dynamics and the development of structural and spatial heterogeneity in Pacific Northwest forests. Canadian Journal of Forest Research 41 :2276–2291. https://doi.org/10.1139/x11-128

Kane VR, McGaughey RJ, Bakker JD, et al (2010b) Comparisons between field- and LiDAR-based measures of stand structural complexity. Can J For Res 40 :761–773. https://doi.org/10.1139/X10-024

Karna YK, Penman TD, Aponte C, et al (2020) Persistent changes in the horizontal and vertical canopy structure of fire-tolerant forests after severe fire as quantified using multi-temporal airborne lidar data. Forest Ecology and Management 472 :118255. https://doi.org/10.1016/j.foreco.2020.118255

Karna YK, Penman TD, Aponte C, Bennett LT (2019) Assessing Legacy Effects of Wildfires on the Crown Structure of Fire-Tolerant Eucalypt Trees Using Airborne LiDAR Data. Remote Sensing 11 :2433. https://doi.org/10.3390/rs11202433

Kim H-J, Tomppo E (2006) Model-based prediction error uncertainty estimation for k-nn method. Remote Sensing of Environment 104 :257–263. https://doi.org/10.1016/j.rse.2006.04.009

Kim S, Hinckley T, Briggs D (2011) Classifying individual tree genera using stepwise cluster analysis based on height and intensity metrics derived from airborne laser scanner data. Remote Sensing of Environment 115 :3329–3342. https://doi.org/10.1016/j.rse.2011.07.016

Kneeshaw DD, Bergeron Y (1998) Canopy Gap Characteristics and Tree Replacement in the Southeastern Boreal Forest. Ecology 79 :783–794. https://doi.org/10.1890/0012-

9658(1998)079%5B0783:CGCATR%5D2.0.CO;2

Kneeshaw D, Gauthier S (2003) Old growth in the boreal forest : A dynamic perspective at the stand and landscape level. Environmental Reviews 11 :S99–S114. https://doi.org/10.1139/a03-010

Koenig K, Höfle B (2016) Full-Waveform Airborne Laser Scanning in Vegetation Studies—A Review of Point Cloud and Waveform Features for Tree Species Classification. Forests 7 :198. https://doi.org/10.3390/f7090198

Korhonen L, Korpela I, Heiskanen J, Maltamo M (2011) Airborne discrete-return LIDAR data in the estimation of vertical canopy cover, angular canopy closure and leaf area index. Remote Sensing of Environment 115 :1065–1080. https://doi.org/10.1016/j.rse.2010.12.011

Lacointe A (2000) Carbon allocation among tree organs : a review of basic processes and representation in functional-structural tree models. Annals of Forest Science 57 :521–533. https://doi.org/10.1051/forest:2000139

Larson AJ, Lutz JA, Gersonde RF, et al (2008) Potential Site Productivity Influences the Rate of Forest Structural Development. Ecological Applications 18 :899–910. https://doi.org/10.1890/07-1191.1

LAStools (2019) Efficient LiDAR Processing Software

Leblanc M, Bélanger L (2000) La sapinière vierge de la forêt Montmorency et de sa région : une forêt boréale distincte. Ministère des Ressources naturelles du Québec

Leboeuf A, Vaillancourt É (2013b) Guide de photo-interprétation des essences forestières du Québec méridional (partie 2 et 3 : espèces feuillues et le rehaussement d'image). Bibliothèque et archives nationales du Québec, Québec

Leboeuf A, Vaillancourt É (2013a) Guide de photo-interprétation des essences forestières du Québec méridional (partie 1 : espèces résineuses). Bibliothèque et archives nationales du Québec, Québec

Lefsky MA, Cohen WB, Harding DJ, et al (2002) Lidar remote sensing of above-ground biomass in three biomes. Global Ecology and Biogeography 11 :393–399. https://doi.org/10.1046/j.1466-822x.2002.00303.x

Lefsky MA, Hudak AT, Cohen WB, Acker SA (2005) Geographic variability in lidar predictions of forest stand structure in the Pacific Northwest. Remote Sensing of Environment 95 :532–548

LeMay V, Maedel J, Coops NC (2008) Estimating stand structural details using nearest

neighbor analyses to link ground data, forest cover maps, and Landsat imagery. Remote Sensing of Environment 112 :2578–2591. https://doi.org/10.1016/j.rse.2007.12.007

Liaw A, Wiener M (2002) Classification and Regression by randomForest. R News 2 :18–22

Lim K, Treitz P, Wulder M, et al (2003) LiDAR Remote Sensing of Forest Structure. Progress in Physical Geography 27 :88–106. https://doi.org/10.1191/0309133303pp360ra

Liu J, Skidmore AK, Heurich M, Wang T (2017) Significant effect of topographic normalization of airborne LiDAR data on the retrieval of plant area index profile in mountainous forests. ISPRS Journal of Photogrammetry and Remote Sensing 132 :77–87. https://doi.org/10.1016/j.isprsjprs.2017.08.005

Liu J, Skidmore AK, Jones S, et al (2018) Large off-nadir scan angle of airborne LiDAR can severely affect the estimates of forest structure metrics. ISPRS Journal of Photogrammetry and Remote Sensing 136 :13–25. https://doi.org/10.1016/j.isprsjprs.2017.12.004

Lundberg SM, Lee S-I (2017) A Unified Approach to Interpreting Model Predictions. Advances in Neural Information Processing Systems 30 :4765–4774

MacArthur RH, Horn HS (1969) Foliage Profile by Vertical Measurements. Ecology 50 :802–804

Magnussen S, Eggermont P, LaRiccia VN (1999) Recovering Tree Heights from Airborne Laser Scanner Data. Forest Science 45 :407–422. https ://doi.org/https://doi.org/10.1093/forestscience/45.3.407

Maltamo M, Kinnunen H, Kangas A, Korhonen L (2020) Predicting stand age in managed forests using National Forest Inventory field data and airborne laser scanning. For Ecosyst 7 :44. https://doi.org/10.1186/s40663-020-00254-z

Maltamo M, Packalén P, Suvanto A, et al (2009) Combining ALS and NFI training data for forest management planning : a case study in Kuortane, Western Finland. European Journal of Forest Research 128 :305–317. https://doi.org/10.1007/s10342-009-0266-6

Maltamo M, Packalén P, Yu X, et al (2005) Identifying and quantifying structural characteristics of heterogeneous boreal forests using laser scanner data. Forest Ecology and Management 216 :41–50. https://doi.org/10.1016/j.foreco.2005.05.034

Martin-Ducup O (2017) Étude de la structure et de la dynamique des houppiers à partir de données de LIDAR terrestre. Phd, Université du Québec à Rimouski

Martin-Ducup O, Schneider R, Fournier RA (2016) Response of sugar maple (Acer saccharum, Marsh.) tree crown structure to competition in pure versus mixed stands. Forest Ecology

and Management 374 :20–32. https://doi.org/10.1016/j.foreco.2016.04.047

Mayer DG, Butler DG (1993) Statistical validation. Ecological Modelling 68 :21–32. https://doi.org/10.1016/0304-3800(93)90105-2

McRoberts RE (2009) Diagnostic tools for nearest neighbors techniques when used with satellite imagery. Remote Sensing of Environment 113 :489–499. https://doi.org/10.1016/j.rse.2008.06.015

McRoberts RE (2011) Satellite image-based maps : Scientific inference or pretty pictures ? Remote Sensing of Environment 115 :715–724. https://doi.org/10.1016/j.rse.2010.10.013

McRoberts RE (2012) Estimating forest attribute parameters for small areas using nearest neighbors techniques. Forest Ecology and Management 272 :3–12. https://doi.org/10.1016/j.foreco.2011.06.039

Mehtätalo L (2006) Eliminating the effect of overlapping crowns from aerial inventory estimates. Can J For Res/Rev can rech for 36 :1649–1660. https ://doi.org/https://doi.org/10.1139/x06-066

Meyer D, Dimitriadou E, Hornik K, et al (2019) e1071 : Misc functions of the department of statistics, probability theory group (formerly : E1071), TU wien

Moeur M, Stage AR (1995) Most Similar Neighbor : An Improved Sampling Inference Procedure for Natural Resource Planning. Forest Science 41 :337–359

Moudrý V, Klápště P, Fogl M, et al (2020) Assessment of LiDAR ground filtering algorithms for determining ground surface of non-natural terrain overgrown with forest and steppe vegetation. Measurement 150 :107047. https://doi.org/10.1016/j.measurement.2019.107047

Mrkvička T, Myllymäki M, Jílek M, Hahn U (2020) A one-way ANOVA test for functional data with graphical interpretation. Kybernetika 432–458. https://doi.org/10.14736/kyb-2020-3-0432

Mrkvička T, Roskovec T, Rost M (2019) A Nonparametric Graphical Tests of Significance in Functional GLM. Methodol Comput Appl Probab. https://doi.org/10.1007/s11009-019-09756-y

MRNFQ (2005) Forest resource protection and development objectives general forest management plans 2007-2012 :implementation document. Ministère des ressources naturelles, de la faune et des parcs, Québec

MRNQ (2007) Norme de photo-interprétation (version provisoire). Direction des inventaires

forestiers, Gouvernement du Québec

Muss JD, Mladenoff DJ, Townsend PA (2011) A pseudo-waveform technique to assess forest structure using discrete lidar data. Remote Sensing of Environment 115 :824–835. https://doi.org/10.1016/j.rse.2010.11.008

Myllymäki M, Mrkvička T (2020) GET : Global envelopes in R. arXiv :191106583 [statME]

Myllymäki M, Mrkvička T, Grabarnik P, et al (2017) Global envelope tests for spatial processes. Journal of the Royal Statistical Society B 79 :381–404. https://doi.org/10.1111/rssb.12172

Naesset E (2004) Practical large-scale forest stand inventory using a small-footprint airborne scanning laser. Scandinavian Journal of Forest Research 19 :164–179. https://doi.org/10.1080/02827580310019257

Næsset E (2004) Effects of different flying altitudes on biophysical stand properties estimated from canopy height and density measured with a small-footprint airborne scanning laser. Remote Sensing of Environment 91 :243–255. https://doi.org/10.1016/j.rse.2004.03.009

Newton AC (2007) Forest ecology and conservation : a handbook of techniques. Oxford University Press, USA

Nyström M, Holmgren J, Olsson H (2012) Prediction of tree biomass in the forest–tundra ecotone using airborne laser scanning. Remote Sensing of Environment 123 :271–279. https://doi.org/10.1016/j.rse.2012.03.008

Oliver CD, Larson BC (1996) Forest Stand Dynamics, Updated Edition. Wiley

Ørka HO, Næsset E, Bollandsås OM (2009) Classifying species of individual trees by intensity and structure features derived from airborne laser scanner data. Remote Sensing of Environment 113 :1163–1174. https://doi.org/10.1016/j.rse.2009.02.002

Palace MW, Sullivan FB, Ducey MJ, et al (2015) Estimating forest structure in a tropical forest using field measurements, a synthetic model and discrete return lidar data. Remote Sensing of Environment 161 :1–11. https://doi.org/10.1016/j.rse.2015.01.020

Papa D de A, Almeida DRA de, Silva CA, et al (2020) Evaluating tropical forest classification and field sampling stratification from lidar to reduce effort and enable landscape monitoring. Forest Ecology and Management 457 :117634. https://doi.org/10.1016/j.foreco.2019.117634

Parker GG, Harmon ME, Lefsky MA, et al (2004) Three-dimensional structure of an old-growth Pseudotsuga-Tsuga canopy and its implications for radiation balance, microclimate,

and gas exchange. Ecosystems 7 :440–453

Parker GG, Russ ME (2004) The canopy surface and stand development : assessing forest canopy structure and complexity with near-surface altimetry. Forest Ecology and Management 189 :307–315. https://doi.org/10.1016/j.foreco.2003.09.001

Pebesma E (2004) Multivariable geostatistics in S : the gstat package. Computers & Geosciences 30 :683–691. https://doi.org/10.1016/j.cageo.2004.03.012

Pebesma E, Heuvelink G (2016) Spatio-temporal interpolation using gstat. RFID Journal 8 :204–218

Pedlar JH, McKenney DW, Lawrence K, et al (2014) A Comparison of Two Approaches for Generating Spatial Models of Growing-Season Variables for Canada. J Appl Meteor Climatol 54 :506–518. https://doi.org/10.1175/JAMC-D-14-0045.1

Perron J-Y, Morin P (2002) Normes d'inventaire forestier. Placettes-échantillons permanentes. Direction des inventaires forestiers, Forêt Québec, Ministère des Ressources naturelles et de la Faune, Gouvernement du Québec, Québec

Pienaar LV, Turnbull KJ (1973) The Chapman-Richards Generalization of Von Bertalanffy's Growth Model for Basal Area Growth and Yield in Even - Aged Stands. Forest Science 19 :2–22

Pommerening A (2002) Approaches to quantifying forest structures. Forestry 75 :305–324. https://doi.org/10.1093/forestry/75.3.305

Pothier D, Savard F (1998) Actualisation des tables de production pour les principales espèces forestières du Québec. Ministère des Ressources naturelles

Power H, LeMay V, Berninger F, et al (2012) Differences in crown characteristics between black (Picea mariana) and white spruce (Picea glauca). Canadian Journal of Forest Research 42 :1733–1743

Power H, Schneider R, Berninger F (2014) Understanding changes in black (Picea mariana) and white spruce (Picea glauca) foliage biomass and leaf area characteristics. Trees 28 :345–357. https://doi.org/10.1007/s00468-013-0953-2

Pretzsch H (2009) Forest dynamics, growth and yield : from measurement to model. Springer, Berlin

Pretzsch H, Dieler J (2012) Evidence of variant intra- and interspecific scaling of tree crown structure and relevance for allometric theory. Oecologia 169 :637–649. https://doi.org/10.1007/s00442-011-2240-5

Puettmann K, Coates KD, Messier CC (2009) A critique of silviculture : managing for com-

plexity. Island Press, Washington DC

Purves DW, Lichstein JW, Pacala SW (2007) Crown Plasticity and Competition for Canopy Space : A New Spatially Implicit Model Parameterized for 250 North American Tree Species. PLoS ONE 2 :e870. https://doi.org/10.1371/journal.pone.0000870

Quinn P, Beven K, Chevallier P, Planchon O (1991) The prediction of hillslope flow paths for distributed hydrological modelling using digital terrain models. Hydrological Processes 5 :59–79. https://doi.org/10.1002/hyp.3360050106

R Core Team (2020) R : A Language and Environment for Statistical Computing version 3.6.3. R Foundation for Statistical Computing, Vienna, Austria

R Development Core (2012) R : A Language and Environment for Statistical Computing. Vienna, Austria

Racine EB, Coops NC, St-Onge B, Bégin J (2014) Estimating Forest Stand Age from LiDAR-Derived Predictors and Nearest Neighbor Imputation. Forest Science 60 :128–136. https ://doi.org/http://dx.doi.org/10.5849/forsci.12-088

Ramsay J, Hooker G, Graves S (2009) Functional Data Analysis with R and MATLAB. Springer New York, New York, NY

Ramsay J, Silverman BW (2005) Functional data analysis, 2nd edn. Springer, New York

Räty J, Vauhkonen J, Maltamo M, Tokola T (2016) On the potential to predetermine dominant tree species based on sparse-density airborne laser scanning data for improving subsequent predictions of species-specific timber volumes. For Ecosyst 3 :1. https://doi.org/10.1186/s40663-016-0060-0

Raymond P, Bédard S, Tremblay S, Larouche C (2010) La coupe progressive irrégulière, un outil prometteur pour la mise en oeuvre de l'aménagement écosystémique au Québec. Ministère des Ressources naturelles et de la Faune, Direction de la recherche forestière

Ribeiro MT, Singh S, Guestrin C (2016) "Why Should I Trust You ?" : Explaining the Predictions of Any Classifier. In : Proceedings of the 22nd ACM SIGKDD International Conference on Knowledge Discovery and Data Mining. Association for Computing Machinery, New York, NY, USA, pp 1135–1144

Richardson JJ, Moskal LM (2011) Strengths and limitations of assessing forest density and spatial configuration with aerial LiDAR. Remote Sensing of Environment 115 :2640–2651. https://doi.org/10.1016/j.rse.2011.05.020

Riggins JJ, Tullis JA, Stephen FM (2009) Per-segment Aboveground Forest Biomass Estimation Using LIDAR-Derived Height Percentile Statistics. GIScience & Remote Sensing

46 :232–248. https://doi.org/10.2747/1548-1603.46.2.232

Roberts DR, Bahn V, Ciuti S, et al (2017b) Cross-validation strategies for data with temporal, spatial, hierarchical, or phylogenetic structure. Ecography 40 :913–929. https://doi.org/10.1111/ecog.02881

Roberts DR, Bahn V, Ciuti S, et al (2017a) Cross-validation strategies for data with temporal, spatial, hierarchical, or phylogenetic structure. Ecography 40 :913–929. https://doi.org/10.1111/ecog.02881

Roussel J-R, Auty D, Coops NC, et al (2020) lidR : An R package for analysis of Airborne Laser Scanning (ALS) data. Remote Sensing of Environment 251 :112061. https://doi.org/10.1016/j.rse.2020.112061

Roussel J-R, Béland M, Caspersen J, Achim A (2018) A mathematical framework to describe the effect of beam incidence angle on metrics derived from airborne LiDAR : The case of forest canopies approaching turbid medium behaviour. Remote Sensing of Environment 209 :824–834. https://doi.org/10.1016/j.rse.2017.12.006

Roussel J-R, Caspersen J, Béland M, et al (2017) Removing bias from LiDAR-based estimates of canopy height : Accounting for the effects of pulse density and footprint size. Remote Sensing of Environment 198 :1–16. https://doi.org/10.1016/j.rse.2017.05.032

Ruel J-C, Roy V, Lussier J-M, et al (2007) Mise au point d'une sylviculture adaptée à la forêt boréale irrégulière. The forestry chronicle 83 :367–374

Schütz J-P (1997) Sylviculture. Presses polytechniques et universitaires romandes, Lausanne

Seavy NE, Viers JH, Wood JK (2009) Riparian bird response to vegetation structure : a multiscale analysis using LiDAR measurements of canopy height. Ecological Applications 19 :1848–1857. https://doi.org/10.1890/08-1124.1

Seber GAF, Lee AJ (2003) Linear regression analysis. Wiley-Interscience, Hoboken, N.J.

Settles B (2009) Active learning literature survey. University of Wisconsin-Madison Department of Computer Sciences

Stark SC, Leitold V, Wu JL, et al (2012) Amazon forest carbon dynamics predicted by profiles of canopy leaf area and light environment. Ecology Letters 15 :1406–1414. https://doi.org/10.1111/j.1461-0248.2012.01864.x

Straub C, Koch B (2011) Enhancement of bioenergy estimations within forests using airborne laser scanning and multispectral line scanner data. Biomass and Bioenergy 35 :3561–3574. https://doi.org/10.1016/j.biombioe.2011.05.017

Tackenberg O (2007) A New Method for Non-destructive Measurement of Biomass, Growth

Rates, Vertical Biomass Distribution and Dry Matter Content Based on Digital Image Analysis. Ann Bot 99 :777–783. https://doi.org/10.1093/aob/mcm009

Thomas RQ, Hurtt GC, Dubayah R, Schilz MH (2008) Using lidar data and a height-structured ecosystem model to estimate forest carbon stocks and fluxes over mountainous terrain. Canadian Journal of Remote Sensing 34 :S351–S363. https://doi.org/10.5589/m08-036

Thorpe HC, Astrup R, Trowbridge A, Coates KD (2010) Competition and tree crowns : A neighborhood analysis of three boreal tree species. Forest Ecology and Management 259 :1586–1596. https://doi.org/10.1016/j.foreco.2010.01.035

Treitz P, Lim K, Woods M, et al (2012) LiDAR Sampling Density for Forest Resource Inventories in Ontario, Canada. Remote Sensing 4 :830–848. https://doi.org/10.3390/rs4040830

Ung CH, Bernier PY, Raulier F, et al (2001) Biophysical site indices for shade tolerant and intolerant boreal species. Forest Science 47 :83–95

Vanclay J (1994) Sustainable timber harvesting : simulation studies in the tropical rainforests of north Queensland. Forest Ecology and Management 69 :299–320

Vaughn NR, Moskal LM, Turnblom EC (2012) Tree Species Detection Accuracies Using Discrete Point Lidar and Airborne Waveform Lidar. Remote Sensing 4 :377–403. https://doi.org/10.3390/rs4020377

Vierling KT, Bässler C, Brandl R, et al (2010) Spinning a laser web : predicting spider distributions using LiDAR. Ecological Applications 21 :577–588. https://doi.org/10.1890/09-2155.1

Vierling KT, Vierling LA, Gould WA, et al (2008) Lidar : shedding new light on habitat characterization and modeling. Frontiers in Ecology and the Environment 6 :90–98. https://doi.org/10.1890/070001

Wasser L, Day R, Chasmer L, Taylor A (2013) Influence of Vegetation Structure on Lidar-derived Canopy Height and Fractional Cover in Forested Riparian Buffers During Leaf-Off and Leaf-On Conditions. PLoS One 8 : https://doi.org/10.1371/journal.pone.0054776

Weber TC, Boss DE (2009) Use of LiDAR and supplemental data to estimate forest maturity in Charles County, MD, USA. Forest Ecology and Management 258 :2068–2075. https://doi.org/10.1016/j.foreco.2009.08.001

Weiskittel AR, Kershaw JA, Hofmeyer PV, Seymour RS (2009) Species differences in total and vertical distribution of branch- and tree-level leaf area for the five primary conifer

species in Maine, USA. Forest Ecology and Management 258 :1695–1703. https://doi.org/10.1016/j.foreco.2009.07.035

White JC, Wulder MA, Varhola A, et al (2013a) A best practices guide for generating forest inventory attributes from airborne laser scanning data using an area-based approach. Natural Resources Canada, Canadian Forest Service, Canadian Wood Fibre Centre, Victoria, BC.

White J, Wulder M, Vastaranta M, et al (2013b) The Utility of Image-Based Point Clouds for Forest Inventory : A Comparison with Airborne Laser Scanning. Forests 4 :518–536. https://doi.org/10.3390/f4030518

Wilkes P, Jones SD, Suarez L, et al (2016) Using discrete-return airborne laser scanning to quantify number of canopy strata across diverse forest types. Methods in Ecology and Evolution 7 :700–712. https ://doi.org/https://doi.org/10.1111/2041-210X.12510

Winkler AM, Ridgway GR, Webster MA, et al (2014) Permutation inference for the general linear model. NeuroImage 92 :381–397. https://doi.org/10.1016/j.neuroimage.2014.01.060

Woods M, Lim K, Treitz P (2008) Predicting forest stand variables from LiDAR data in the Great Lakes – St. Lawrence forest of Ontario. THE FORESTRY CHRONICLE 84 :13

Woods M, Pitt D, Penner M, et al (2011) Operational implementation of a LiDAR inventory in Boreal Ontario. The Forestry Chronicle 87 :512–528

Wulder MA, White JC, Nelson RF, et al (2012) Lidar sampling for large-area forest characterization : A review. Remote Sensing of Environment 121 :196–209. https://doi.org/10.1016/j.rse.2012.02.001

Zimble D, Evans DL, Carlsonc GC, et al (2003) Characterizing vertical forest structure using small-footprint airborne LiDAR. Remote Sensing of Environment 87 :171–182. https://doi.org/10.1016/S0034-4257(03)00139-1